공학박사 학위논문

Dynamic Substructuring for Evaluating Vibro-acoustic Performance:

Virtual Parameters and Virtual Point Transformation

시스템의 음향 진동 성능 평가를 위한 동특성 합성기법:

가상 매개 변수 및 가상 지점 변환

2020년 8월

서울대학교 대학원

기계항공공학부

김 준 구

Dynamic Substructuring for Evaluating Vibro-acoustic Performance:

Virtual Parameters and Virtual Point Transformation

by

Jun Gu Kim

A Dissertation
Submitted to the Faculty of

School of Mechanical and Aerospace Engineering

at

Seoul National University

in Partial Fulfillment of
the Requirements for the Degree of

Doctor of Philosophy

August 2020

Dynamic Substructuring for Evaluating Vibro-acoustic Performance:

Virtual Parameters and Virtual Point Transformation

시스템의 음향 진동 성능 평가를 위한 동특성 합성기법: 가상 매개 변수 및 가상 지점 변환

지도교수 강 연 준

이 논문을 공학박사 학위논문으로 제출함

2020년 4월

서울대학교 대학원

기계항공공학부

김 준 구

김준구의 공학박사 학위논문을 인준함

2020년 6월

위 원 장 _____

부위원장 _____

위 원 _____

위 원 _____

위 원 _____

ABSTRACT

Dynamic Substructuring for Evaluating Vibro-acoustic Performance:

Virtual Parameters and Virtual Point Transformation

Jun Gu Kim

School of Mechanical and Aerospace Engineering

The Graduate School

Seoul National University

Generally, a mechanical system consists of various substructures that cause noise and vibration problems. This thesis proposes a dynamic substructuring method for the estimation of the dynamic characteristics of a coupled mechanical system based on substructure characteristics.

The first phase of this thesis presents a method for the estimation of rotational stiffness at the coupled points of an assembled system based on a dynamic substructuring method. Conventional test-based rotational stiffness evaluation methods are sensitive to measurement errors and

require a specialized jig for testing. In contrast, given that the proposed method uses the natural frequency shift phenomenon that results from the addition of mass, the measurement error is relatively small, and the accuracy is improved by excluding the interference of other modes. In addition, the proposed method solves the problem due to the complexity of the conventional method by changing the fixed condition of the system using frequency response function (FRF)-based substructuring (FBS) modeling; thus, it does not require a specialized jig for fixing parts. In this manuscript, the concepts of trial mass, virtual mass, and virtual spring are introduced to systematically explain the proposed method and its application based on frequency shifts. The results of the experiments conducted on a vehicle shock absorber verify the utility of the proposed method.

In the second phase, a novel transfer path analysis (TPA) method based on a dynamic substructuring model is proposed. With the dynamic substructuring model, the FRF information of a base system can be used to evaluate the stiffness addition effect at the measurement points instead of adding the actual stiffness. In the proposed method, a spring with an infinite stiffness is virtually added to a specific transfer path among various possible paths, such that the specific path is removed. Hence, the

virtual spring significantly reduces the contribution of the specific path. This method is more implementable and applicable than existing TPA methods (i.e., conventional TPA and operational TPA), as it does require part removal or the correlation information between the signals. To verify the feasibility of the FBS-based TPA method, it was applied to a significant road noise phenomenon. The test results confirm that the proposed method can be applied to the TPA of suspension linkages and vehicle bodies.

In the final phase of this thesis, an improved dynamic substructuring model is presented based on the estimated FRF information at a coupling point between substructures. An assembled system generally consists of two or more such substructures, which are typically connected by a bolt. To ensure an accurate estimation of the dynamic characteristics of the assembled system, an accurate measurement of the joint properties is required. However, in most practical cases, physical constraints prevent such measurements at actual coupling points. Accordingly, this study proposes a method that uses generalized coupling properties to estimate the dynamic characteristics of a new coupling system based on the characteristics of the original substructure. In this process, the concept of virtual point transformation was used to estimate accurate FRFs at the

coupling points of the assembled system based on convenient measurements. Thereafter, the proposed method was validated using a hard-mount vehicle suspension in a test jig and on an actual vehicle body for estimating the vibration characteristics of the assembled system. This research contributes towards the accurate estimation of the dynamic properties of bolt-assembled systems in several practical applications.

Keywords: Dynamic substructuring, FRF-based substructuring, Trial mass, Virtual mass, Virtual spring, Rotational stiffness, Transfer path analysis, Virtual point transformation

Student Number: 2015-20723

TABLE OF CONTENTS

LIST OF TABLES

LIST OF FIGURES

CHAPTER 1

GENERAL INTRODUCTION

1.1 Research background and motivation of the work

In recent years, as the use of conventional internal combustion engines has been decreasing, the proportion of road noise perceived by drivers inside vehicles has been increasing in contrast to the power train (P/T) noise, as shown in Fig. 1.1 [68]. Accordingly, road noise has become an important design consideration in the automobile industry. In general, road noise with a frequency below 500 Hz is considered as structure-borne noise is caused by the irregular interactions between the wheels of the travelling vehicle and the road surface. The noise is transmitted from the wheel to the interior sound pressure level (SPL) via the suspension, which acts as a transfer path. This mechanism is depicted in Fig. 1.2. Therefore, modifying the transfer path (i.e., suspension) can lead to an improvement in the vibro-acoustic performance of the vehicle with respect to road noise.

However, the vehicle body styling, and consequently its interior SPL

construction, are only determined during the final phase of the vehicle development process, as depicted in Fig. 1.3. This implies that the scope of viable design considerations available for the interior SPL at this stage is limited by earlier design choices. Therefore, by omitting the impact of body styling on the vibro-acoustic performance, the results obtained from analyses conducted during earlier phases of the development process are insufficient. In addition, the noise, vibration, and harshness (NVH) performance conflicts with the ride and handling (R&H) or durability performance of the vehicle, as depicted in Fig. 1.4. For this reason, vehicle development that focuses on the NVH performance alone while neglecting other performance indicators is unreliable. Therefore, in the vehicle development process, it is necessary to determine the optimum performance to achieve a suitable trade-off among the abovementioned parameters. Hence, to reduce road-induced noise during the development of vehicles, NVH engineers typically conduct several trial-and-error cycles and repeated/redundant experiments. Therefore, an independent study on the suspension is required without consideration of the vehicle body to avoid this inefficient iterative process.

For this reason, a V-shaped development process is established, as depicted in Fig. 1.3. To improve the vibro-acoustic performance of the vehicle, developers first select the target vehicle as a benchmark, and then repeatedly

analyze the system modules and part-level cascading. Thereafter, the part-level components are integrated. This V-shaped development process is superior to the conventional serial process, which involves the repetitive evaluation of the suspension at each level. Moreover, the V-shaped process is more time- and cost-efficient.

Meanwhile, a general mechanical system comprises various substructures that can cause noise and vibration issues. Moreover, noise and vibration issues that were unanticipated in the early single-product design phases may arise in the final mass production phase of the completed system. This necessitates the evaluation of the systems under their final assembled conditions. However, most mechanical systems, such as automobiles, consist of multiple components and thus, individually assessing each component's contribution to noise and vibration can be challenging, given the short development period typically associated with automobile manufacturing. Therefore, to reduce the level of noise or vibration in the overall system, it is necessary to investigate the frequency response characteristics of each individual substructure and use these characteristics to predict the overall assembled system behavior. In particular, it is critical to obtain the frequency response function (FRF) information for each substructure in the initial development stages to facilitate the performance prediction of the system.

Consequently, various approaches have recently been developed to reduce the road noise. However, in this process, it was also necessary to consider the experimental inefficiency with respect to the vehicle NVH and to shorten the duration of the vehicle development process for reducing road noise as described above. In this context, the aim of this study was to improve the vibro-acoustic performance of the vehicle suspension and develop an estimation model of its vibro-acoustic performance in the practical vehicle development process. Numerical modeling was conducted to evaluate the rotational stiffness of suspension components, and a dynamic substructuring method was developed to estimate the dynamic characteristics of the target system.

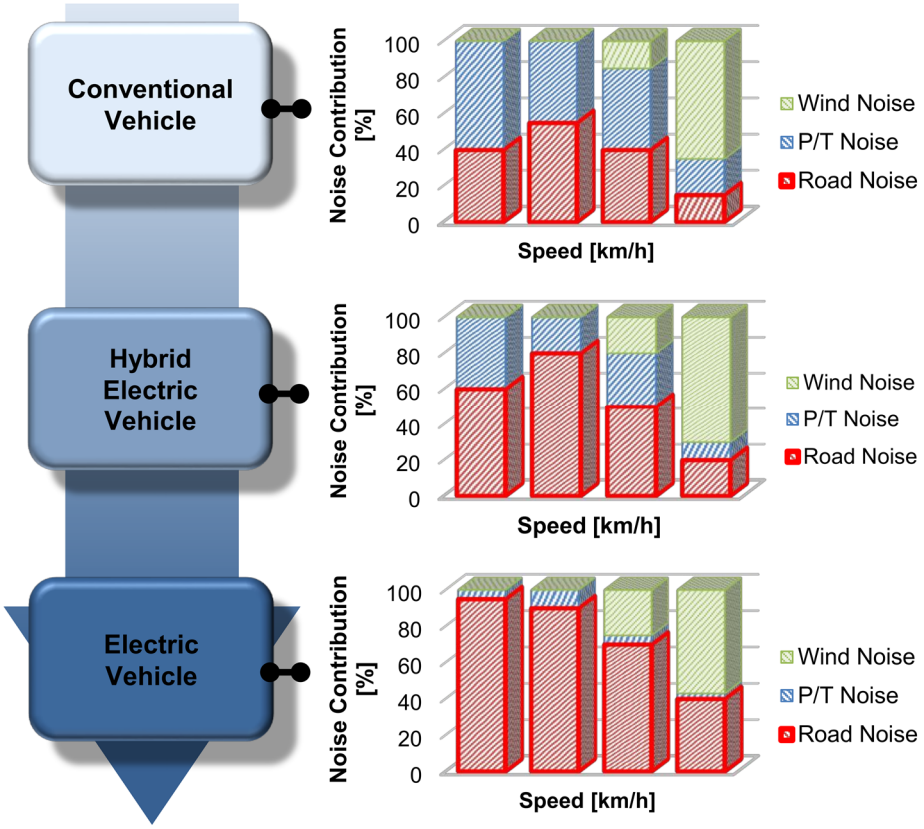

Figure 1.1 Noise-contribution ratio with respect to vehicle type.

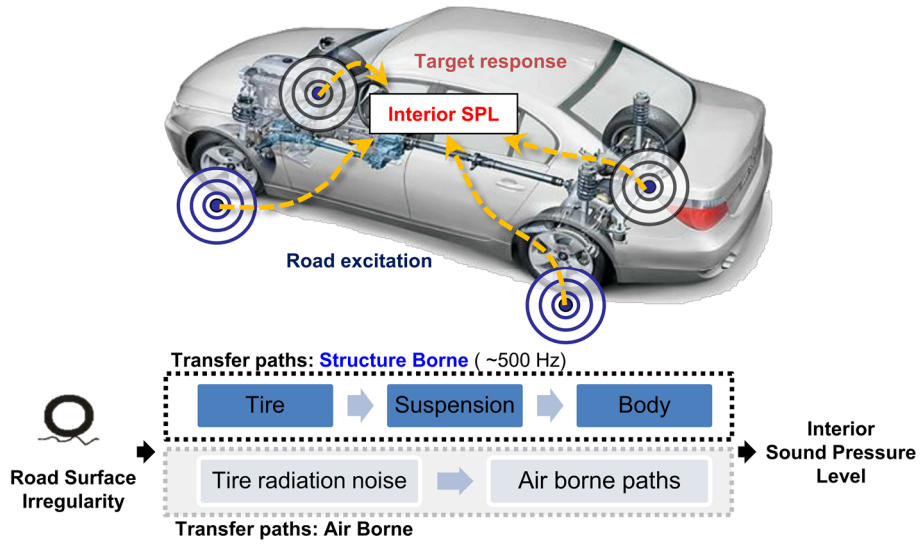

Figure 1.2 Road noise and transfer paths of vehicle.

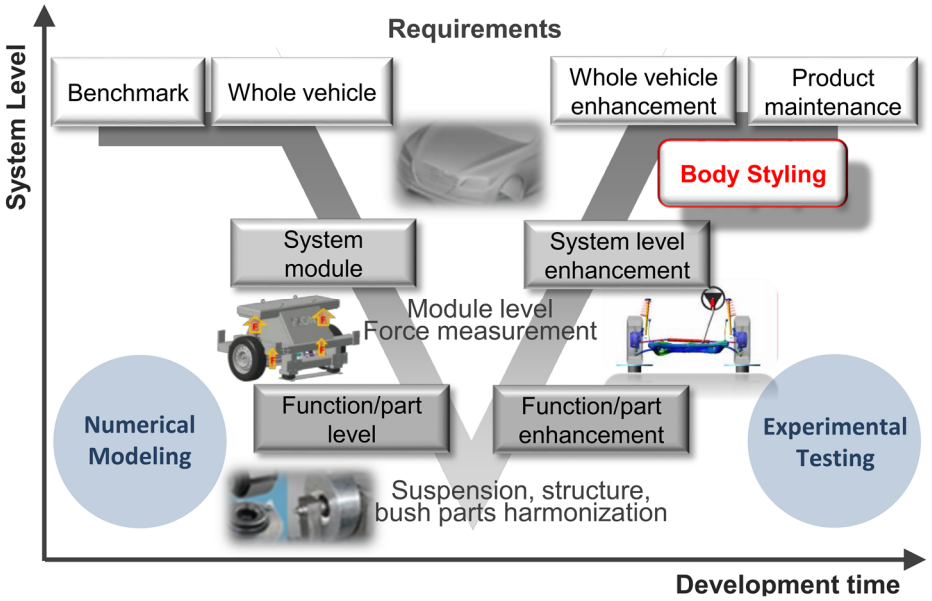

Figure 1.3 V-shaped vehicle development process.

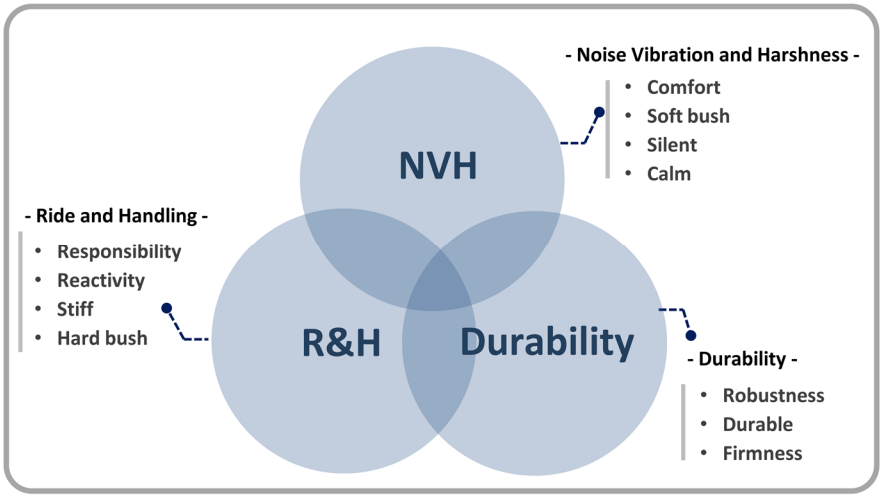

Figure 1.4 Conflicting performances in vehicle development process.

1.2 Literature reviews

To evaluate the joint stiffness of system, various studies have been conducted. Kang et al. [1] conducted a study on the selection of support stiffness parameters to obtain optimal modal properties with reference to previous work on the vibration characteristics of flexibly supported systems. Elishakoff and Lin [2] studied the vibrational characteristics of a beam with a rotational spring at its ends, using the dynamic-edge-effect method. Chang et al. [3] studied the dynamic response of a beam with an internal hinge installed on foundations with unknown parameters. Grossi and Quintana [4] conducted a modal analysis on a beam with an arbitrarily located internal hinge; the ends of the beam were elastically restrained to prevent rotational and translational motion. Wang [5] conducted further research on the optimal design of a support for a beam with elastically-restrained boundaries, with focus on practical use cases. In addition, Wang et al. [6] conducted a study on joint identification based on the partially measured FRF, based on estimations. In addition, Mehrpouya et al. [7] employed the inverse receptance coupling (IRC) method to estimate joint properties using FRFs measured from the assembled structures. Recently, a joint parameter updating algorithm [8] and a finite element (FE) model updating method [9] were proposed for the identification of joint

properties with improved accuracy. Moreover, an analytical approach was proposed by Segovia-Eulogio et al. [10] for the evaluation of the dynamic stiffness of a material using equations that satisfy the equilibrium conditions within the system. Čelič et al. [11] also proposed a method to identify joint properties by considering rotational effects. To identify the stiffness at a connection point, most of these studies were based on the dynamic modeling method. However, these methods have practical limitations when used to evaluate stiffness, especially rotational stiffness. For example, Čelič used sections of the FE model in the experimental verification, as the FRFs of the rotational degrees of freedom (RDOFs) could not be experimentally determined [11]. Therefore, a specialized jig that fixes the system is generally required for the evaluation of rotational stiffness, which is inefficient, given that the jig requires design and manufacture. Furthermore, the results are generally influenced by the different modes or measurement errors. Hence, there are many practical limitations to the test-based stiffness evaluation methods, as detailed above.

In contrast to the previously mentioned methods, studies were conducted on the identification of the system characteristics using response data, instead of FRFs. In particular, an operational modal analysis (OMA) was introduced for application to modal analyses using only operational data, namely,

transmissibility. Similarly, studies were conducted on the improvement of the system identification accuracy [12] and damage detection [13,14] using only transmissibility. Joo [15] recently developed a technique to identify boundary characteristics based on transmissibility. The methods that require only the response data for the estimation or evaluation the dynamic properties of a system provide many advantages with respect to experimental simplicity. In particular, the automobile industry imposes stiffness reinforcement requirements on several parts based on OMA obtained only from vehicle operational data. Although this provides insight into parts with lack stiffness, it cannot satisfy quantitative requirements. Thus, besides several experimental advantages, it is difficult to evaluate rotational stiffness in practical cases using existing methods. Previous studies were focused on the measurement or observation of the stiffness. However, this differs from the focus of this study, which is the control of stiffness with respect to the NVH. Hence, the aim of this study was to develop a method for evaluating rotational stiffness based on simple NVH experiments, without an FE model or a test jig for the fixing of a target system.

Meanwhile, the FRF-based substructuring (FBS) method is a commonly used technique to predict the dynamics when two or more substructures are assembled or disassembled. The FBS technique has been investigated by many

researchers to date. Among them, de Klerk et al. [16,17] summarized the history of dynamic substructuring and transfer path analysis (TPA) techniques using the FBS method. Tsai and Chou [18] proposed an identification method for single bolt joint properties using the FBS method. Yang et al. [19] conducted advanced research on the identification of joint parameters using a coupled stiffness matrix. In particular, they did not consider a joint as a translational or rotational spring, as is the case in the conventional method. Instead, they identified the translational and rotational stiffness of the joint by applying the substructure synthesis method, considering the model as a coupled stiffness matrix. Ren and Beards extended the methods to reduce the measurement error [20,21]. They derived a system model with multiple joints to consider mass, stiffness, and damping, unlike previous studies. Subsequently, Ren et al. [22] used the generalized coupling technique to eliminate the measurement error in the application of the FBS method. In addition, a study on substructure coupling considering the rotational degree of freedom was conducted by Liu and Ewins [23]. Zhen and Lim [24] identified the critical element of a multi-coupling system without information on the substructures, which differentiates it from the general FBS method. Allen [25] proposed an experimental procedure to remove the dynamic effects of flexible fixtures using the modal substructuring method. Recently, various applications based on these FBS modeling method

have been investigated [26,27,28]. In particular, in numerous studies, attempts have been made to apply these dynamic substructuring methods to automotive systems. Recently, Seijs and Klerk have expanded their research to hybrid dynamic models by introducing a system equivalent model mixing technique [29]. Kim et al. [30] introduced a derivation method to estimate the transfer forces at suspension mounting points using the FBS modeling method. Based on the results of previous research, in this study, the dynamic substructuring technique was employed to evaluate the rotational rigidity of the system components. In addition, the focus of this study was on the development of a method for rotational stiffness evaluation. This thesis proposes an estimation method for the rotational stiffness. In this process, the peak frequency shift of an FRF using a test mass was used. Furthermore, an FBS model was used to apply a virtual mass instead of an actual test mass, for experimental convenience. In the proposed dynamic substructuring model, a method is recommended for the estimation of the dynamic characteristics of the system with the modification of the measured FRFs based on virtual masses and virtual springs.

From another aspect, many studies have been conducted based on the estimation of the dynamic characteristics for the design of entire systems. To predict the dynamic characteristics of assembled systems in which two or more

substructures are coupled or decoupled, dynamic substructuring methods or synthesis techniques are typically employed. In many studies [6,7,8,9], FRF information was used to determine the coupled system characteristics. In particular, Ewins [33,34] examined the application of system parameters using FRFs, and proposed a method to identify structure modal properties. Different approaches to the dynamic substructuring method using FRFs have therefore been evaluated, as detailed above [11,18,19,20,21,22]. In subsequent research, Čelič et al. [52] employed a numerical simulation method to verify the effects of the joint characteristics due to coordinate reduction. Klerk and Rixen [16] presented a concise literature review and summary of dynamic substructuring techniques. Furthermore, Moorhouse et al. [26] used a dynamic substructuring method and the blocked force occurring at a joint interface to apply a TPA technique in an operational state. Seijs [27,28] presented a synthesis technique to predict the dynamic characteristics of an assembled automotive steering-column system. The work of Seijs and Klerk [29] introduced a hybrid dynamic model using the system equivalent model mixing technique. In general, dynamic substructuring techniques are used in the development of numerical models such as FE analyses, to identify substructure characteristics. In several studies conducted on dynamic substructures, Lagrange multipliers and Boolean matrices were employed to solve problems using parallel-processing computers.

Moreover, Cho et al. [53] suggested a reduction process to improve computing efficiency based on proper orthogonal decomposition.

Despite the above numerical model-improvement studies, there are many practical limitations to dynamic substructuring with respect to physical tests, especially in the automotive field; thus, restricting the test-based estimation models used to evaluate the dynamic characteristics of coupling systems. Seijs et al. [17,27,54] conducted a practical physical study using the substructuring technique. In these studies, the concept of virtual point (VP) and post-processing techniques for transforming measured signals using interface deformation matrices (IDMs) have been proposed to overcome these practical problems. In addition, Kang et al. [30,55,56,57] conducted practical physical studies using a test jig to develop a vehicle suspension system by applying a dynamic substructuring technique, under the consideration of the limitations of practical testing. In a study conducted by Häußler and Rixen [58], various techniques for improving the physical experiment-based dynamic substructuring method were proposed based on the application of interface-deformation modes.

1.3 Overview of the present work

This thesis is organized as follows. Chapter 2 presents the derivation of a general dynamic substructuring method. Chapter 3 details formulations for the estimation of the rotational stiffness model derived from the governing equations of the system, for the determination of the natural frequency of the target system. In this process, the frequency shift phenomenon with mass addition is used. By modeling the variation of the natural frequency of the target system FRF due to the use of the actual trial mass, the rotational stiffness of the target system can be estimated. Furthermore, an FBS model was used to apply a virtual mass instead of the actual trial mass, for experimental convenience. In the proposed dynamic substructuring model, a method is presented for estimating the dynamic characteristics of the system by modifying the measured FRFs based on virtual masses and virtual springs. In addition, a numerical simulation that accurately considers the moments of inertia of the trial masses and the accelerometers is derived for more general cases. Based on the simulation results, the principle of virtual mass, for which the volume can be considered as negligible, is used to more easily conduct the experiment. In addition, the accuracy of the results of the proposed method is verified, as presented.

In Chapter 4, a novel approach to transfer path analysis is introduced based on the virtual spring principle, which is an alternative to the conventional TPA, thus simplifying the experimental process. The proposed approach can rapidly evaluate each contribution of the transfer paths to determine which path should be modified first to reduce noise and vibration.

In Chapter 5, a dynamic substructuring model is presented to estimate the vibroacoustic performance of an entire system assembled with substructures. In the proposed method, the virtual point concept is adopted to allow for physical measurements at the joint point in practical implementation when measurements at the coupling points are impractical. In addition, generalized coupling properties (GCPs) are presented for accurate estimations. To verify that this method improves the estimation accuracy in the dynamic substructuring method, a test jig and an actual vehicle suspension were used. The verification results confirm the feasibility of the extended substructuring model in practical cases.

Finally, the conclusions and recommendations are outlined in Chapter 5, which summarizes the results of this thesis, in addition to the limitations of the study and scope of future research.

1.4 Contributions

The aim of this work is threefold: first, to formulate a rotational stiffness evaluation model for improving the vibroacoustic performance of vehicle components, and second, to evaluate the contribution of the transfer path using a dynamic substructuring model. Third, to derive a dynamic substructuring model for the estimation of the dynamic characteristics of a system, and the practical improvement of its estimation accuracy.

In Chapter 3, a novel method is presented for evaluating rotational stiffness with respect to simple NVH experiments, without an FE model or a test jig, based on the virtual spring principle. In conventional methods, a finite element (FE) model is required, as the rotational stiffness is difficult to measure. In several cases, especially in the development process, it is difficult to obtain an FE model [11]. In addition, to evaluate the rotational stiffness, the angular displacement and torque data in the rotational direction should be determined, which requires a specialized test jig for fixing the part. However, these practical limitations are overcome by the proposed method. Furthermore, the proposed method can ensure experimental simplicity by the application of a virtual mass instead of the actual trial mass. Therefore, the proposed method can be employed to evaluate the rotational stiffness using simple FRF measurement

instruments in most practical cases where FE models or specialized test jigs are unavailable.

In addition, a novel TPA approach based on the virtual spring principle is presented in Chapter 4. This approach is an alternative to conventional TPA methods, as it simplifies the experimental process. In this process, the virtual spring can significantly reduce the contribution of the specific transfer path. Thus, the amount of time consumed for the evaluation of the transfer path is considerably reduced by using the proposed technique. This is a major contribution, given that the method significantly shortens the industrial development process, especially in the automobile field.

Chapter 5 details the prediction of the dynamic characteristics of a final assembled structure based on the FRFs of individual substructures evaluated using test jigs in the early development stages. The advantages of the proposed method allow for developers to predict the performance of a part in its intended system, irrespective of the differences in system coupling properties. Hence, the dynamic characteristics of an assembled system can be calculated based on the measured joint property and the FRFs of each substructure, thus allowing for the development process required for evaluation of the system to be significantly shortened. In addition, the results of the proposed method are more accurate than those of the conventional methods, as data at an actual joint point

between two substructures can be estimated, instead of using the data from coupling peripherals in physical tests or analytical models. The proposed method is applicable to almost all assumed rigid boundary conditions with respect to sensor attachment, which includes the bolt assembly. Thus, the proposed pre-test process using a test jig in the early design phase allows for the selection of suitable design parameters early in the development process, especially for the solution of noise and vibration problems, which results in a more accurate estimation of the assembled system characteristics.

As mentioned above, this thesis proposes a more practical and theoretical model throughout the development process, for the improvement of the automotive NVH performance, which can be extended to related research in the vehicular NVH field.

CHAPTER 2

INTRODUCTION TO DYNAMIC SUBSTRUCTURING

2.1 Introduction

This chapter introduces general assumptions for the dynamic substructuring model and provides an overview of this method. In most cases, mechanical systems are composed of many parts, and each part requires independent development, especially in the vehicle development process. Thus, the dynamic substructuring technique is useful for predicting the dynamic characteristics of complex assembled systems, as discussed in Chapter 1. A dynamic substructuring model can be represented by a combination of substructures. Accordingly, there are interrelations among the dynamics at a coupling interface between substructures. Thus, the dynamic characteristics of a target system can be predicted in their assembled state. This method allows for the prediction of the dynamic characteristics of a target system by relating the characteristics of individual subcomponents to those of an assembled system.

The substructuring technique is derived from the Thévenin theorem or Norton equivalent theorem, which facilitates the physical interpretation of the system by replacing complex electrical circuits with simple equivalent models [63]. This substructuring technique applies the equivalent theorem to the physical system, and it is mainly used to estimate the dynamic characteristics of a system [16,27]. Moreover, it is generally applied for the solution of structural problems, as it is a common approach [18,21,25]. Extensive studies were conducted on substructuring methods in various fields. For example, the FBS has been used as a tool for sensitivity analysis by Lee [65]. Moreover, the modeling of joint points and system optimization were mainly conducted using the dynamic substructuring method.

Among the various approaches to the substructuring method, the most common approach is based on the receptance coupling (RC) method, which synthesizes the FRF of an assembly system with the use of two independent substructures [18]. Although not discussed in detail herein, the RC method can be generalized to the generalized RC (GRC) method in more general coupled structures [66,67]. The general dynamic substructuring model and assumptions are derived based on the force equilibrium and compatibility conditions. To model an assembled system in which two substructures are coupled, it is necessary to consider the interface coupling point. As depicted in Fig. 2.1, the

assembled system consists of individual substructures. The force equilibrium and compatibility conditions at the coupling point are as follows:

$$u_j^{AB.A} = u_j^{AB.B}, \tag{1.1}$$

$$f_j^{AB.A} + f_j^{AB.B} = 0. \tag{1.2}$$

Here, u and f are the displacement and force at a coupling point, respectively. In addition, the subscript "j" is the joint point of the system. The superscripts "AB. A" and "AB. B" indicate that they were measured on the "A" and "B" sides of the coupling point of the coupled system "AB," respectively. A dynamic substructuring model to identify the characteristics of all systems is based on the two equations above. This concept is used throughout this thesis.

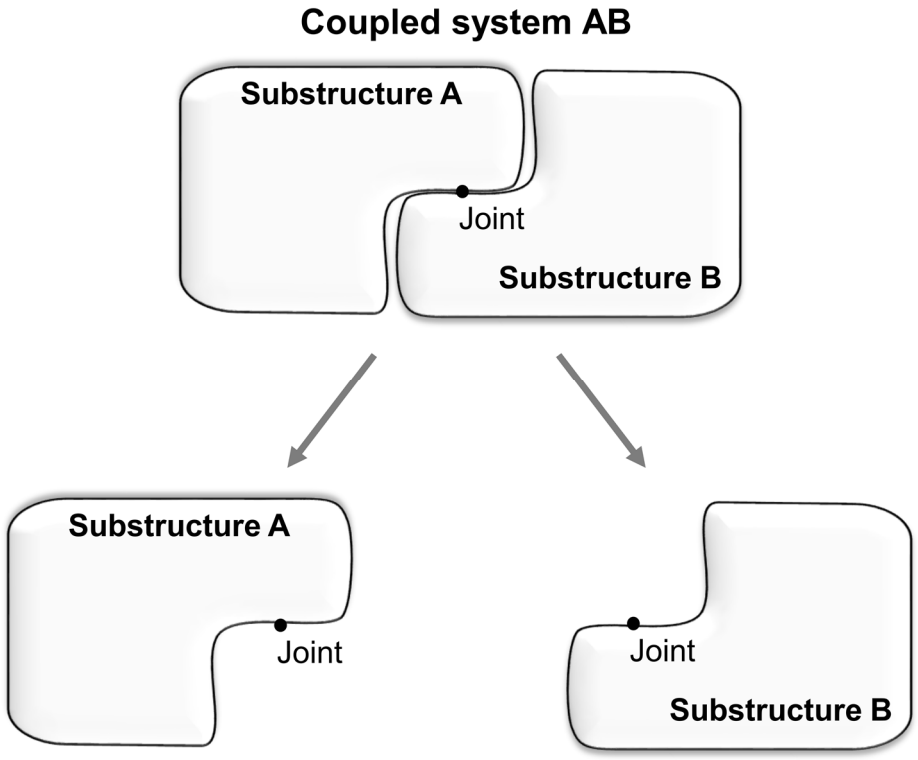

Figure 2.1 Coupled system consisting of substructures.

2.2 Summary

This chapter introduces the fundamental concepts and assumptions of the dynamic substructuring model used throughout this thesis. The dynamic substructuring model makes assumptions related to the force equilibrium and the compatibility conditions of the displacement at the joint point of the system. Based on these two assumptions, the dynamic substructuring is derived as presented in all the subsequent chapters.

CHAPTER 3

VIRTUAL PARAMETERS FOR ESTIMATING ROTATIONAL STIFFNESS

3.1 Introduction

The noise, vibration, and harshness (NVH) problems are common to mechanical systems in the industrial field. However, in most cases, the addition of weight or damping to address these issues is generally avoided to maintain the integrity of the designed systems. Moreover, detailed design requirements such as the shape, dimensions, and materials significantly restrict the adjustable parameters, and the design modifications cannot be implemented in practical applications; which is the case for vehicle development. Recently, vehicle development is focused on the reduction of costs and total mass for the improvement of fuel and the overall efficiency of a vehicle. In these cases, one solution is to enhance the stiffness of the vehicle parts or systems, which is a critical physical parameter in general NVH problems. Hence, the target stiffness in the NVH performance improvement studies should be measurable and

suitable to ensure applicability. In particular, a stiffness-change-oriented improvement approach is required to minimize the performance variations of other design parameters (durability, ride, and handling), especially when addressing NVH problems.

Meanwhile, a specific type of motion occurs when a part rotates with respect to another part. This case can be modeled as two parts connected by a hinge and rotational spring (see Fig. 3.1). These phenomena mainly occur at joints where the local stiffness is discontinuous. There are two classical methods used to estimate the translational stiffness, which is expandable to rotational stiffness, by sensing at two points. The first is a static stiffness evaluation method [31,32], and the second is a curve-fitting method [33,34,35]. Given that the static stiffness evaluation of machine tools is critical, Shuzi modeled the static stiffness of spindles mounted in bearings to evaluate the performance of machine tools [31]. Similarly, Wang conducted stiffness modeling of parallel kinematic machines (PKMs) [32]. Ewins [33,34] established a method to obtain system parameters, which includes stiffness, based on the FRF. The curve fitting technique was applied to the FRF in various studies on system identification [35]. For more practical cases, in the conventional static stiffness evaluation method, one part is fixed and exerts a force or moment on the other part, and the force and displacement or moment

and angle are measured, as illustrated in Fig. 3.2(a). The static stiffness evaluation method requires jigs for fixing one part and sensing for the other rotating part. Therefore, these conventional methods [11,68,69,71,72,73] are generally time-consuming and difficult to apply to non-standard specimens in comparison with the present method, as presented in Table 3.1. Furthermore, the static method cannot isolate only one specific mode; thus, its results may include the effects of other modes, in addition to the rotational mode. Another problem is that static stiffness is generally different from dynamic stiffness, which is dependent on the type of materials. In contrast, the measurement process of a curve fitting method is similar to that of the static stiffness evaluation method, with the exception that this method employs an impact hammer and accelerometers, as shown in Fig. 3.2(b). The curve-fitting method is a suitable estimation method for the stiffness line from the transfer functions, which indicates that the FRFs of translational or rotational motion (e.g., acceleration over force and rotational acceleration over moment) are within the stiffness-dominant frequency range. In general, the stiffness-dominant frequency range is lower than the first natural frequency, as shown in Fig. 3.3(a). Thus, this method can produce erroneous results if this range is narrow (see Fig. 3.3(b)) or there are other natural frequencies lower than that of a rotational mode (see Fig. 3.3(c)). This method also requires jigs for fixing one part,

although it does not require jigs for the sensing of the other rotating part. Alternative methods for stiffness estimation are joint parameter identification methods [6,19,20,22,36] that use FBS [16,18,21]. These methods are especially suitable for joints; and they do not require jigs, as they accommodate measurements under free-free boundary conditions; however, they require the FRF information of individual parts and the assembled system.

The method proposed in this chapter does not require jigs, unlike classical methods, as it allows for measurements under free-free boundary conditions using FBS, for simplicity [65]. Moreover, the proposed method does not require the FRF information of individual parts, given that the FBS method simply facilitates the conversion of the free-free boundary conditions into free-fixed conditions, unlike the joint parameter identification methods. This allows for a simpler and more efficient stiffness estimation. Moreover, the proposed method can yield more reliable results, as it uses only the natural frequency of a rotational mode and is insensitive to measurement errors and other modes. The results of several experiments conducted on a shock absorber verified the superior performance of the proposed method.

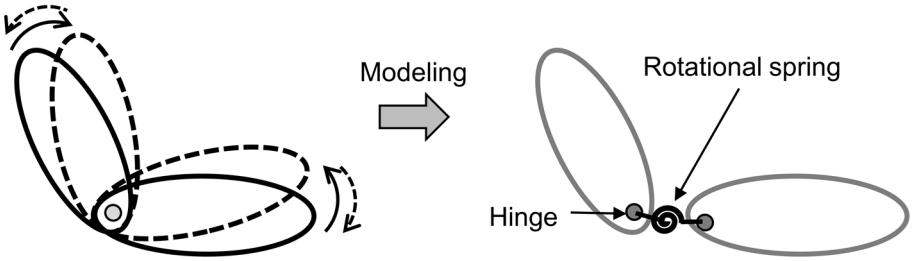

Figure 3.1 Rotational motion and its modeling based on a hinge and rotational spring.

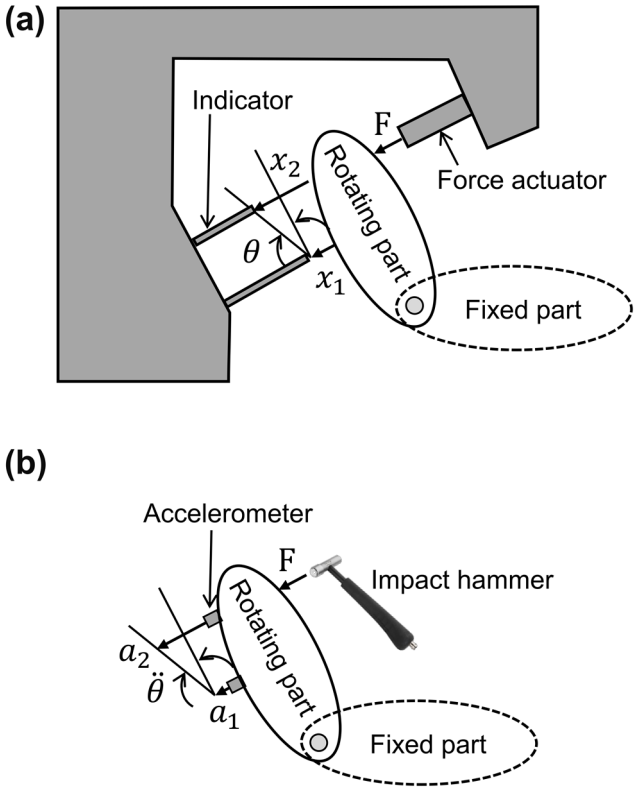

Figure 3.2 Two classical stiffness estimation methods: (a) static method and (b) FRF curve-fitting method.

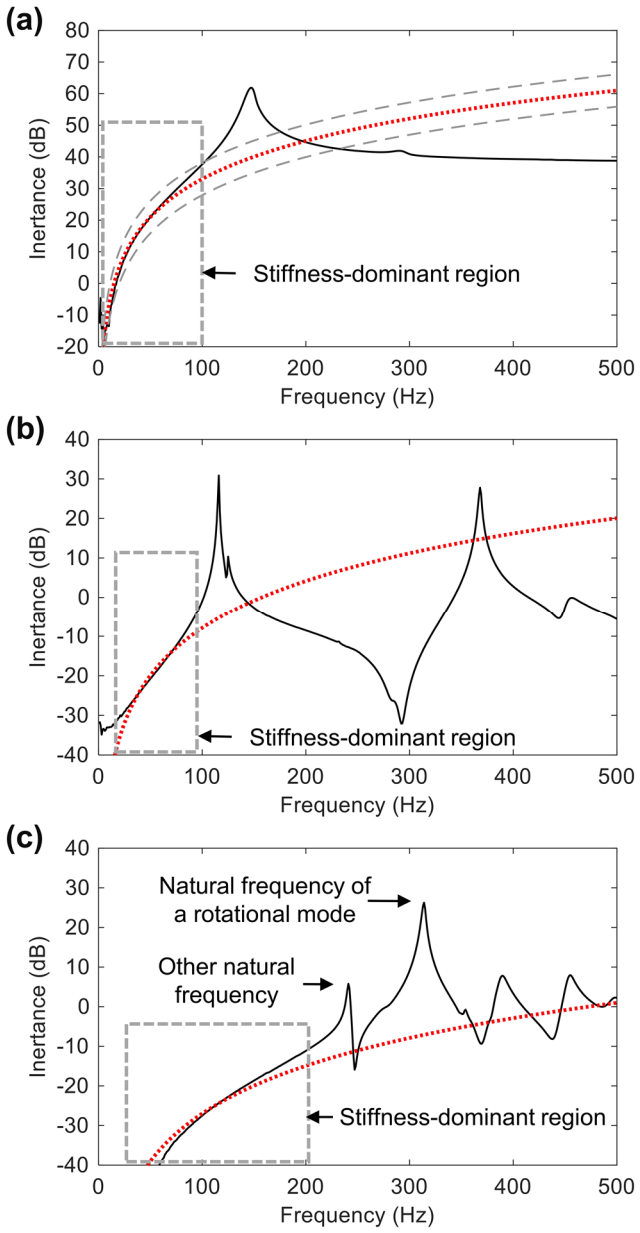

Figure 3.3 Examples of curve fitting method for estimating stiffness: (a) ideal case, (b) case wherein stiffness-dominant region is narrow, and (c) case wherein a natural frequency is lower than that of a rotational mode (solid line: measured FRF, dotted line: stiffness curve fitting line).

Table 3.1 Comparison of the contributions presented in this study with the limitations found in previous works.

Previous studies	Present study
Conventional rotational stiffness measurement: • Requires dedicated test jig for fixing • Experimentally complex	**Estimation model by using virtual parameters:** • Employs a simple test in most practical cases where FE models or specialized jigs are unavailable • Insensitive to measurement error and other modes

3.2 Theoretical concepts

3.2.1 Concept of trial masses

This study uses the natural frequency shift of a rotational mode by changing the moment of inertia to estimate the rotational stiffness. Let us consider the model illustrated in Fig. 3.4(a), which has a fixed part and a rotating part. The natural frequency f_0 of the rotating part is

$$f_0 = \frac{1}{2\pi}\sqrt{\frac{k_\theta}{I_0}}, \tag{3.1}$$

where k_θ is the rotational stiffness and I_0 is the moment of inertia of the rotating part on its hinge [37]. If a trial mass is added to the rotating part, as shown in Fig. 3.4(b), its natural frequency changes into f_1, which is given by

$$f_1 = \frac{1}{2\pi}\sqrt{\frac{k_\theta}{I_0 + I_1 + m_1 h^2}}, \tag{3.2}$$

where m_1 is the weight of the trial mass, I_1 is its moment of inertia on the

mass center, and h is the distance from the hinge to the trial mass. The denominator $I_0 + I_1 + m_1 h^2$ is the resultant moment of inertia of the rotating part on the hinge. In this process, all the additional trial masses are regarded as being point masses. A more generic form, which considers the volume of the trial mass, is given in Appendix A.

Let us add another trial mass to a point different from the first trial mass. Then, the natural frequency f_2 becomes

$$f_2 = \frac{1}{2\pi}\sqrt{\frac{k_\theta}{I_0 + I_2 + m_2(h+L)^2}}, \tag{3.3}$$

where m_2 is the weight of the second trial mass, I_2 is its moment of inertia, and L is the distance from the first trial mass to the second trial mass. This study considers k_θ, I_0, and h in Eqs. (3.1)–(3.3) as unknown parameters and other properties as known, considering real experimental situations. The distance h can be known if the location of a hinge is known; however, this study considers this distance as an unknown parameter for more general cases.

Dividing f_0^2 by f_1^2 and rearranging leads to

$$\frac{f_0^2}{f_1^2} - 1 = \frac{I_1 + m_1 h^2}{I_0}. \tag{3.4}$$

In a similar manner, for f_0^2 and f_2^2,

$$\frac{f_0^2}{f_2^2} - 1 = \frac{I_2 + m_2 (h + L)^2}{I_0}. \tag{3.5}$$

The ratio of Eq. (3.5) to Eq. (3.4), γ, is given by

$$\gamma = \frac{f_0^2 / f_2^2 - 1}{f_0^2 / f_1^2 - 1} = \frac{I_2 + m_2 (h + L)^2}{I_1 + m_1 h^2}. \tag{3.6}$$

Eq. (3.6) can be used to find the second order equation for h, as follows:

$$(\gamma m_1 - m_2) h^2 - 2 m_2 L \cdot h + \gamma I_1 - I_2 - m_2 L^2 = 0. \tag{3.7}$$

The general solution of a second order equation expresses the distance h, as follows:

$$h = \frac{m_2 L + \sqrt{(m_2 L)^2 - (\gamma m_1 - m_2)(\gamma I_1 - I_2 - m_2 L^2)}}{\gamma m_1 - m_2}. \tag{3.8}$$

Eqs. (3.6) and (3.8) imply that distance h can be calculated by measuring the weights of trial masses, their moments of inertia, distance, and natural frequencies. Considering trial masses without volumes (that is, $I_1 = I_2 = 0$), Eq. (3.8) can be simplified as follows:

$$h = \frac{m_2 L + \sqrt{(m_2 L)^2 + \gamma m_1 m_2 L^2 - (m_2 L)^2}}{\gamma m_1 - m_2} = \frac{L}{\sqrt{\gamma\, m_1/m_2} - 1}. \tag{3.9}$$

After calculating the distance h, the moment of inertia I_0 can be obtained by substituting the value of h into Eq. (3.4):

$$I_0 = \frac{I_1 + m_1 h^2}{f_0^2/f_1^2 - 1}. \tag{3.10}$$

Considering trial masses without volumes, Eq. (3.10) can be simplified as follows:

$$I_0 = \frac{m_1 h^2}{f_0^2/f_1^2 - 1}. \tag{3.11}$$

The result of this approximation process is used to apply the virtual mass

concept in subsequent sections. Eventually, the calculation of I_0 makes it possible to estimate rotational stiffness k_θ by substituting its value into Eq. (3.1):

$$k_\theta = (2\pi f_0)^2 I_0. \tag{3.12}$$

These processes imply that the rotational stiffness can be estimated using trial masses and measuring the natural frequencies.

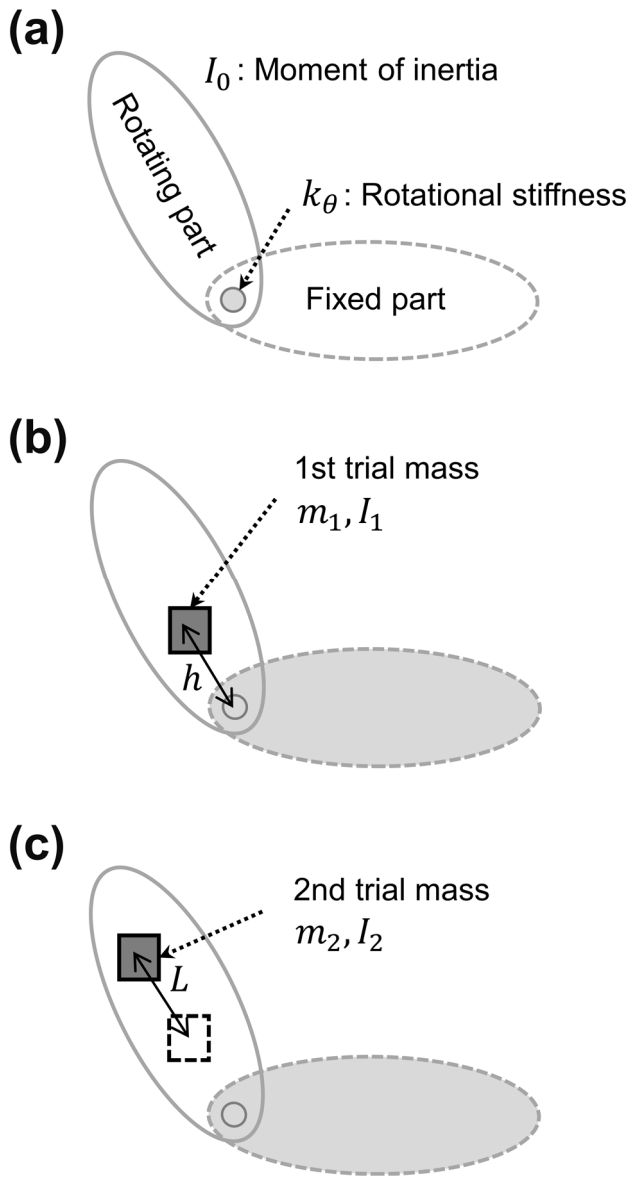

Figure 3.4 Theoretical models of proposed method for estimating rotational stiffness: (a) base system, (b) base system and first trial mass, and (c) base system and second trial mass.

3.2.2 Concept of virtual masses

The realization of trial masses may be difficult or time-consuming, especially in cases where the trial masses are heavy to ensure the sufficient FRF separation to evaluate the rotational stiffness, as mentioned in the previous section, or in cases where their attachment surfaces do not allow for the attachment of sensors or trial masses. An alternative method is the replacement of the actual trial masses with FRF information, which can be realized using FBS.

Consider a coupled system consisting of a base and an added system, combined at a joint (Fig. 3.5). The physical relation of this system can be described as follows:

$$\begin{bmatrix} \mathrm{u}_o \\ \mathrm{u}_j^{base} \\ \mathrm{u}_j^{added} \end{bmatrix} = \begin{bmatrix} \mathrm{H}_{o,i} & \mathrm{H}_{o,j} & 0 \\ \mathrm{H}_{j,i} & \mathrm{H}_{j,j}^{base} & 0 \\ 0 & 0 & \mathrm{H}_{j,j}^{added} \end{bmatrix} \begin{bmatrix} \mathrm{f}_i \\ \mathrm{f}_j^{base} \\ \mathrm{f}_j^{added} \end{bmatrix}. \tag{3.13}$$

Here, u_x and f_x are the displacement and excitation force at point x, respectively. $\mathrm{H}_{y,x}$ is the transfer function from the input force at point x to response point y (i.e., $\mathrm{H}_{o,i}$ and $\mathrm{H}_{o,j}$ are the transfer function from the input force f_i to the output response u_o, and from the force at the joint f_j to the

output response u_o in the coupled system, respectively). In addition, the superscripts "$base$" and "$added$" indicate that they were measured on the base and added sides of the coupling point, respectively.

In general, force equilibrium and compatibility are assumed at the interface, and they can be expressed as follows:

$$u_j^{base} = u_j^{added}, \tag{3.14}$$

$$f_j^{base} + f_j^{added} = 0. \tag{3.15}$$

Substituting Eq. (3.15) into (3.13), Eq. (3.13) can be rewritten as follows:

$$\begin{bmatrix} u_o \\ u_j^{base} \\ u_j^{added} \end{bmatrix} = \begin{bmatrix} H_{o,i} & H_{o,j} & 0 \\ H_{j,i} & H_{j,j}^{base} & 0 \\ 0 & 0 & H_{j,j}^{added} \end{bmatrix} \begin{bmatrix} f_i \\ f_j^{base} \\ -f_j^{base} \end{bmatrix}. \tag{3.16}$$

Then, solving for f_j^{base} using Eq. (3.14), the following is obtained:

$$f_j^{base} = -\left(H_{j,j}^{base} + H_{j,j}^{added}\right)^{-1} H_{j,i} f_i. \tag{3.17}$$

As a result, the response at the output point of the coupled system is expressed as follows:

$$u_o = \mathrm{H}_{o,i}^{coupled} \mathrm{f}_i, \tag{3.18}$$

where

$$\mathrm{H}_{o,i}^{coupled} = \mathrm{H}_{o,i} - \mathrm{H}_{o,j}\left(\mathrm{H}_{j,j}^{base} + \mathrm{H}_{j,j}^{added}\right)^{-1}\mathrm{H}_{j,i}\,. \tag{3.19}$$

Here, Eq. (3.19) is a modified form of the equation developed by Tsai and Chou [18].

Assuming that the added system is a simple mass without volume, Eq. (3.19) can be rewritten as follows:

$$\mathrm{H}_{o,i}^{coupled} = \mathrm{H}_{o,i} - \mathrm{H}_{o,j}\left(\mathrm{H}_{j,j}^{base} + 1/M\right)^{-1}\mathrm{H}_{j,i}\,, \tag{3.20}$$

where M is the weight of the added mass and $1/M$ is its transfer function or inertance. Eq. (3.20) implies that the mass effect added to the base system can be predicted without realizing it if all the related FRFs of the base system are given. This process is referred to as “adding a virtual mass” in this thesis.

Virtual trial masses can directly replace real trial masses by using accelerometers and impact hammers at the points of real trial masses. Therefore, stiffness can be estimated without realizing trial masses; thus, its experiment becomes simpler and more convenient.

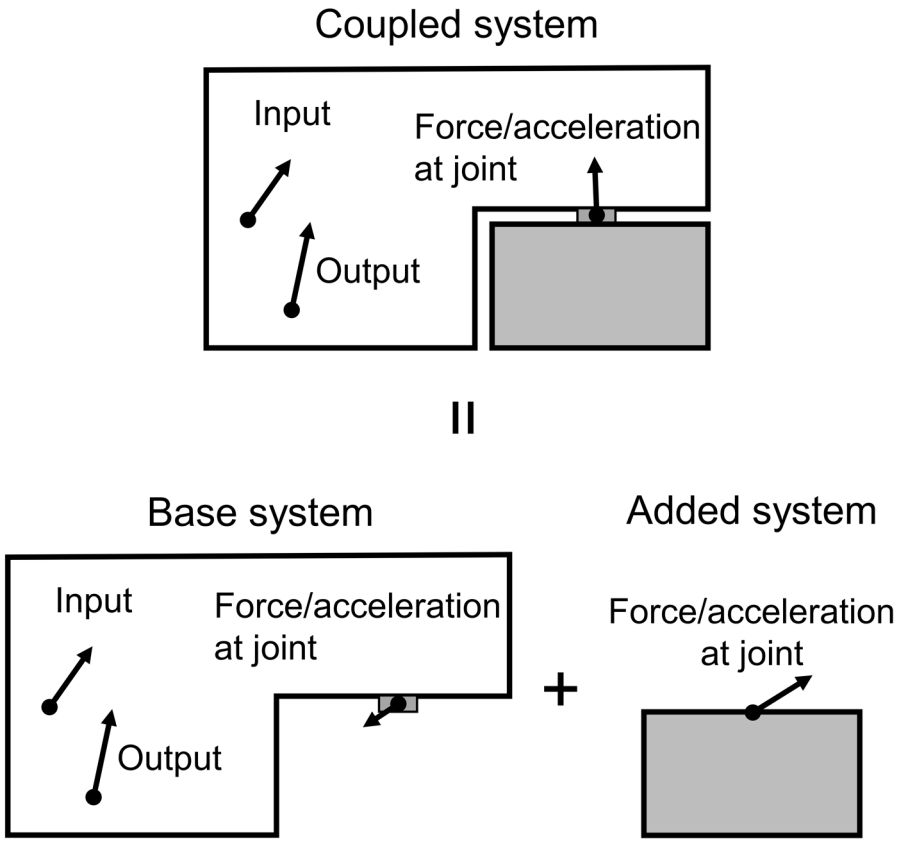

Figure 3.5 Coupled system composed of a base and an added system.

3.2.3 Concept of virtual springs

In this section, a method is proposed to estimate the rotational stiffness of a test specimen that can be considered to be connected by a hinge and rotational spring. As described in the previous sections, this method requires the fixing of one part while allowing the other part to rotate freely; that is, the test specimen should have a free-fixed boundary condition. Therefore, the existing methods require a jig that can implement a fixed boundary condition for the measurement of rotational stiffness. The proposed method is also likely to require jigs for the fixation, which often makes the experiments time-consuming and difficult to perform, as mentioned in the introduction of this chapter. This section describes a virtual spring concept that overcomes this limitation.

Similar to the derivation method of the virtual trial mass introduced in the previous section, the FBS makes the concept of a virtual spring possible. If the added system is a simple spring, as illustrated in Fig. 3.6, the transfer function $\mathrm{H}_{o,i}^{coupled}$ of the coupled system in Eq. (3.19) can be expressed as

$$\mathrm{H}_{o,i}^{coupled} = \mathrm{H}_{o,i} - \mathrm{H}_{o,j}\left(\mathrm{H}_{j,j}^{base} - \omega^2/k\right)^{-1}\mathrm{H}_{j,i}\,, \tag{3.21}$$

where k is the stiffness of the spring, ω is the angular frequency, and $-\omega^2/k$ is the transfer function or inertance of the spring. Eq. (3.21) implies that the stiffness effect of a spring added to a base system can be predicted without realizing it if all the related FRFs of the base system (i.e. $H_{o,i}$, $H_{o,j}$, $H_{j,i}$ and $H_{j,j}^{base}$) are given. In this thesis, this process is referred to as "adding a virtual spring." If there are multiple springs, one can predict their effects in multiple steps by using Eq. (3.21) or a single step by changing Eq. (3.21) to a matrix. These processes are referred to as multi-step two co-ordinate coupling (MTC) and pseudo co-ordinate coupling (PCC), respectively [21].

Virtual springs with infinite stiffness can replace the need to fix one part. Fig. 3.7 illustrates this consideration. Fixing one part is physically identical to connecting the part to the ground with no vibration by numerous springs with infinite stiffness. A few springs with infinite stiffness can approximate numerous springs if the movement of the part to be fixed is negligible. Then, a few virtual springs with infinite stiffness can replace a few real springs if accelerometers are mounted at the same points as the real springs and all the related FRFs are measured, as mentioned above. This consideration concludes that FBS can change a free-free boundary condition into a free-fixed boundary. The rotational stiffness estimation method, therefore, is expandable to a free-free boundary condition through the adoption of virtual springs.

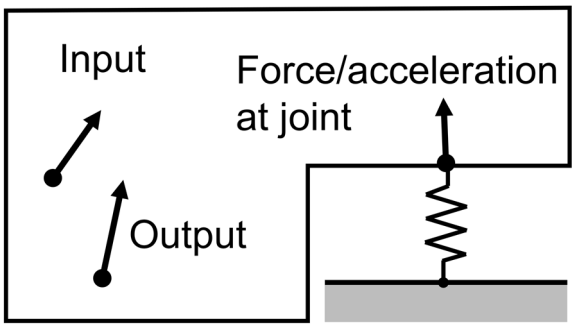

Figure 3.6 Coupled system composed of a base and a simple spring.

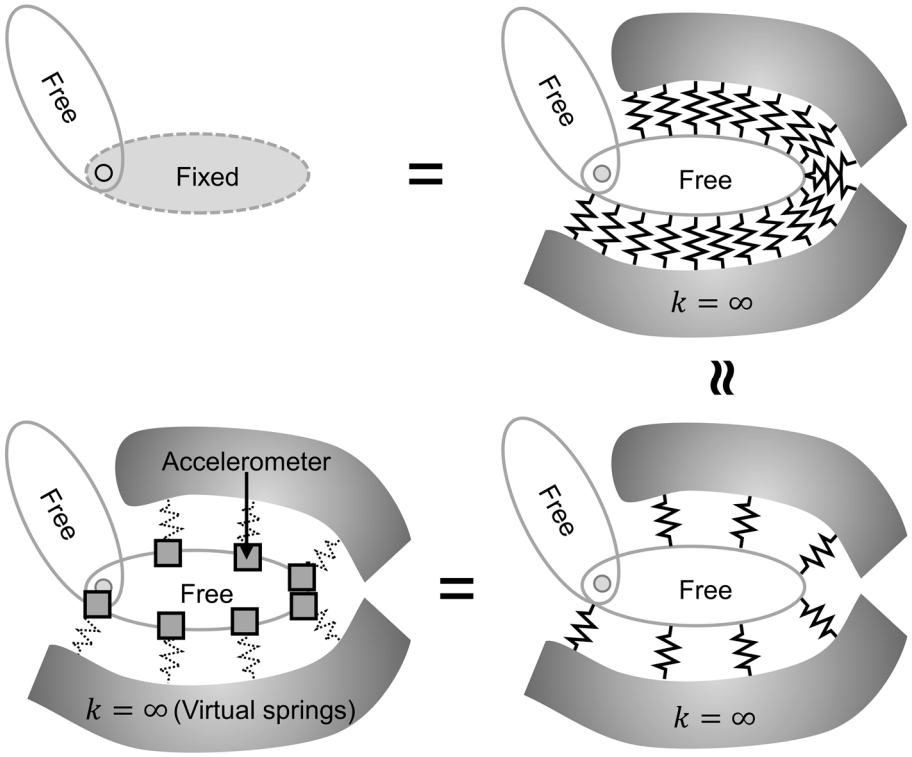

Figure 3.7 Replacement of free-fixed boundary conditions with free-free boundary conditions.

3.3 Experimental validation

3.3.1 Validation of trial masses

In this study, experiments were conducted on a vehicle shock absorber to verify the concept of a trial mass for estimating rotational stiffness. The shock absorber is externally composed of a body and rod, as shown in Fig. 3.8(a). Two jigs (e.g., brackets) fix the body to an anti-vibration plate and there is no restriction on the rod [38,39,40]. Thus, the body is the fixed part and the rod is the rotating part, as shown in Fig. 3.4(a). Fig. 3.8(b) shows the mode shape of the shock absorber at a natural frequency. The rod appears to rotate on the body, as explained in Section 3.2.1. An impact hammer and an accelerometer were used for measuring the natural frequency of the rotational mode. The impact hammer with a force transducer excited the rod end, and the accelerometer was mounted near the exciting point. The natural frequency of the rotational mode was derived by the transfer function, which was obtained from the previously mentioned setting. The impact hammer was a B&K 2806-002 model, and the accelerometers were PCB 365A15 ICP models. All the signals were measured using an LMS SCADAS mobile FFT analyzer. The frequency resolution for the analysis was 1 Hz.

The experiment used two types of trial masses: relatively heavy trial masses of approximately 1 kg and relatively light trial masses of approximately 0.3 kg. The trial masses have to conclude the same stiffness values regardless of the trial masses used because trial masses are simply estimation tools and do not change the stiffness itself. The main objective of this experiment was to check whether the two types of trial masses produce the same results.

Fig. 3.9 shows the measurement cases. The first step was to measure the natural frequency of the shock absorber itself. The second step was to measure the natural frequency when the first trial mass was added to the rod. The third step was to measure it when the second trial mass was added. Table 3.2 lists the detailed specifications and natural frequencies. The positions of the trial masses were measured at the junction of the body and rod. Fig. 3.10 shows their transfer functions.

Table 3.3 lists the experimental results. The estimated hinge position was approximately 1.4 cm away from the junction of the body and rod. This value appears to be reasonable, considering that the length of the rod is over 20 cm. The stiffness values estimated from the two types of trial mass differ by 3.3 %, although different trial masses and natural frequencies were used to calculate them. Such differences can be ignored in normal automotive NVH problems. Therefore, these experimental results show that the trial mass concept offers a

valid means of estimating the rotational stiffness.

Additional numerical studies were conducted to verify that these estimation results were reasonable. To investigate the effects of the trial mass volume on the estimation, a natural frequency prediction simulation for the system was performed according to the trial mass volume change. The results shown in Fig. 3.11 show the estimation error for the first and second natural frequencies according to the height and radius of the cylindrical trial mass. These results allow the accuracy of the proposed model to be verified because the estimation error of the natural frequency due to the volume change of the trial mass is limited to less than 3.5 %. The results also provide a criterion for neglecting the volume of the trial mass, as described in Section 3.2.1. They are also the basis for the use of the virtual mass to be applied in the following section.

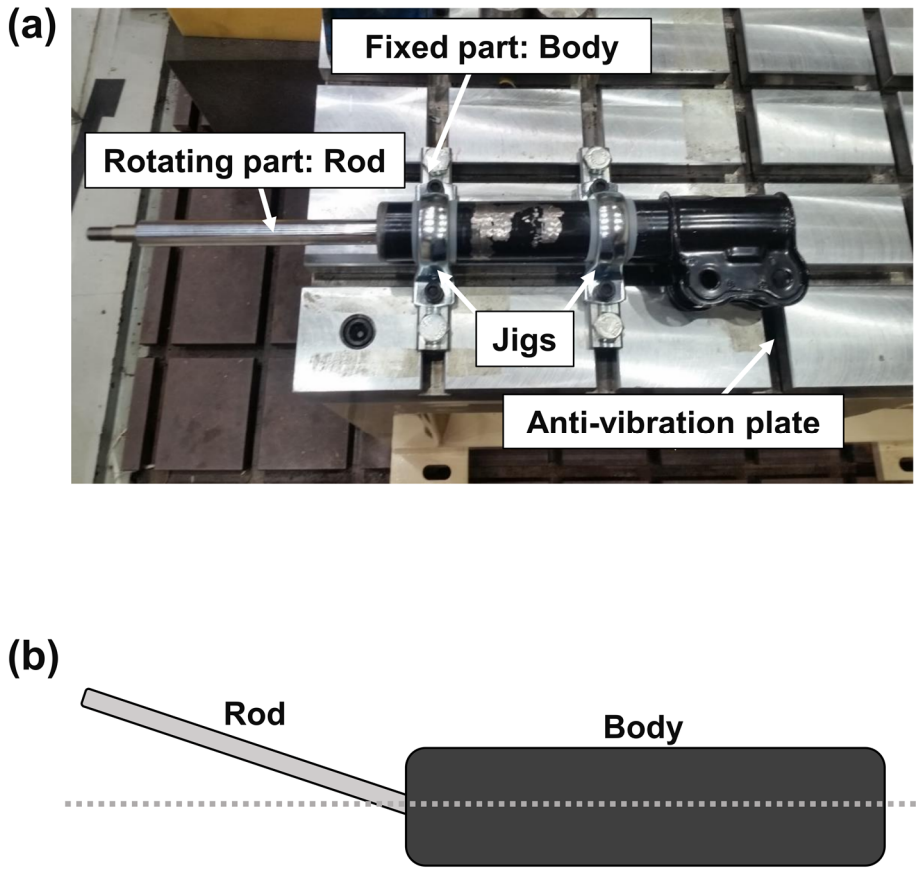

Figure 3.8 Shock absorber used as test specimen for verifying the proposed method: (a) experimental setup and (b) mode shape at a natural frequency.

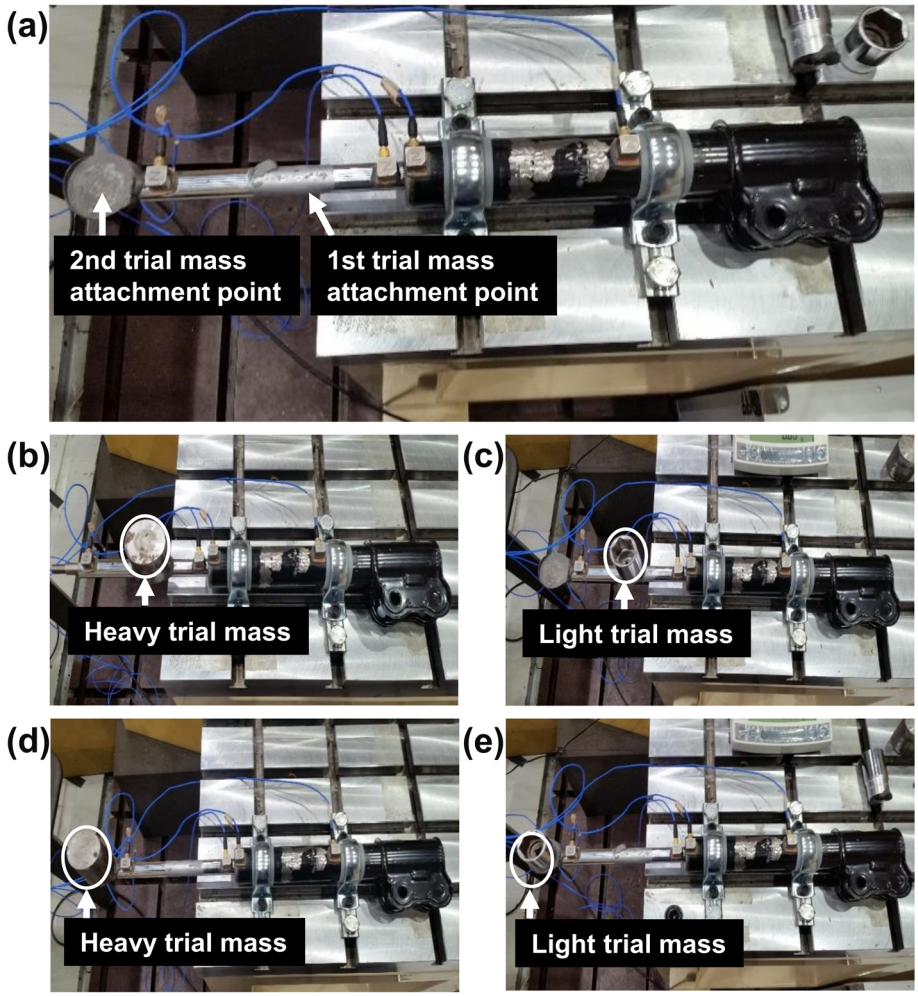

Figure 3.9 Measurement setup: (a) base system, (b) with a heavy trial mass on the first trial mass attachment point of the base system, (c) with a light trial mass on the first trial mass attachment point of the base system, (d) with a heavy trial mass on the second trial mass attachment point of the base system, and (e) with a light trial mass on the second trial mass attachment point of the base system.

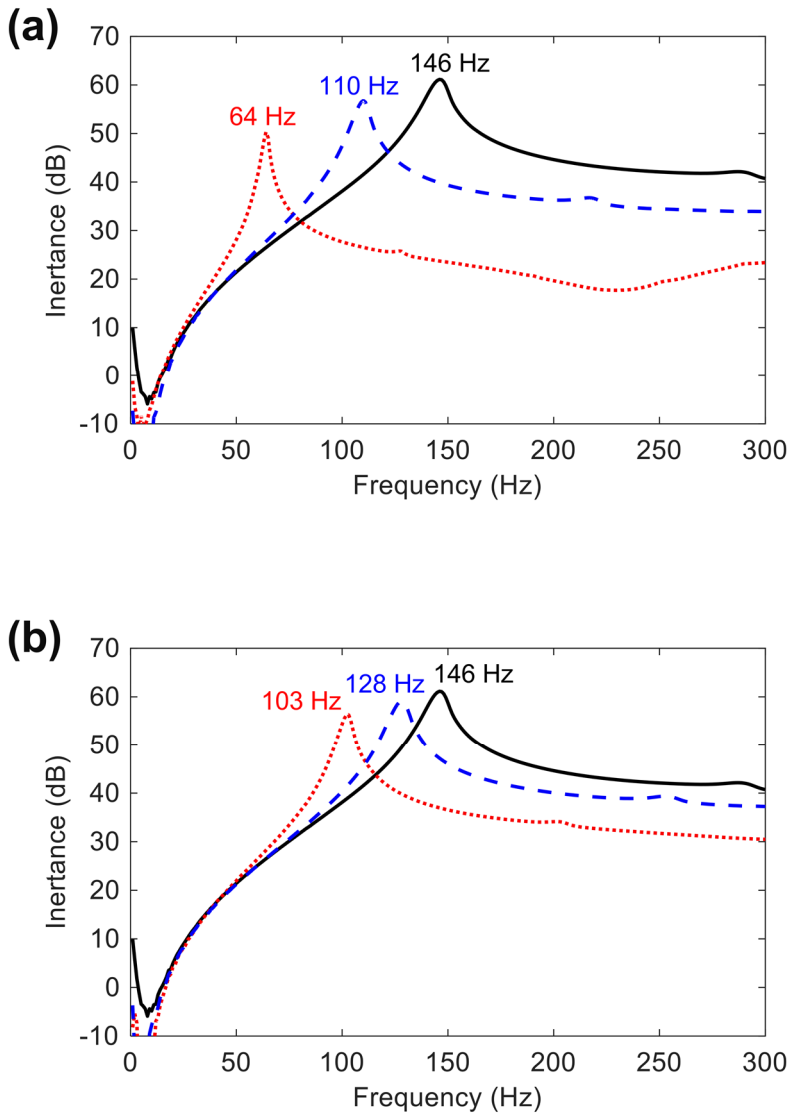

Figure 3.10 Change in transfer functions due to trial mass effect: (a) case of heavy trial mass and (b) case of light trial mass. (solid line: base system, dashed line: base system with each trial mass at the first trial mass attachment point, dotted line: base system with each trial mass at the second trial mass attachment point)

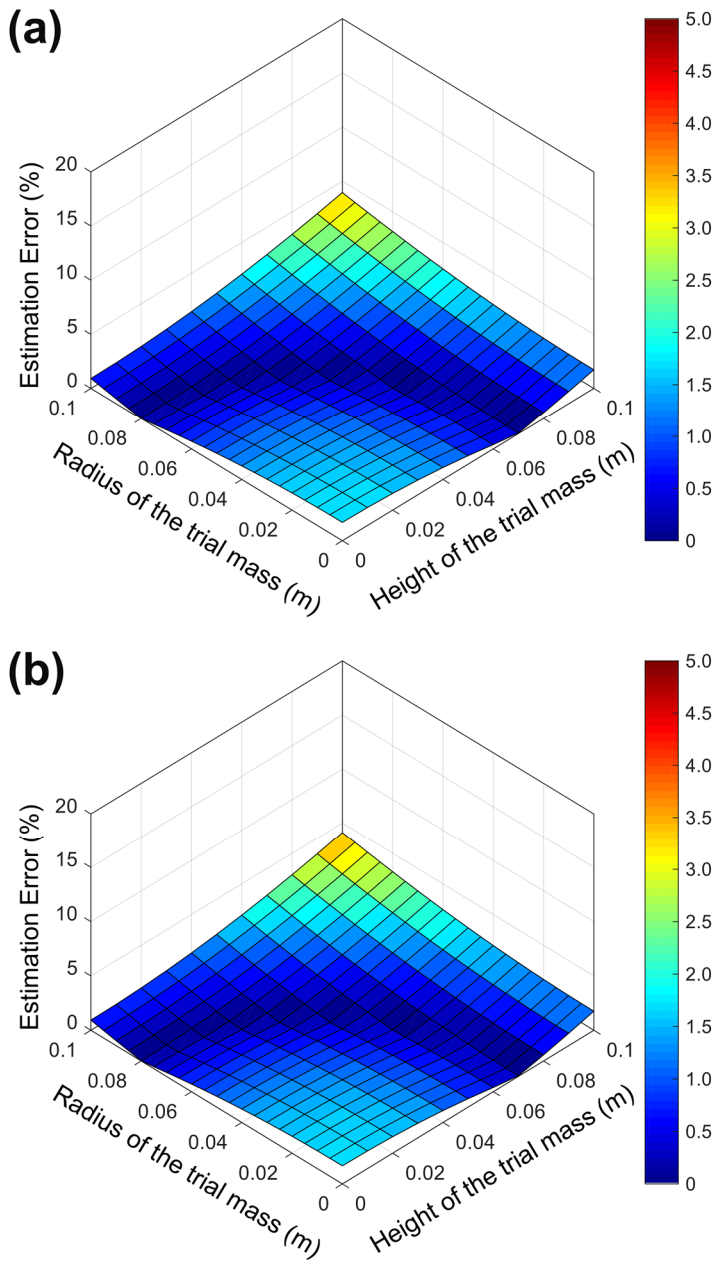

Figure 3.11 Errors between estimated and measured natural frequency when applying (a) the first trial mass and (b) the second trial mass.

Table 3.2 Experimental specifications and natural frequencies for verifying trial masses.

Specifications and natural frequencies		Heavy case	Light case
Base system	Natural frequency (Hz, f_0)	146	
Base system with first trial mass	Weight (kg, m_1)	1.03	0.369
	Moment of inertia ($\times 10^{-5}$ kg·m^2, I_1)	46.1	9.69
	Position of the trial mass (m, x_1)	-0.0840	-0.0920
	Natural frequency (Hz, f_1)	110	128
Base system with second trial mass	Weight (kg, m_2)	1.00	0.259
	Moment of inertia ($\times 10^{-5}$ kg·m^2, I_2)	31.3	7.03
	Position of the trial mass (m, x_2)	-0.225	-0.22
	Natural frequency (Hz, f_2)	64	103

※ Distance L of Eq. (3.3) from the first trial mass to the second is calculated by $x_1 - x_2$

Table 3.3 Experimental results for verifying trial masses.

Results	Heavy case	Light case
Distance from hinge to first trial mass (m, h)	0.0985	0.106
Hinge position (m, $x_1 + h$)	0.0145	0.0142
Moment of inertia of the rotating part ($\times 10^{-5}$ kg·m^2, I_0)	1,370	1,410
Rotational stiffness ($\times 10^4$ N·m/rad, k_θ)	**1.15**	**1.19**

3.3.2 Validation of virtual masses

Two more experiments were performed on another shock absorber to check if virtual masses can replace real masses. One experiment used real trial masses for estimating the stiffness of the shock absorber. Its procedure is identical to that outlined in the prior section, and Figs. 3.12(a) and (b) show the real trial masses. Virtual trial masses were applied in the other experiment. Two accelerometers were mounted at the same points as the real trial masses and an impact hammer was used to hit the accelerometers, as shown in Figs. 3.12(c) and (d). Fig. 3.13 shows the transfer functions when a virtual trial mass of 2 kg was applied.

Table 3.4 lists the specifications and results obtained in the two experiments. Virtual trial masses with various weights can be used for estimating stiffness by simply changing M in Eq. (3.14); thus, stiffnesses were calculated by varying the virtual masses from 0.5 kg to 3.0 kg in increments of 0.5 kg and averaged. The results obtained using virtual masses are very similar to those obtained using real masses, and the values differ by 1.1 %. These results demonstrate that virtual trial masses can replace real trial masses in estimating stiffness.

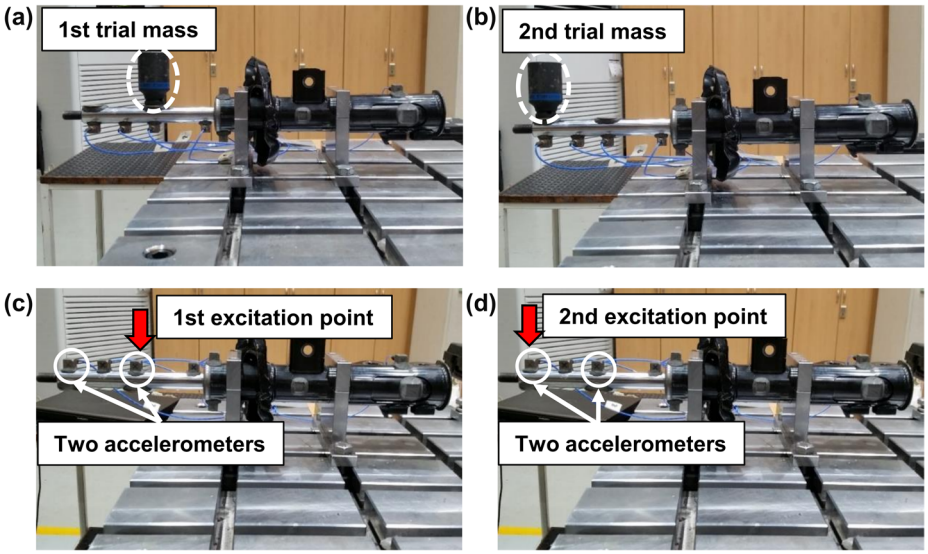

Figure 3.12 Experimental setups for verifying virtual trial masses: real trial mass (a) at first trial mass attachment point, and (b) at second trial mass attachment point. Virtual trial mass applied to (c) first attachment point and (d) second attachment point.

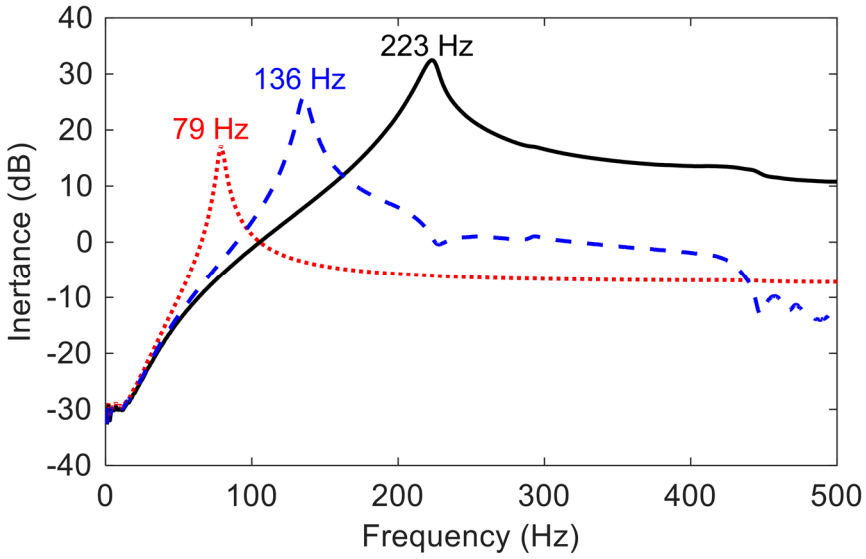

Figure 3.13 Representative transfer functions when 2 kg virtual masses are applied (solid line: base system, dashed line: base system with virtual mass at the first point, dotted line: base system with virtual mass at the second point).

Table 3.4 Experimental specifications, natural frequencies, and results for verifying virtual trial masses.

	Specification		Frequency			Results			
	$m_1 = m_2$ (kg)	$I_1 = I_2$ ($\times$ 10^{-5} kg·m^2)	f_0 (Hz)	f_1 (Hz)	f_2 (Hz)	h (m)	Hinge position, $x_1 + h$ (m)	I_0 ($\times$ 10^{-5} kg·m^2)	k_θ ($\times$ 10^4 N·m/rad)
Real	0.501	13.2	223	174	126	0.108	0.013	924	**1.81**
Virtual	0.5	0	223	186	135	0.091	-0.004	949	1.86
	1.0		223	164	106	0.089	-0.006	937	1.84
	1.5		223	148	89	0.087	-0.008	887	1.74
	2.0		223	136	79	0.087	-0.008	902	1.77
	2.5		223	126	71	0.087	-0.008	880	1.73
	3.0		223	118	66	0.089	-0.006	922	1.81
Average						**0.088**	-0.007	913	**1.79**

※ First position x_1 is -0.095 m, and second position x_2 is -0.185 m.

3.3.3 Validation of virtual springs

One additional experiment was performed on the same shock absorber described in Section 3.3.2 to verify the virtual spring concept. The shock absorber had a free-free boundary condition, as shown in Fig. 3.14; that is, the body was not fixed. This experiment used a total of four accelerometers. Two accelerometers were mounted on the body for virtual springs and were used only for restricting rigid body motion. Another two accelerometers were mounted on the rod for the virtual trial masses, similar to that described in the prior section. The measurement procedure was similar to that described in Section 3.3.2, except for additionally hitting the two accelerometers on the body to obtain FRFs related to virtual springs.

The first analysis involved application of virtual springs with infinite stiffness to change the free-free boundary condition into a free-fixed boundary condition. Fig. 3.15 shows the transfer functions from the force to the acceleration at a point on the rod. The result of applying virtual springs with infinite stiffness to the free-free boundary condition is similar to that of the free-fixed boundary condition described in the prior section. The difference between their natural frequencies is 2.2 %.

Virtual masses were added to the transfer functions derived by applying

virtual springs to the free-free boundary condition experiment for estimating the rotational stiffness. Table 3.5 summarizes the results of the experiment. The stiffness value differs by 1.7 % from that obtained using real trial masses described in Section 3.3.2. These results show that the virtual spring concept is useful for replacing a free-fixed boundary condition experiment with a free-free boundary condition.

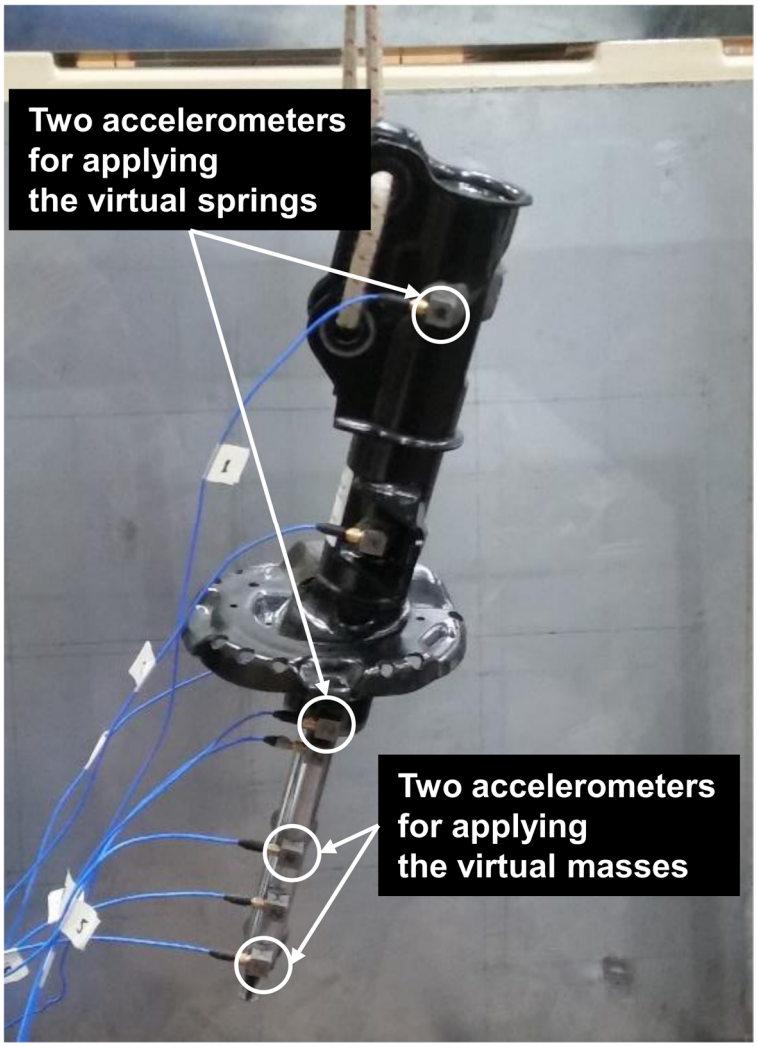

Figure 3.14 Experimental setup for verifying virtual springs.

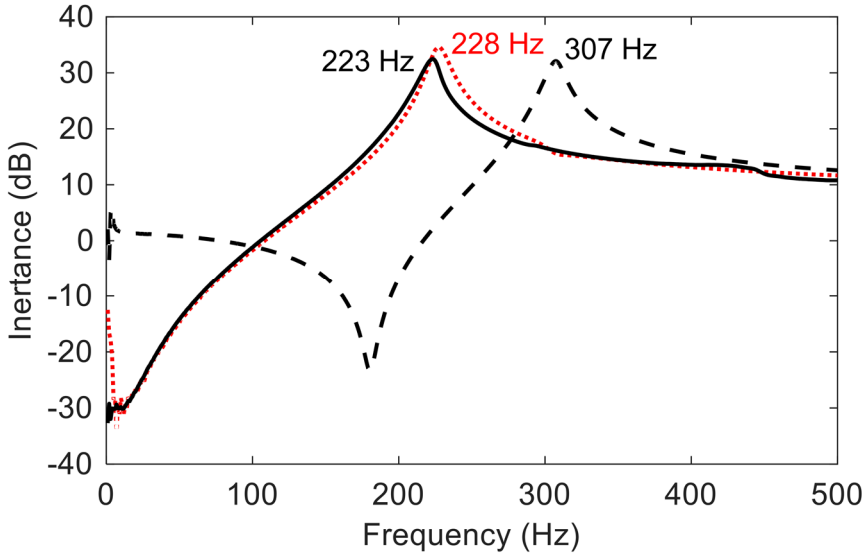

Figure 3.15 Verification results of virtual spring effect (solid line: free-fixed boundary condition, dashed line: free-free boundary condition, dotted line: free-free boundary condition with virtual springs).

Table 3.5 Experimental specifications, natural frequencies, and results for verifying virtual springs.

	Specification		Frequency			Results			
	$m_1 = m_2$ (kg)	$I_1 = I_2$ ($\times$ 10^{-5} kg·m^2)	f_0 (Hz)	f_1 (Hz)	f_2 (Hz)	h (m)	Hinge position, $x_1 + h$ (m)	I_0 ($\times$ 10^{-5} kg·m^2)	k_θ ($\times$ 10^4 N·m/rad)
Application of virtual masses after using virtual springs	0.5	0	228	192	139	0.087	-0.008	930	1.91
	1.0			170	109	0.085	-0.010	910	1.87
	1.5			153	91	0.083	-0.012	854	1.75
	2.0			138	81	0.090	-0.005	935	1.92
	2.5			130	73	0.085	-0.010	879	1.80
	3.0			122	67	0.085	-0.010	867	1.87
Average						0.086	-0.009	896	1.84

※ First position x_1 is -0.095 m, and second position x_2 is -0.185 m.

3.4 Summary

In this chapter, a novel method is proposed to estimate rotational stiffness using a natural frequency shift by adding mass to the test specimen. In this process, the concept of trial masses is introduced. The concepts of virtual trial masses and virtual springs based on the FBS method are also introduced for the convenience of testing.

To estimate the rotational stiffness, a dedicated test jig is usually needed. In such cases, the angular displacement and torque data in the rotational direction are required to evaluate the rotational stiffness, as shown in Fig. 3.2. Consequently, a special test jig for fixing parts is required. Moreover, if the experiment for estimating the stiffness of the system is made impossible by physical constraints, the FE model is used as a substitute estimation method [11]. In this case, and as previously described, the system's FE model is necessary owing to the difficulty experienced with regard to obtaining the required measurements. Furthermore, developing and validating an FE model in the development process can be a challenging task, with the analytical verification alone deserving of a separate study.

Therefore, the method proposed in this study can be used to evaluate the rotational stiffness with simple FRF measuring instruments in most practical

cases where FE models are not available, or where the manufacture of test jigs is not possible. Specifically, this proposed method can estimate the stiffness only with FRFs of a specimen measured under free-free boundary condition without a test jig for fixation. This is because virtual masses can replace real trial masses, and virtual springs with infinite stiffness can replace free boundary conditions with fixed boundary conditions. This method was validated experimentally with respect to vehicle components. Several experiments were conducted on the shock absorbers of a vehicle to confirm the applicability of these concepts for estimating rotational stiffness.

An advantage of the proposed method is that it is relatively insensitive to measurement errors and excludes the interference of other modes, as it is only based on the natural frequencies of a rotational mode, unlike classical methods. Another advantage is that the proposed method does not require jigs to fix a part, in addition to the FRFs of individual parts. Therefore, the method is more efficient and convenient than other methods.

However, there are several challenges. For example, Fig. 3.16 presents a coupled system that comprises a knuckle and a shock absorber. Due to its complex shape, the modification of the trial mass formulation for the inclusion of more geometry variables may be required. Its stronger coupling may require more virtual springs to consider the deformation and the rigid body motion of

a fixed part. Therefore, in future research, model studies for extended application to systems with complex shapes or coupling conditions and experiments for verification should be conducted. The results reported in this chapter are reliable and can serve as a basis for the solution of more difficult problems.

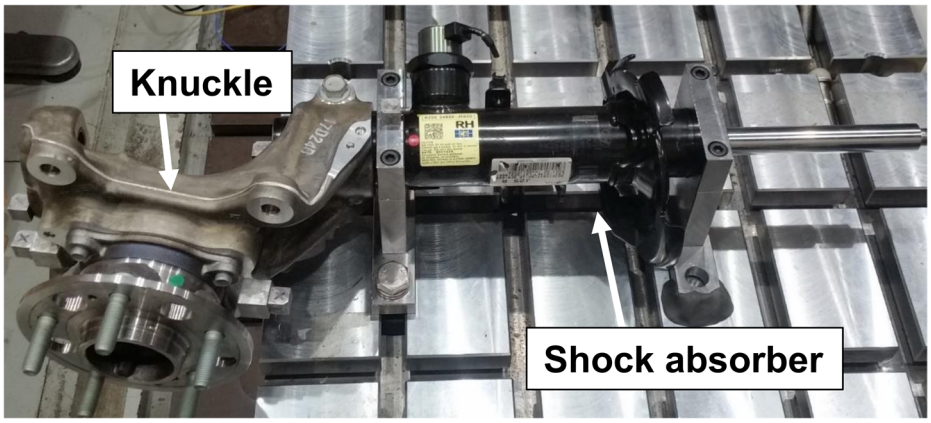

Figure 3.16 Coupled knuckle/shock absorber system.

CHAPTER 4

TRANSFER PATH ANALYSIS USING A VIRTUAL SPRING

4.1 Introduction

Transfer path analysis is a process of determining the priorities of various possible paths from a noise and vibration source to an output response. To reduce responses such as noise, it is necessary to determine efficient transfer paths with respect to noise transmission and isolation. This analysis mainly considers the NVH field of vehicular design. In particular, the structure-borne road noise of a vehicle can be attributed to road–tire interactions, which excite the suspension linkages and numerous other vehicle parts. Consequently, these parts generate interior noise. Figure 4.1 presents the transmission process of road noise and its transfer function with respect to the interior noise. Considering the development cycle of a vehicle with numerous parts, it is necessary to conduct TPA at an early stage, especially for the improvement of the vibro-acoustic performance. Moreover, by the selection of a critical path for

each individual frequency band, the time and energy required for NVH performance improvements can be significantly reduced.

The TPA has been widely used in various fields [17,27]. Based on the similarity between methods, the TPA can be classified into two types: conventional TPA and operational TPA (OTPA), which is detailed in this section. The two methods have been modified for various systems since the introduction of the TPA. In particular, they have been used as representative methods for evaluating the NVH performance of vehicles [41].

The conventional TPA is one of the most classical TPA methods. To use this method, all the force and transfer functions related to the NVH phenomenon should be measured to evaluate the transfer paths. For the structure-borne road noise of a vehicle, the conventional TPA facilitates the measurement of all the operational forces and transfer functions with respect to individual links, calculates their contributions to the interior noise, and determines their priorities. This method is theoretically complete, as it based on all the information related to the transfer paths. However, it requires the removal and reattachment of parts to accurately determine the transfer functions. Therefore, this method is time-consuming, can only be applied to removable parts, and should be carefully conducted for repeatability. An additional drawback is that it requires the matrix inversion process to obtain the operating

force [42,43,44,45], which can lead to computational errors. (Table 4.1)

The OTPA uses correlations between inputs (e.g., external forces) and outputs [46,47], thereby reducing the experimental complexity observed in the conventional TPA [48,49]. The method is practically simpler to implement than the conventional TPA, as it does not require the removal of parts. However, the OTPA is not useful for systems with correlated inputs. In particular, for a structure-borne road noise, this method is only suitable for the contribution analysis of the front and rear tires, and not that of the suspension links, given that they are excited and linked by the same tires. Hence, the OTPA is more limited than the conventional TPA.

Due to the disadvantages of the above two methods, a simpler and more applicable method is required. This section proposes a method based on an FBS model, for the evaluation of the contribution of noise transfer paths (i.e., FBS-based TPA). In this study, a virtual spring was applied to a target system using the FBS-based model; thus, the variation trend of the system characteristics with respect to the variations in the stiffness were predicted. The improvement priority of the transfer paths can be selected by the analysis of this trend. The proposed method requires the FRFs or transfer functions of the target system. Therefore, it eliminates the need to remove or re-assemble individual parts and the need of signal correlation information as illustrated in Fig. 4.2. These

characteristics increase the simplicity and applicability of the proposed method, when compared with the conventional and operational TPA methods.

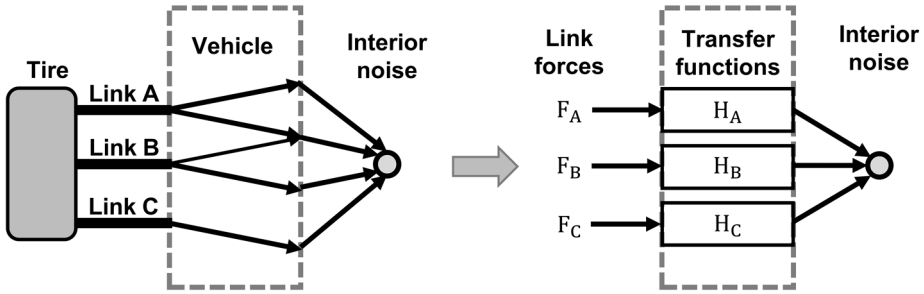

Figure 4.1 Schematic of a structure-borne road noise.

Table 4.1 Study contributions for performing TPA in comparison with previous works.

	Conventional TPA	**FBS-based TPA**
Advantages	• Estimates the interior SPL in operational condition of vehicles	• No removal process required • No need for matrix inversion process to estimate operational force • Can quickly evaluate the transfer path contribution in general cases (not in a specific operational condition) • Useful in a multi-path TPA
Disadvantages	• Removal work required • Cause the operational force estimation error by the matrix inversion calculation • Contribution analysis of transfer path can be evaluated only for a specific operational condition • Computational load in large systems with multiple transfer paths	• Cannot estimate the interior SPL (an operational data measurement step is required)

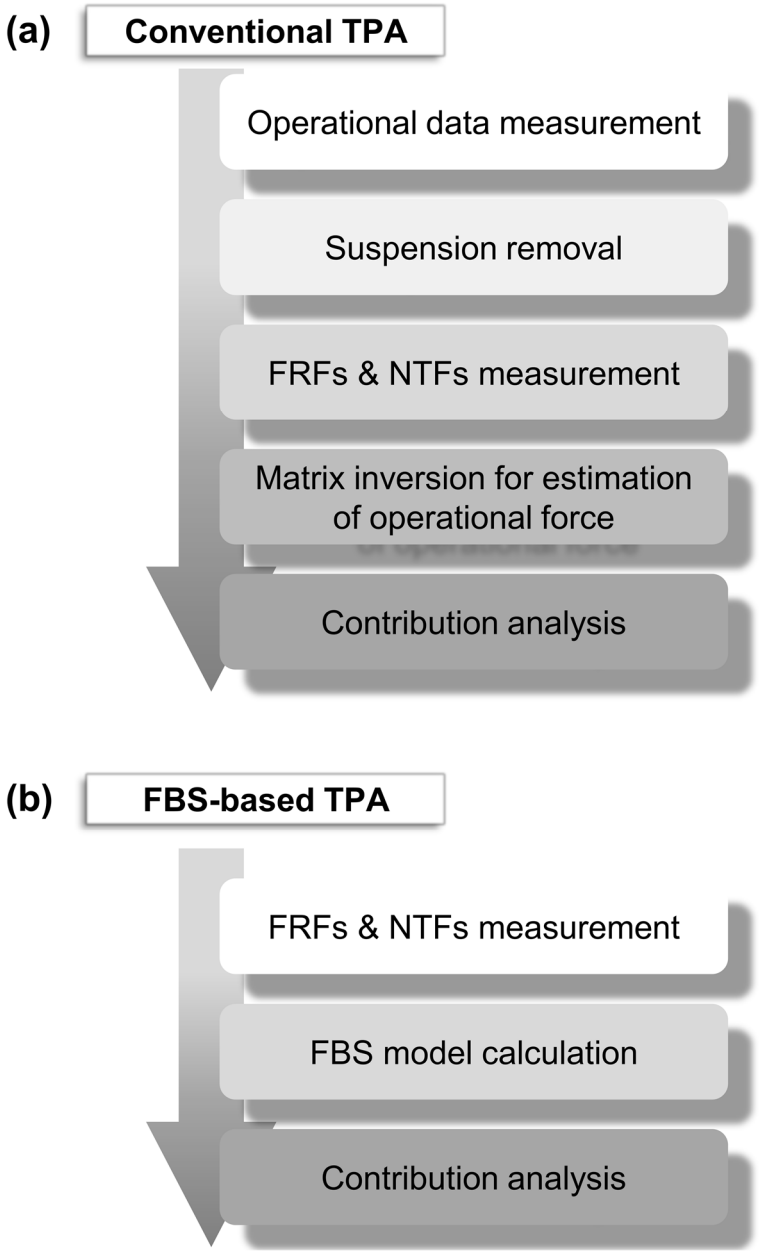

Figure 4.2 Experimental and analytical TPA process: (a) conventional TPA, and (b) FBS-based TPA.

4.2 Conventional TPA

Conventional TPA is a classical method that enables the tracing of vibro-acoustic energy transmission from the noise source to the target position throughout the transfer pathways. Therefore, this method enables the identification of the critical path for vibro-acoustical transmission. Noise response at a target position can be represented as follows:

$$\mathrm{P}_{\mathrm{target}} = \sum_{i=1}^{n} \mathrm{P}_i^{\mathrm{op}}, \tag{4.1}$$

where $\mathrm{P}_{\mathrm{target}}$ is the noise response at the target position caused by the specific noise source in an operational condition, and it is estimated by the product of the noise transfer (NTF) function summation from the i-th to n-th paths with the exerted operating forces $\mathrm{F}_i^{\mathrm{op}}$ at those paths as follows:

$$\mathrm{P}_i^{\mathrm{op}} = \mathrm{F}_i^{\mathrm{op}} \times \mathrm{NTF}_i. \tag{4.2}$$

Here, NTF_i is the noise transfer function in the i-th path, expressed as the ratio of the response P_i at the target point when a specific force F_i is applied

to the path. (i.e., $\mathrm{NTF}_i = \mathrm{P}_i/\mathrm{F}_i$.)

Meanwhile, since the operational force cannot be directly measured, the estimated value of the force is generally used using the matrix inversion method. In this method, the operational force can be estimated as follows:

$$\mathrm{F}^{\mathrm{op}} = \mathrm{H}^{-1} \times \mathrm{a}^{\mathrm{op}}. \tag{4.3}$$

Herein, F^{op} is an $n \times 1$ operational force spectrum vector and a^{op} is an $m \times 1$ operational acceleration spectrum vector. In addition, H represents an $m \times n$ unitary matrix comprising FRFs between the force applied at each transfer path and the response accelerations. Meanwhile, these FRFs are obtained by using an impact hammer test with accelerometers located in the periphery of the transfer path when the noise source is physically removed. This is called the 'matrix inversion method' and Eq. (4.3) is required for the computation.

Meanwhile, the singular value decomposition (SVD) technique is required to perform this matrix inversion computation in Eq. (4.3). The FRFs matrix H is decomposed into unitary matrices $[\mathrm{U}]_{m\times m}$, $[\mathrm{V}]^{\mathrm{T}}_{n\times n}$, and a non-negative real diagonal matrix $[\Sigma]_{m\times n}$ as follows:

$$\mathrm{H} = [\mathrm{U}][\Sigma][\mathrm{V}]^{\mathrm{T}}, \tag{4.4}$$

where

$$[\Sigma] = \begin{bmatrix} \sigma_1 & & & \\ & \sigma_2 & & \\ & & \ddots & \\ & & & \sigma_n \end{bmatrix}. \tag{4.5}$$

Herein, σ represents the singular value that can provide the information of orthogonality for estimating the solution set. Therefore, m should be equal or larger than n to estimate the operational force accurately (recall n is the number of the transfer paths).

However, this conventional TPA method using the matrix inversion method with SVD techniques tends to be vulnerable to errors due to the computational processes mentioned above. Therefore, careful consideration is required for precise experimentation and post-processing.

4.3 FBS-based TPA

The FBS theory allows for the estimation of the FRFs of a coupled system based on the FRFs of individual systems. Considering a coupled system that comprises a base and an added system (recall Fig. 3.5). The coupled system can be assembled by the combination of two sub-systems at a joint point. Force equilibrium and compatibility conditions can be applied at the point connecting the two sub-systems. As described in the previous section, the following is obtained based on transfer function of a coupled system, as expressed by Eq. (3.19):

$$\mathrm{H}_{o,i}^{coupled} = \mathrm{H}_{o,i}^{base} - \mathrm{H}_{o,j}^{base}\left(\mathrm{H}_{j,j}^{base} + \mathrm{H}_{j,j}^{added}\right)^{-1}\mathrm{H}_{j,i}^{base}. \qquad (4.6)$$

In Eq. (4.6), $\mathrm{H}_{o,i}^{coupled}$ is the transfer function due to the input force at the point *i* to the output acceleration at the point *o* in the coupled system. Similarly, $\mathrm{H}_{o,i}^{base}$, $\mathrm{H}_{o,j}^{base}$, and $\mathrm{H}_{j,i}^{base}$ are the transfer functions measured between the input and output, joint and output, and input and joint of the base system, respectively. Moreover, $\mathrm{H}_{j,j}^{base}$ and $\mathrm{H}_{j,j}^{added}$ are the driving point inertances measured at the joint points of the base and added systems, respectively.

In general, when a system (or a part) is added to a vehicle, the FRFs of Eq. (4.6), with the exception $\mathrm{H}_{j,j}^{added}$, can be measured; thus, the terms are known. Assuming that the added system is a simple spring with one connected to a rigid wall and the other to a base system (recall Fig. 3.6), Eq. (4.6) can be rewritten similar to Eq. (3.21), as follows:

$$\mathrm{H}_{o,i}^{coupled} = \mathrm{H}_{o,i}^{base} - \mathrm{H}_{o,j}^{base}\left(\mathrm{H}_{j,j}^{base} - \omega^2/k\right)^{-1}\mathrm{H}_{j,i}^{base}. \qquad (4.7)$$

In Eq. (4.7), k is the stiffness of the spring, ω is the angular frequency, and $-\omega^2/k$ is the transfer function of the spring. The FRF information of the base system can be easily obtained in an actual experimental, as mentioned above. Equation (4.7) indicates that the stiffness effect of a spring added to the base system can be predicted if only the FRFs of the related base system are known. As introduced in Section 3.2.3, this process is referred to as "the addition of a virtual spring." It may be preferable to use a virtual spring, as it is difficult to add a real spring. In addition, an actual spring can generate additional effects (such as the mass effect) and cannot assume arbitrary stiffness values such as infinity.

The virtual spring can be applied to the TPA of vehicle suspension. For example, a case wherein a spring is incorporated in the transfer path of a

structure-borne road noise can be considered as follows. If the virtual spring is added at the attachment point of a specific suspension link, as shown in Fig. 4.3, and its stiffness tends to infinity, the attachment stiffness of the specific link also tends to infinity. Thus, the displacement (or acceleration) of the attachment point is zero, and the specific link does not result in the vibration of any vehicle parts. In particular, the virtual spring with an infinite stiffness produces the effect of eliminating a specific path. Therefore, if the link is the main transfer path of the structure-borne noise, which affects the sound pressure level (SPL) of the vehicle interior, the SPL can be significantly reduced by application of virtual spring with an infinite stiffness and the removal of the transfer path. Thus, the virtual spring can be used for evaluating the transfer path. In practice, a spring with infinite stiffness cannot be realized. Moreover, applying the virtual spring concept can allow for the realization of a spring with infinite stiffness. The virtual spring plays the same role as that of an actual spring, and only requires the FRF information, instead of the mounting of an actual spring. In addition, the virtual spring can assume any arbitrary stiffness value, including infinity, thus allowing for the prediction of the trend of the dynamic behavior of a system with respect to variation in the stiffness without the modification of the actual stiffness. The virtual spring can provide path directions that should be prioritized to reduce the structure-borne noise.

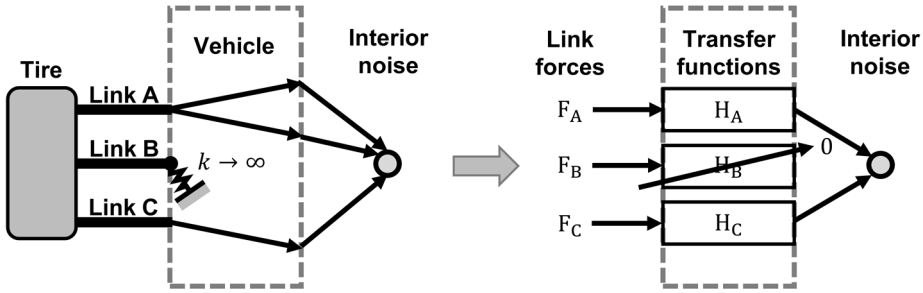

Figure 4.3 Schematic diagrams showing the application of the virtual spring at the attachment point of a suspension link.

4.4 Experimental validation

4.4.1 Specific road noise phenomenon

In this study, the significant road noise phenomenon of a vehicle was employed to test the effectiveness of the proposed FBS-based TPA method. The vehicle, which has a MacPherson strut-type front suspension, was manufactured by the Hyundai Motor Company. The suspension is excited from the knuckle under operating conditions, as shown in Fig. 4.4. The major links include a front lower arm, a rear lower arm, and a damper-strut. Moreover, it comprises minor linkages such as a stabilizer bar and a tie rod.

The vehicle exhibits a unique road noise phenomenon, which can be confirmed by measuring the interior SPL of the vehicle under operating conditions of 60 km/h on a proving ground. Figure 4.5(a) reveals that the road noise significantly reduces at approximately 160 Hz, when the strut bar that connects the strut housing to the dash panel (as shown in Fig. 4.5(b)) is eliminated. This phenomenon reveals that the damper-strut is a major transfer path. Many studies have been conducted on damper-strut exciting noise [40,50,51]. In operation, the excitations due to road–tire interactions are transmitted to the interior of the vehicle through the damper-strut (and its

housing motion in the y-direction), strut bar, and dash panel (vibration in the x-direction), as shown in Fig. 4.6.

As shown in Fig. 4.7, the transfer functions from the force acting on a wheel in the y-direction to the interior noise were compared before and after the removal of the strut bar. Moreover, the excitation point of the target vehicle is indicated. The results reveal that the elimination of the strut bar facilitates the reduction in the interior noise due to the excitation of the wheel. The changes in the SPL contribution at other frequency bands due to the removal of the strut bar were negligible. The results indicate that the strut bar contributes to the interior SPL at approximately 160 Hz. In this study, the transfer function from the input (i.e., the force acting on a wheel in the y-direction) to the output (i.e., interior SPL) was used to verify the effectiveness of the FBS-based TPA.

To obtain the FRF information of all the paths, accelerometers were attached along each path. The FRFs were measured using a B&K 2806-002 impact hammer and PCB 365A15 ICP type tri-axial accelerometers. A Brüel & Kjær diffuse field 4942-A-21 microphone was also used to obtain the interior SPL of the vehicle under operational conditions and the noise transfer function (NTF) from the impact hammer excitation to the interior SPL. All the signals were measured using an LMS SCADAS mobile FFT analyzer.

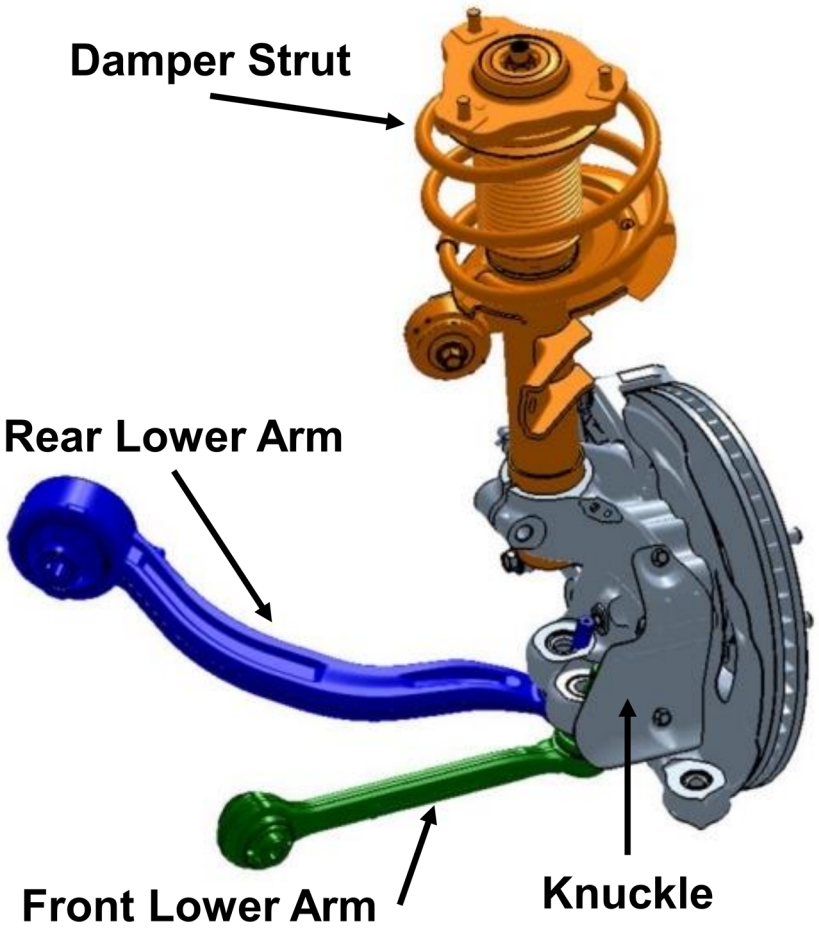

Figure 4.4 Definition of the transfer paths: knuckle, front lower arm, rear lower arm, and damper strut.

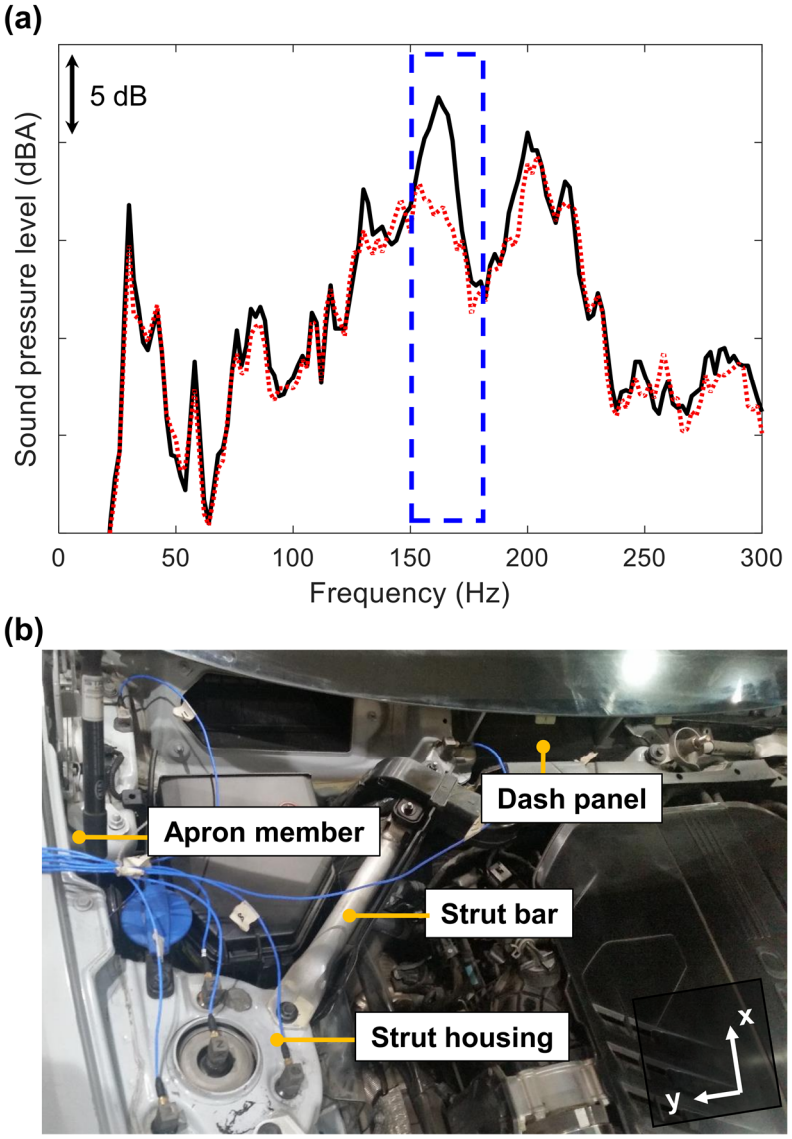

Figure 4.5 Specific road noise phenomena and the target system in which road noise occurs: (a) interior sound pressure level of target vehicle under operational conditions of 60 km/h (i.e., road noise) (solid line: base system, dotted line: system without a strut bar), and (b) a strut bar and several engine room components.

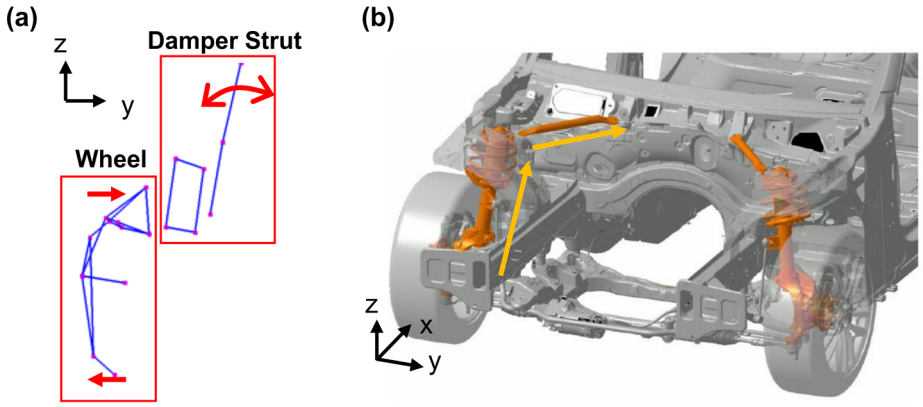

Figure 4.6 Transfer path of the road noise in the target system: (a) motion of wheels and damper struts of the target vehicle, and (b) significant transfer path at approximately 160 Hz in the target vehicle.

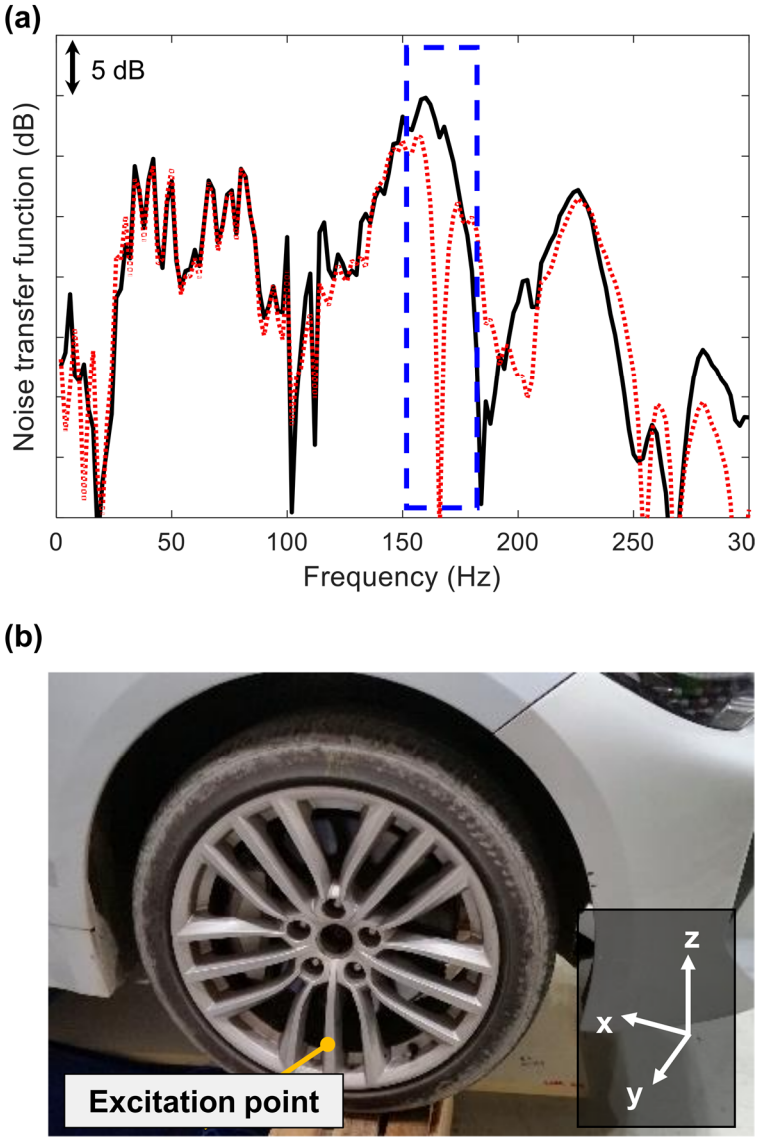

Figure 4.7 Changes in the system characteristic before and after the removal of the strut bar: (a) transfer function from the force acting on a wheel in the y-direction to the interior noise of the target vehicle (solid line: base system, dotted line: system without a strut bar), and (b) excitation point of the vehicle.

4.4.2 Suspension link TPA

To conduct the suspension link TPA of the target vehicle using a virtual spring, the accelerometers were mounted at the connecting points between the four linkages (i.e., the tie rod, the front lower arm, the rear lower arm, and the damper-strut) and the vehicle body, as shown in Fig. 4.8. The linkages serve as paths that connect the knuckle at the front-tire side to the vehicle body or sub-frame. In the feasibility test, the vehicle chassis in the original state, i.e., without any additional stiffness, corresponded to the base system in Eq. (4.7), and the arbitrarily added virtual spring was considered as the added system.

The first step in the suspension link TPA involves measuring the transfer functions due to the wheel excitation. In this step, $H_{o,i}^{base}$ and $H_{j,i}^{base}$, as expressed by Eq. (4.7), can be obtained by applying the impact hammer excitation method in the y-direction of the wheel. Similarly, the remaining dynamic properties (e.g., $H_{o,j}^{base}$, and $H_{j,j}^{base}$) at the connecting points of the base system can be obtained. In this case, the impact hammer excitation method is used to measure the inertance by exciting the accelerometer itself, which is attached to the connecting point between the tie rod and the sub-frame. This second procedure allows for the virtual spring to be added at the connecting point between the tie rod and the sub-frame (i.e., at the accelerometer

attachment point, as shown in Fig. 4.8(b)). The remaining procedures involve measuring the transfer functions related to the other linkages, which serve as noise transmitting paths (i.e., the front lower arm, rear lower arm, and damper-strut). The procedures are similar to those applied to the tie rod.

Figure 4.9 presents the transfer functions from the input force acting on the wheel in the y-direction to the interior SPL as an output when a virtual spring with infinite stiffness was applied to the connection point between the damper-strut and the vehicle body. The virtual spring applied along the y-direction resulted in a significant reduction in the interior noise at approximately 160 Hz. The findings are similar to those observed when the strut bar is eliminated. Moreover, the virtual springs in the other directions did not significantly influence the interior noise. Figure 4.10 indicates that the virtual springs applied to the other linkages did not influence the interior SPL at approximately 160 Hz. These results are similar to those predicted in Section 4.4.1, in that the damper-strut is the most significant transfer path of the road noise. Hence, it can be concluded that the FBS-based TPA is experimentally feasible and applicable to the structure-borne road noise of vehicles.

An additional test was conducted to obtain the same results. This test involved the direct addition of the virtual springs to the linkages, and not at their connecting points on the vehicle body. To add the virtual springs, the

accelerometers were mounted on the front lower arm and the damper-strut, as shown in Fig. 4.11. Figure 4.12 reveals that the virtual spring on the front lower arm and the damper-strut help significantly reduced the transfer function. The findings are different from those obtained when applying the virtual spring to the connecting point of the transfer path. The previous results indicate that only the damper-strut path facilitates the reduction in the transfer function when a virtual spring with infinite stiffness is applied to all the paths. This is because the fixation of the front lower arm via the virtual spring has an influence on the vibration of the knuckle. Consequently, the path of the damper-strut is impacted, which reduces the transfer function. Figure 4.13 reveals that the fixation of the front lower arm via the virtual spring has an influence on the damper-strut as the transfer path.

In conclusion, a virtual spring applied to a specific link itself can influence the specific path of the link and the paths of other links, as shown in Fig. 4.14. This indicates that the suspension linkages should not be restricted when conducting the TPA, depending on their original design objectives. Moreover, the addition of virtual springs at the connecting points of the linkages is more suitable than that at the linkages, with respect to the TPA of suspension links.

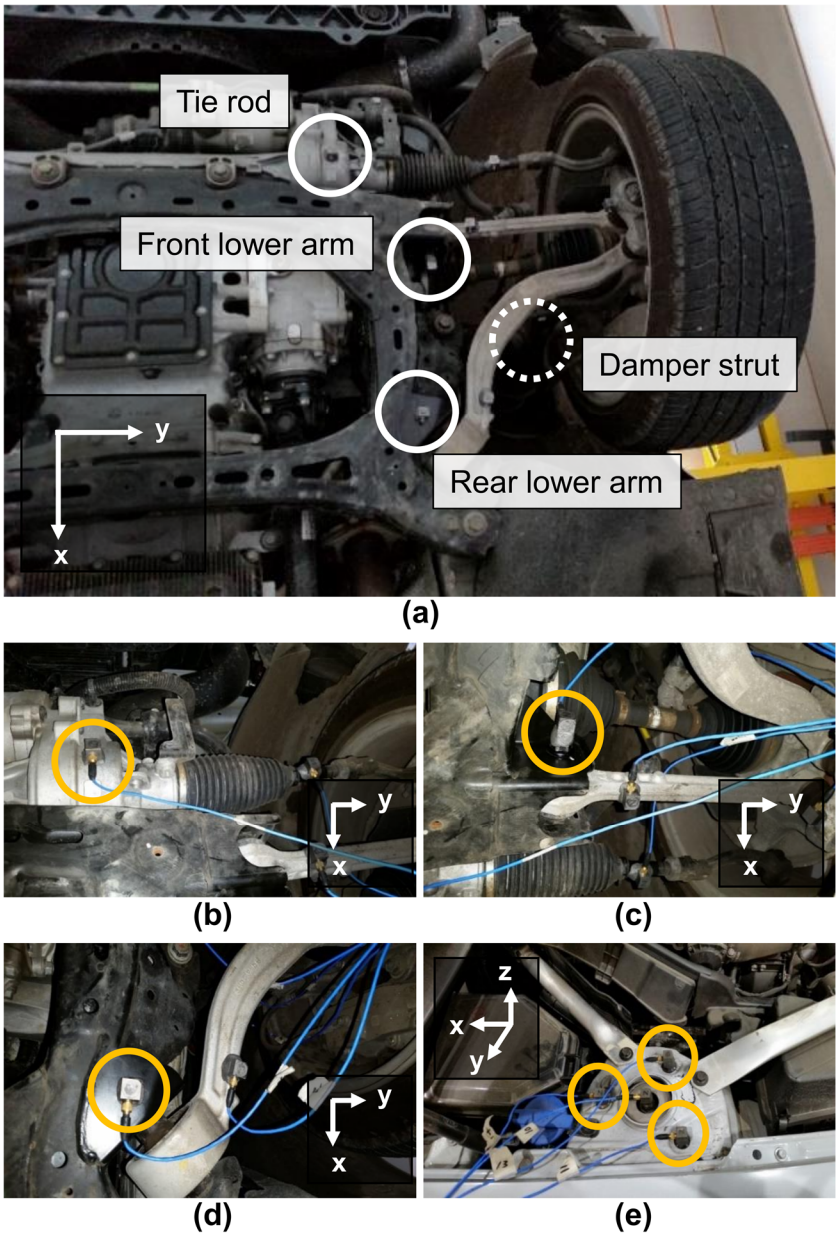

Figure 4.8 Mounting points of accelerometers on the vehicle suspension for the virtual spring application: (a) overall view of the underbody, and the measurement point (b) at the tie rod, (c) at the front lower arm, (d) at the rear lower arm, and (e) at the damper strut.

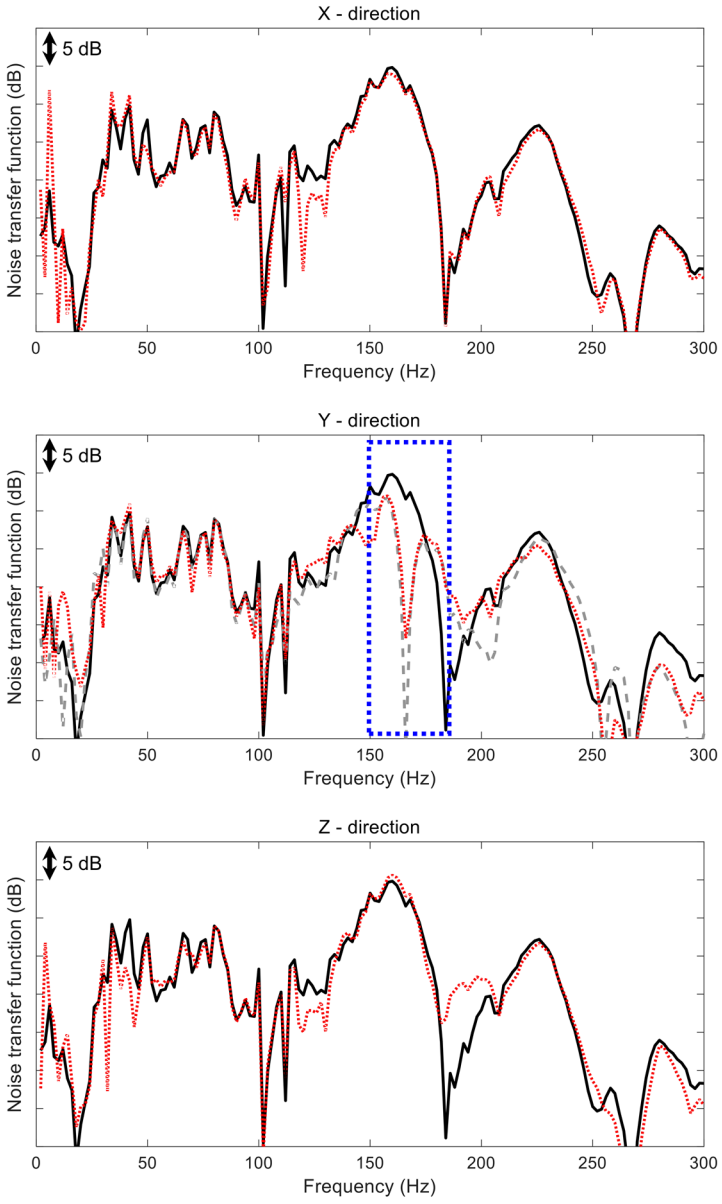

Figure 4.9 Comparison of transfer functions from the input force acting on a wheel in the y-direction to the output interior SPL before and after applying infinite virtual stiffness at the measurement point of the damper strut (solid line: original system, dotted line: system with a virtual spring at the damper strut point, dashed line: system without a strut bar).

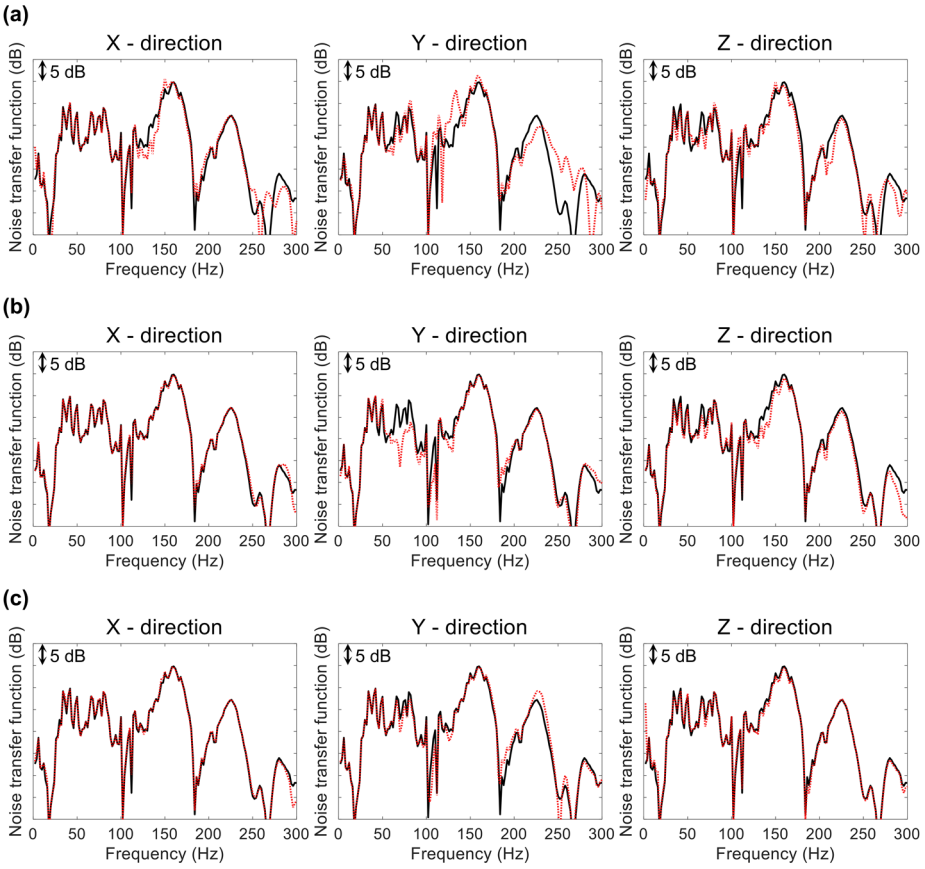

Figure 4.10 Comparison of transfer functions from the input force acting on a wheel in the y-direction to the output interior SPL before and after applying the virtual spring at each point: (a) tie rod, (b) front lower arm, and (c) rear lower arm (solid line: base system, dotted line: system with a virtual spring at each point).

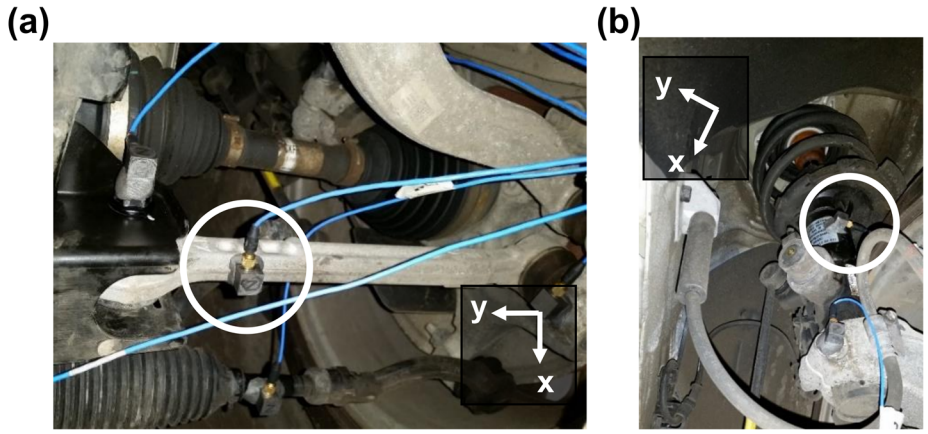

Figure 4.11 Additional accelerometer positions to conduct the suspension link TPA with virtual spring: (a) at the front lower arm, and (b) at the damper strut.

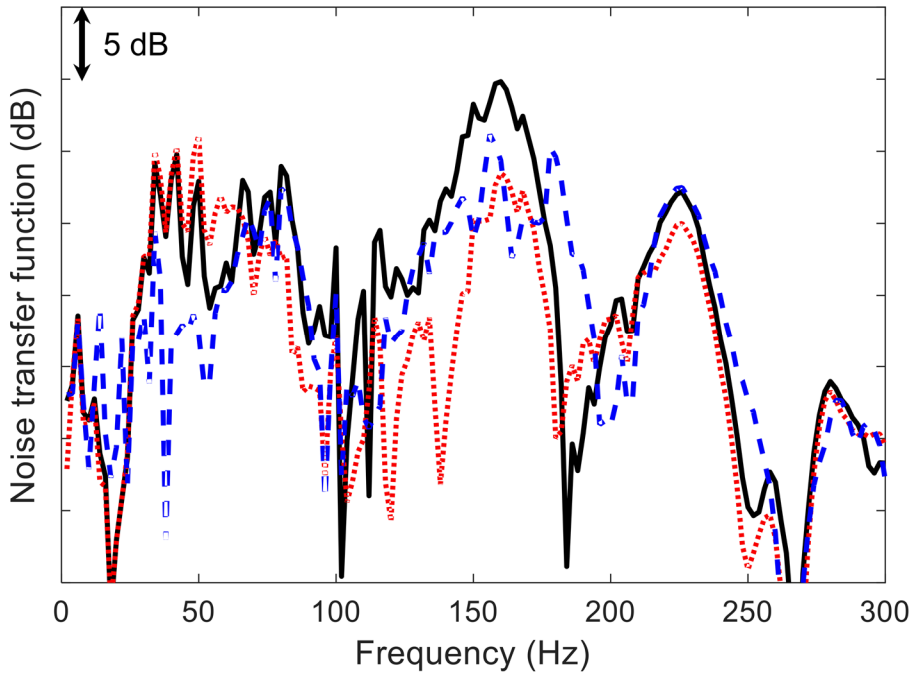

Figure 4.12 Transfer functions from the input force acting on a wheel in the y-direction to the output interior SPL before and after applying the virtual spring at each point (solid line: base system, dotted line: system with a virtual spring at the front lower arm, dashed line: system with a virtual spring at the damper strut).

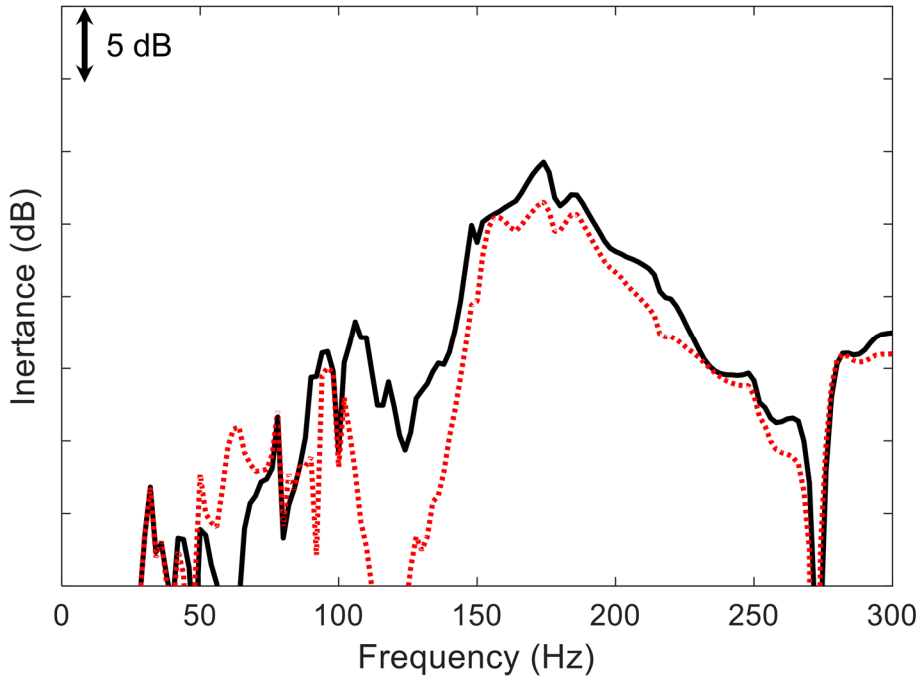

Figure 4.13 Transfer functions from the input force acting on the wheel in the y-direction to the damper strut acceleration in the y-direction when a virtual spring with infinite stiffness is applied to the front lower arm (solid line: base system, dotted line: system with a virtual spring at the front lower arm).

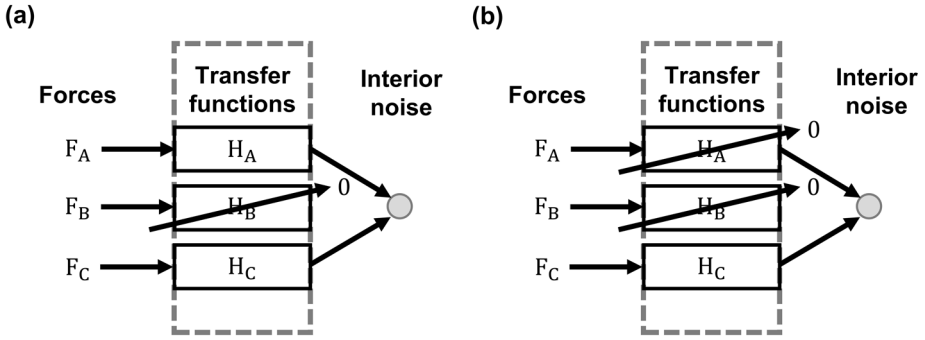

Figure 4.14 Schematic diagrams of the influence on the transfer function as a change in the virtual spring application point: (a) when the virtual spring is applied to the connecting point between a path and the substructure to which it is mounted, and (b) when a virtual spring with infinite stiffness is applied to a specific path B itself.

4.4.3 Body TPA

The FBS-based TPA differs from the conventional TPA in that it does not require the removal of the source connected to the noise transmission path. This is because the original system is considered as a base system, and the virtual spring is considered as an added system in the FBS-based TPA model. Hence, the virtual spring concept does not require a practical decomposition and assembly process, which is advantageous with respect to experimental efficiency. Thus, the proposed method can be applied to a vehicle body that primarily consists of welded parts, which are difficult to remove.

To conduct a feasibility test on the FBS-based TPA method under application to a vehicle body, the road noise phenomenon presented in the previous section was used. An apron member and a strut bar were employed to connect the strut housing to the cabin, as shown in Fig. 4.5(b). To determine which component of the apron member and the strut bar is a more critical path, accelerometers were mounted near the cabin for the application of the virtual springs, as shown in Fig. 4.15.

Figure 4.16 presents the results of adding a virtual spring at the point connecting the strut bar and the cabin. The x-directional virtual spring significantly reduced the interior noise at approximately 160 Hz. However, the

virtual springs along the other directions were found to have no significant influences. Moreover, Fig. 4.17 reveals that the apron member does not have an influence on the interior noise. Based on the results, it can be deduced that the structure-borne noise transmitted from the damper strut is transmitted to the interior cabin via the strut bar, instead of the apron member. This verifies that the proposed method is feasible for the TPA of a vehicle body.

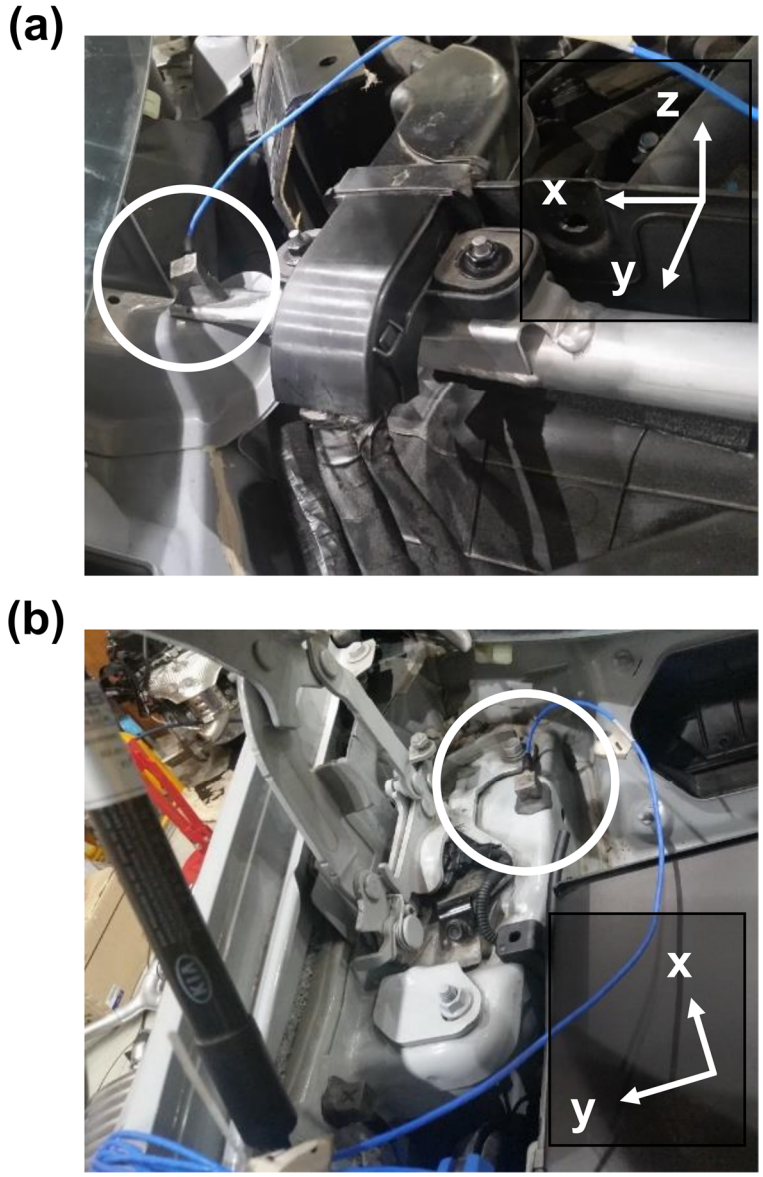

Figure 4.15 Accelerometer positions to conduct the vehicle body TPA using virtual spring: (a) accelerometer mounting point at the strut bar, and (b) accelerometer mounting point at the apron member.

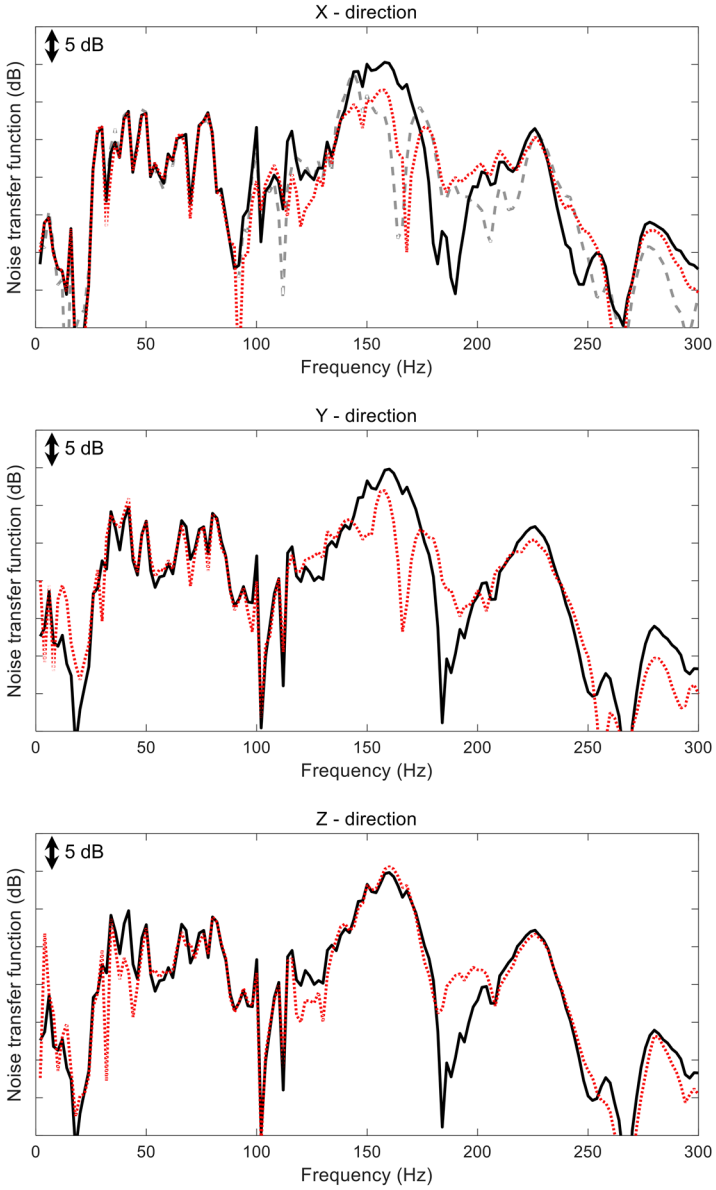

Figure 4.16 Noise transfer functions from the input force acting on a wheel in the y-direction to the interior SPL when a virtual spring with infinite stiffness is applied to the connecting point of the strut bar (solid line: base system, dotted line: system with a virtual spring at the strut bar, dashed line: system without a strut bar).

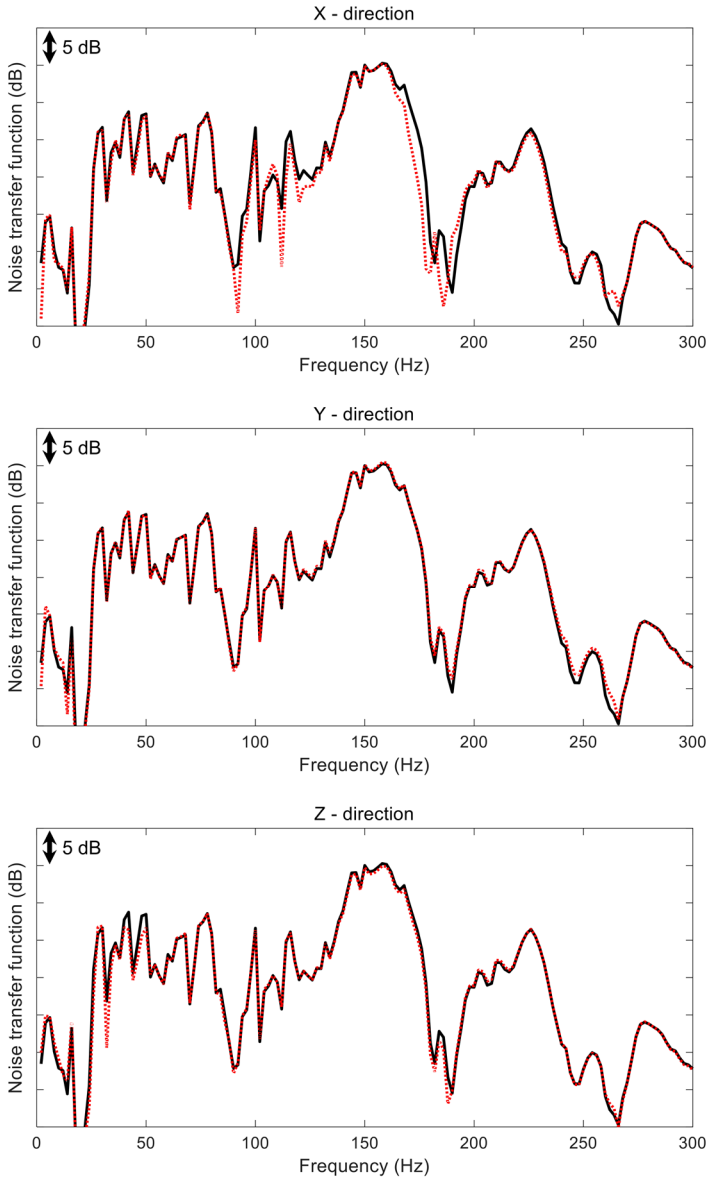

Figure 4.17 Noise transfer functions from the input force acting on a wheel in the y-direction to the interior SPL when a virtual spring with an infinite stiffness is applied to the measurement point of the apron member (solid line: base system, dotted line: system with a virtual spring at the apron member).

4.5 Summary

In this chapter, a novel method for evaluating the transfer path is proposed, which is based on the FBS method [18] and is referred to as FBS-based TPA. In the proposed method, the concept of a virtual spring with an infinite stiffness was applied. Using this method, the effects of a change in the stiffness of the transfer path can be predicted using only the FRF information of the original system. Unlike the conventional TPA, the proposed method is based on the concept of virtual spring [64], thus allowing for the evaluation of the transfer path without a practical decomposition and assembly process. In the conventional TPA method, a decomposition and assembly process of the system is employed, and the contributions of the transfer paths are evaluated by estimating the input forces from a source. The classical TPA methods are disadvantageous with respect to efficiency. In addition, they are erroneous, as they do not accurately reflect the operational conditions of an actual system, such as the boundary conditions to the exclusion of the source. A mathematical error may therefore be induced in the matrix inversion method, which is used to estimate the operating forces of a source in the conventional TPA. Therefore, unlike the conventional evaluation methods, an FBS-based modeling was used to evaluate the transfer path in this study. With the FBS technique, an original

system can be considered as a base system and a virtual spring can be considered as an added system. Thus, the transfer path can be evaluated, and the direction of the stiffness modification for noise improvement can be suggested.

In this study, the feasibility of the proposed method was investigated by applying a series of processes to the suspension link TPA of an actual vehicle. As shown in Figs. 4.5 and 4.7, the strut bar is the main transfer path at 160 Hz in the target system Moreover, a significant road noise phenomenon was considered in this study. The results shown in Fig. 4.9 confirm that the virtual spring has the same effect as that when the actual path is removed. In addition, the sensitivity of the stiffness change can be evaluated by considering an arbitrary stiffness modification using the virtual spring at each point. The results of the proposed method applied to the significant road noise phenomenon confirmed that it can be employed for suspension linkages upon the addition of virtual springs at the attachment points of the linkages. This is because the attachment stiffness of a virtual spring for a specific linkage tends to infinity, and the effect of the spring on the system is the same as that when the transfer path is removed. Moreover, the results revealed that the proposed method is feasible for vehicle bodies that comprise components that are difficult to separate. Based on the findings, parts can be preferentially modified with a high

sensitivity to stiffness modification in the vehicle development process.

In addition, the FBS-based TPA does not require part removal or correlation information between the signals. The results shown in Fig. 4.10 confirm that the correlation between the paths is not required. Therefore, the proposed method is easier to implement and more applicable than the other two representative TPA methods, namely, the conventional and operational TPA methods. Moreover, in comparison with the conventional TPA, which uses the matrix inversion method, a reduced computational load can also be achieved with the proposed method, as shown in Fig. 4.18. As a result of comparing the computational loads [70], the proposed method is considered to be suitable for fast and convenient analysis of multiple transfer paths.

However, the proposed method is only applicable to FRF data at the current stage, and not to the entire spectrum of an actual operation signal. In particular, the proposed method is an FRF-based TPA method; thus, the force characteristics should be considered in the representation of actual phenomena. The force acting on a wheel can be a candidate for vehicle road noise, as detailed in this chapter. The FBS-based TPA requires more data and experience for a wider scope of application. It should be noted that a virtual spring should be added at the attachment point of a link, and not to the actual link, for the TPA of suspension links.

However, despite several limitations, this research proposes a novel transfer path evaluation method, which overcomes the disadvantages of the existing TPA methods. The method is useful to NVH engineers and experimentally efficient with respect to time and energy consumption. Moreover, this method can be used in the actual vehicle development and evaluation process, as it can predict the trend without the experimentally application of stiffness changes to the actual system. By arbitrarily changing the stiffness of the path, the reduction of the SPL in the target system can be predicted without actual experiments. This can improve the efficiency of existing development processes with respect to the time required and cost, by reducing the necessity for repeated vehicle prototype evaluations and improvements. In conclusion, this research presents a novel evaluation method for the transfer paths in the vehicle development stage.

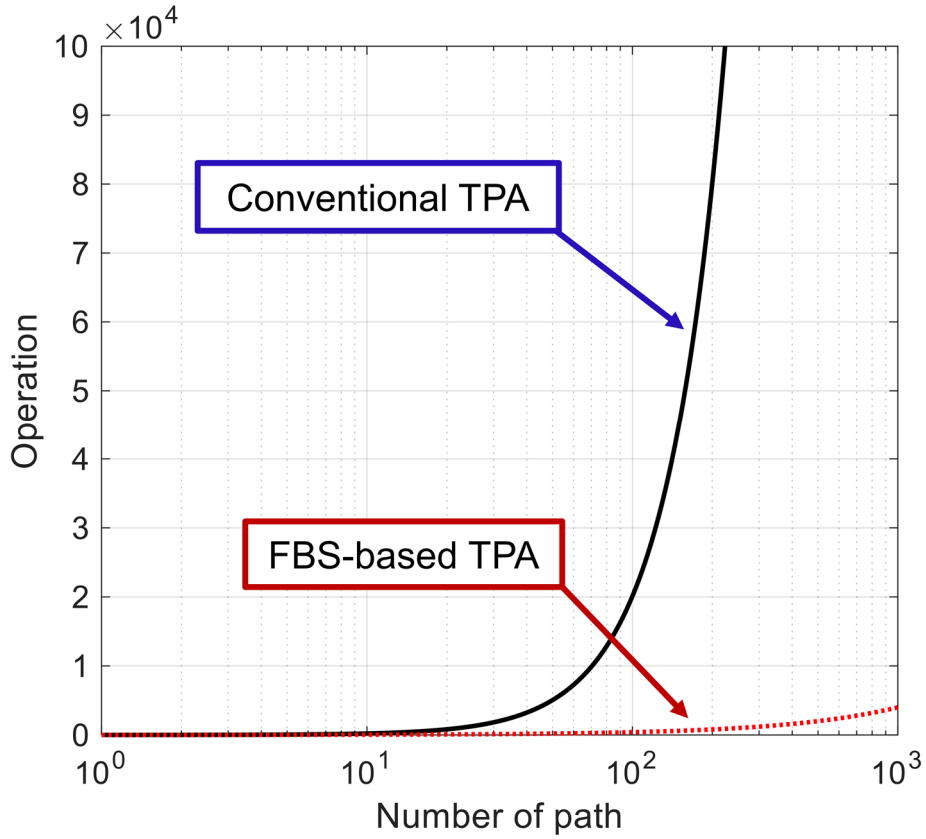

Figure 4.18 Computational load for TPA.

CHAPTER 5

EXPERIMENTAL METHOD FOR IMPROVED ACCURACY OF DYNAMIC SUBSTRUCTURING MODEL

5.1 Introduction

Generally, the vibro-acoustic performance of an assembled system cannot be predicted in the early development phase, prior to the assembly of the entire system. To predict the performance of the entire system, the dynamic properties of the substructure coupling points and the FRFs of each substructure are required. Given that measurements cannot be carried out at the coupling points, previous methods are based on measurements carried out at neighboring locations, which this leads to erroneous results. Moreover, a signal measured at a single point is not sufficiently representative of system characteristics, which leads to further errors in the substructuring model.

Hence, the aim of this study was to predict the dynamic characteristics of a final assembled structure using only the FRFs of single substructures evaluated using test jigs in the early development stages. This method allows

for developers to predict the performance of a part in its intended system by overcoming the differences between system coupling properties. This chapter therefore proposes a method for estimating the dynamic characteristics of a substructure coupling system using the joint properties to improve estimation accuracy. A hybrid method is then presented to realize an efficient and accurate dynamic substructuring model technique based on these properties.

In the proposed method, an assembled system is divided into individual substructures and joint properties. In this process, the virtual point (VP) concept is employed to enable physical measurements at the joint points in practical use cases. The VP is a concept proposed by Seijs for estimating the signal of the non-measurable coupling point from the measured signal [27]. In this present study, a weighting matrix composed of the coherence between the measured signals was proposed to perform the virtual point transformation (VPT). Hence, the dynamic characteristics of an assembled system can be calculated using only the FRFs of each substructure and the estimated joint property obtained from the measurements. Thereafter, the dynamic characteristics of a new coupling system can then be predicted by applying the generalized coupling properties (GCPs) to the examined system. This results in a more accurate estimate of the assembled system characteristics. The results of the proposed method were validated using a test jig and an actual vehicle suspension mount.

5.2 Theoretical concepts

5.2.1 Dynamic substructuring model considering generalized coupling properties

The FRF-based substructuring (FBS) technique is generally used to obtain the dynamic characteristics of a coupling system in which two or more substructures are combined, as shown in Fig. 5.1. Here, the force equilibrium and compatibility conditions at the coupling point can be expressed as follows:

$$\mathrm{u}_j^{\mathrm{AB.A}} = \mathrm{u}_j^{\mathrm{AB.B}}, \tag{5.1}$$

$$\mathrm{f}_j^{\mathrm{AB.A}} + \mathrm{f}_j^{\mathrm{AB.B}} = 0, \tag{5.2}$$

where u and f are the interface displacement and force, respectively; the superscript indicates that the measurement is for substructure A, B, or coupled system AB, such that $\mathrm{AB.A}$ and $\mathrm{AB.B}$ indicate the A and B sides, respectively, of AB; and the subscript j denotes the joint point.

The dynamic characteristics of this coupling system can be expressed as follows:

$$u_o^{AB} = H_{o,i}^{A} f_i^{AB} + H_{o,j}^{A} f_j^{AB.A}, \tag{5.3}$$

$$u_j^{AB.A} = H_{j,i}^{A} f_i^{AB} + H_{j,j}^{A} f_j^{AB.A}, \tag{5.4}$$

$$u_j^{AB.B} = H_{j,j}^{B} f_j^{AB.B}, \tag{5.5}$$

where $H_{y,x}$ is the frequency response function from the input force at point x to the response point y, and the subscripts i and o indicate the input and output points in the derivation process, respectively. Using the conditions of Eqs. (5.1) and (5.2), Eqs. (5.3) to (5.5) can be expressed in matrix form as

$$\begin{bmatrix} u_o^{AB} \\ u_j^{AB.A} \\ u_j^{AB.B} \end{bmatrix} = \begin{bmatrix} H_{o,i}^{A} & H_{o,j}^{A} & 0 \\ H_{j,i}^{A} & H_{j,j}^{A} & 0 \\ 0 & 0 & H_{j,j}^{B} \end{bmatrix} \begin{bmatrix} f_i^{AB} \\ f_j^{AB.A} \\ -f_j^{AB.A} \end{bmatrix}. \tag{5.6}$$

Solving for $f_j^{AB.A}$, the following result is obtained:

$$f_j^{AB.A} = -\left(H_{j,j}^{A} + H_{j,j}^{B}\right)^{-1} H_{j,i}^{AB} f_i^{AB}. \tag{5.7}$$

Using this result, the response at the output point of the coupling system can be expressed as

$$u_o^{\mathrm{AB}} = [\mathrm{H}_{o,i}^{\mathrm{A}} - \mathrm{H}_{o,j}^{\mathrm{A}}\left(\mathrm{H}_{j,j}^{\mathrm{A}} + \mathrm{H}_{j,j}^{\mathrm{B}}\right)^{-1}\mathrm{H}_{j,i}^{\mathrm{A}}]\mathrm{f}_i^{\mathrm{AB}}. \tag{5.8}$$

By employing Eq. (8), the transfer function from the input point to the output point can be defined as follows:

$$\mathrm{H}_{o,i}^{\mathrm{AB}} = \mathrm{H}_{o,i}^{\mathrm{A}} - \mathrm{H}_{o,j}^{\mathrm{A}}\left(\mathrm{H}_{j,j}^{\mathrm{A}} + \mathrm{H}_{j,j}^{\mathrm{B}}\right)^{-1}\mathrm{H}_{j,i}^{\mathrm{A}}, \tag{5.9}$$

which represents a slightly modified form of the equations developed by Tsai [18]. In this manner, the FRF of the coupling system can be predicted using the FRFs of each substructure.

However, coupling systems are generally bolt-assembled in actual implementation. Therefore, the joint properties of the coupling system should be considered, as they can cause a discrepancy between the actual FRF of the coupling system and the FRF estimated using Eq. (5.9). This discrepancy is defined as the dynamic joint property $\mathrm{H_J}$, and it is included in the estimation equation as follows:

$$\mathrm{H}_{o,i}^{\mathrm{AB}} = \mathrm{H}_{o,i}^{\mathrm{A}} - \mathrm{H}_{o,j}^{\mathrm{A}}\left(\mathrm{H}_{j,j}^{\mathrm{A}} + \mathrm{H}_{j,j}^{\mathrm{B}} + \mathrm{H_J}\right)^{-1}\mathrm{H}_{j,i}^{\mathrm{A}}, \tag{5.10}$$

where $\mathrm{H_J}$ is expressed as

$$\mathrm{H_J} = \mathrm{H}_{j,i}^{\mathrm{A}}\left(\mathrm{H}_{o,i}^{\mathrm{A}} - \mathrm{H}_{o,i}^{\mathrm{AB}}\right)^{-1}\mathrm{H}_{o,j}^{\mathrm{A}} - \mathrm{H}_{j,j}^{\mathrm{A}} - \mathrm{H}_{j,j}^{\mathrm{B}}. \tag{5.11}$$

In general, in a bolted joint coupling system, the substructures have similar characteristics at the coupling point. These joint characteristics are referred to generalized coupling properties (GCPs), as they can be generalized in most structures that use the same bolt. Hence, if a new system X is combined with substructure A in which we are interested, the changes in the dynamic behavior of substructure A can be predicted as follows:

$$\mathrm{H}_{o,i}^{\mathrm{AX}} = \mathrm{H}_{o,i}^{\mathrm{A}} - \mathrm{H}_{o,j}^{\mathrm{A}}\left(\mathrm{H}_{j,j}^{\mathrm{A}} + \mathrm{H}_{j,j}^{\mathrm{X}} + \mathrm{H_J}\right)^{-1}\mathrm{H}_{j,i}^{\mathrm{A}}. \tag{5.12}$$

Based on these results the dynamic characteristics of a new coupling system consisting of substructure X and substructure A can be estimated, as shown in Fig. 5.2.

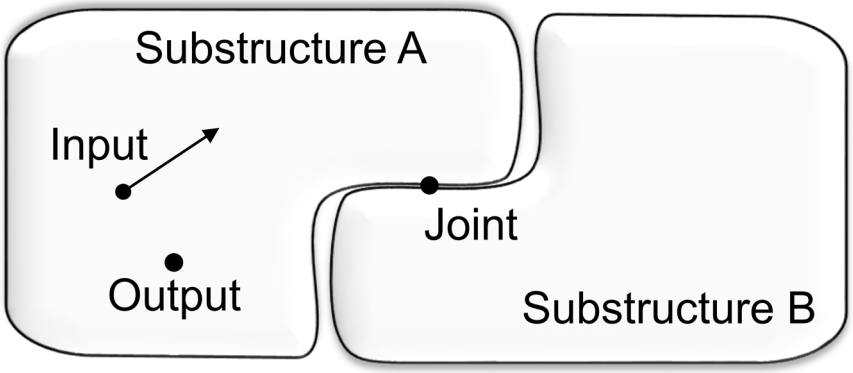

Figure 5.1 Coupling system schematic.

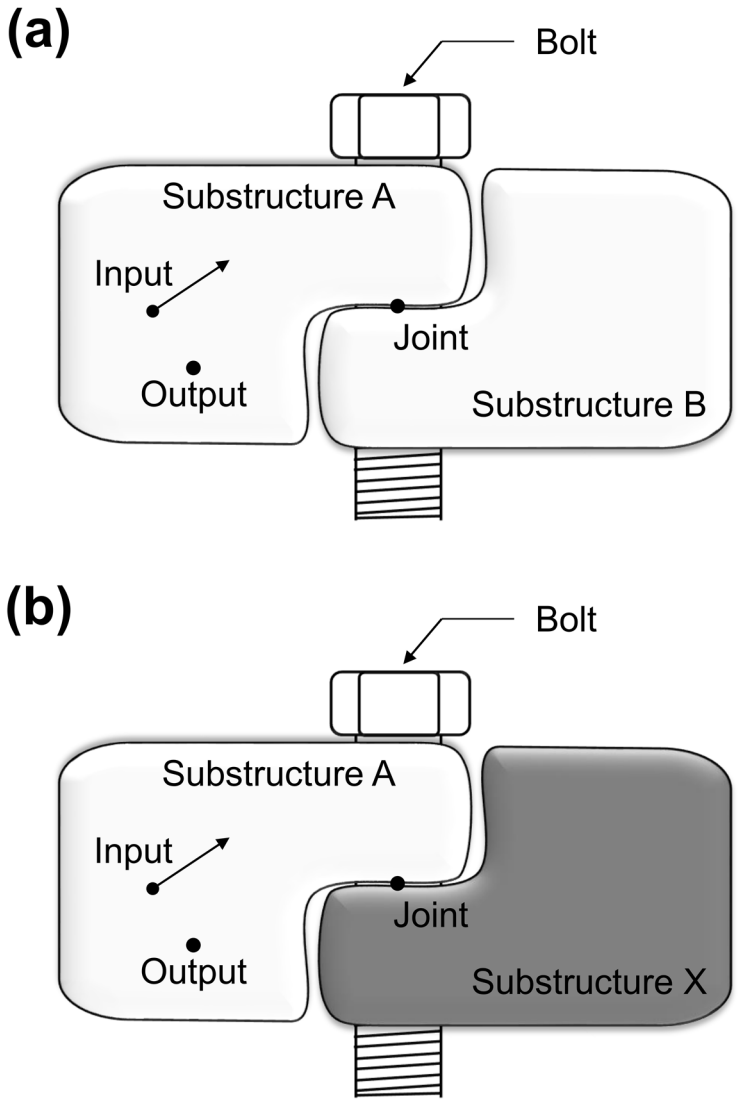

Figure 5.2 Schematics of coupling systems joined by a bolt: (a) substructures A and B; and (b) substructures A and X.

5.2.2 Virtual point transformation method to improve experimental data

5.2.2.1 Virtual point displacement

As discussed in Section 5.2.1, to employ the FBS technique, a force equilibrium and compatibility should be assumed at the point of coupling. However, most actual coupling structures consist of bolted joints instead of ideal point joints, as shown in Fig. 5.3. Therefore, the coupling system is engaged by surface contact at the bolting periphery, instead of via a discrete point. The FRF at the exact joint of the coupling system can therefore not be obtained using a direct measurement. Therefore, when actual data are applied to the approximated FBS model, the predicted dynamic characteristics of the coupling system may be erroneous unless coupling rigidity is guaranteed, which is highly improbable.

To overcome this practical limitation, Rixen et al. [59] introduced the concept of virtual points (VPs). This concept uses measurements at peripheral areas, as shown in Fig. 5.3, to estimate the vibration signals at the coupling point, which are not directly measurable in physical tests. Hence, coordinates are introduced in Fig. 5.4(a) to allow for conversion between the measurable

points and the virtual point (i.e., actual coupling point). This coordinate transformation, which is referred to as VPT, can be applied to a structure with a bolted joint, as shown in Fig. 5.4(b).

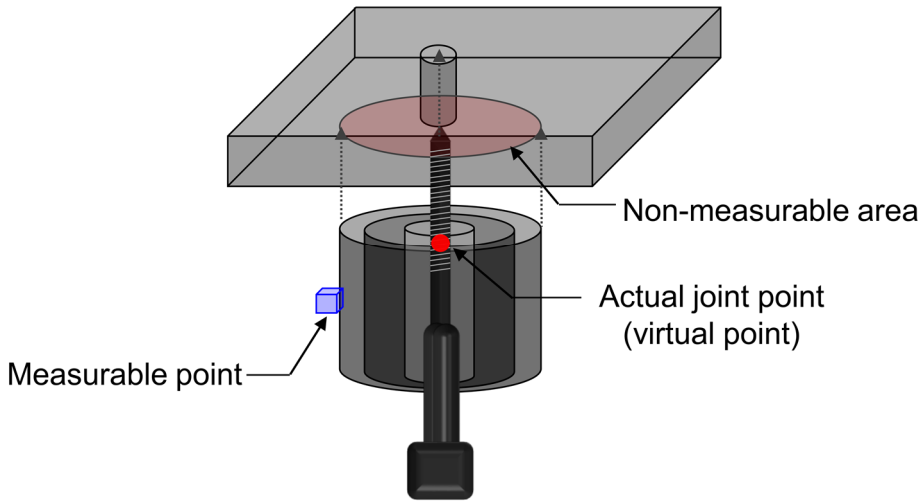

Figure 5.3 Actual configuration of a coupling system with a bolt.

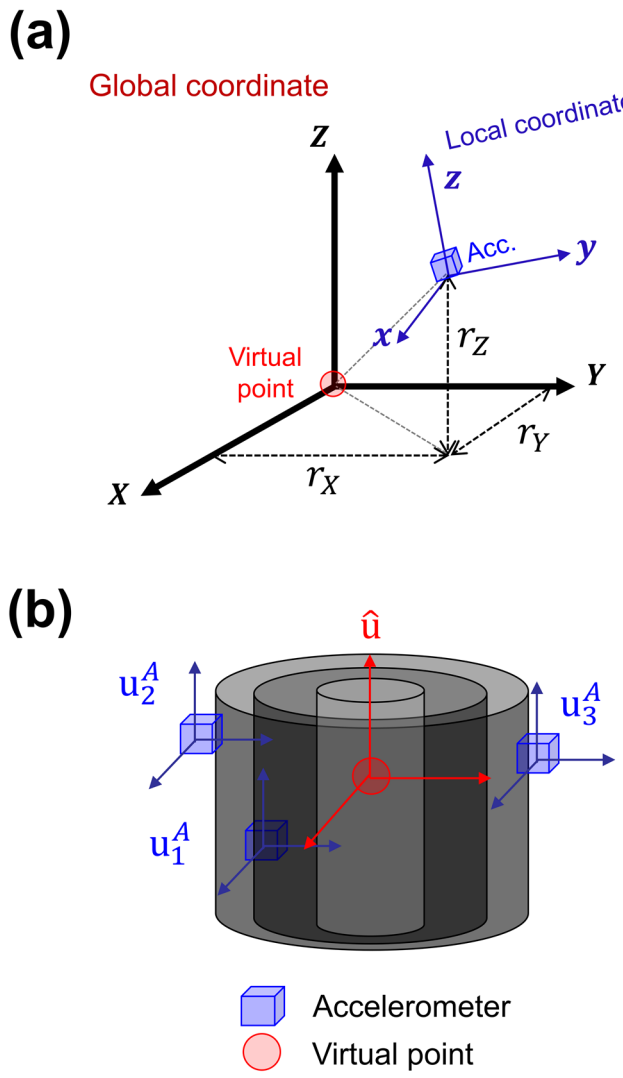

Figure 5.4 Relationship between measurable points and a virtual point (actual coupling point): (a) coordinates and (b) illustration of application to a bolted joint.

To carry out VPT, the dynamics of the coupling point are defined as follows:

$$\mathbf{u} = \mathbf{T}\hat{\mathbf{u}} + \mathbf{e_d}, \tag{5.13}$$

where $\mathbf{u}$ is the displacement vector measured by the sensors, $\hat{\mathbf{u}}$ denotes the virtual point displacement vector at the coupling point estimated using the actual displacement, $\mathbf{T}$ is the transformation matrix, and $\mathbf{e_d}$ is the estimated error of the measured displacement. The measured displacement vector, the virtual point displacement vector, and estimated error are respectively defined as follows:

$$\mathbf{u} = \left[\mathrm{u}_x \; \mathrm{u}_y \; \mathrm{u}_z \right]^{\mathbf{T}}, \tag{5.14}$$

$$\hat{\mathbf{u}} = \left[\hat{\mathrm{u}}_x \;\; \hat{\mathrm{u}}_y \;\; \hat{\mathrm{u}}_z \;\; \hat{\mathrm{u}}_{rx} \;\; \hat{\mathrm{u}}_{ry} \;\; \hat{\mathrm{u}}_{rz} \right]^{\mathbf{T}}, \tag{5.15}$$

$$\mathbf{e_d} = \left[\mathrm{e}_x \; \mathrm{e}_y \; \mathrm{e}_z \right]^{\mathbf{T}}, \tag{5.16}$$

where subscripts x, y, and z represent the local coordinate axes of each point, and rx, ry, and rz represent the rotations around each local axis. Consequently, the transformation matrix $\mathbf{T}$ in Eq. (5.13) is composed of the

orientation matrix and distances from the virtual point to the measurable points as follows:

$$\mathbf{T} = \begin{bmatrix} \emptyset_{x,X} & \emptyset_{x,Y} & \emptyset_{x,Z} \\ \emptyset_{y,X} & \emptyset_{y,Y} & \emptyset_{y,Z} \\ \emptyset_{z,X} & \emptyset_{z,Y} & \emptyset_{z,Z} \end{bmatrix} \begin{bmatrix} 1 & 0 & 0 & 0 & r_Z & -r_Y \\ 0 & 1 & 0 & -r_Z & 0 & r_X \\ 0 & 0 & 1 & r_Y & -r_X & 0 \end{bmatrix}, \quad (5.17)$$

where $\emptyset_{l,G}$ is the cosine of the angle between the local coordinate axis l and global coordinate axis G, and r_G is the distance from the global G-axis of the virtual point to each measureable point.

From Eq. (5.13), the error can be expressed as follows:

$$\mathbf{e_d} = \mathbf{u} - \mathbf{T}\hat{\mathbf{u}} . \quad (5.18)$$

From Eq. (5.18), the cost function to minimize the error can be defined as follows:

$$\mathbf{J}(\hat{\mathbf{u}}) = \frac{1}{2}\mathbf{e_d^T W e_d} , \quad (5.19)$$

where $\mathbf{W}$ represents the diagonal weighting matrix introduced to identify the optimal virtual displacement by applying the Moor–Penrose pseudo-inverse of $\mathbf{T}$ [59]. This weighting matrix can be composed of the measured FRF coherences γ^2 as follows:

$$\mathbf{W} = \begin{bmatrix} \gamma_1^2 & & \\ & \gamma_2^2 & \\ & & \gamma_3^2 \end{bmatrix}, \tag{5.20}$$

where γ_i^2 is the coherence at the *i*-th position in the sensor placement [27]. To obtain the estimated optimal response of the virtual point with minimal errors, Eq. (5.18) is substituted into Eq. (5.19) as follows:

$$\begin{aligned} \mathbf{J}(\hat{\mathbf{u}}) &= \frac{1}{2}(\mathbf{u} - \mathbf{T}\hat{\mathbf{u}})^{\mathbf{T}}\mathbf{W}(\mathbf{u} - \mathbf{T}\hat{\mathbf{u}}) \\ &= \frac{1}{2}(\hat{\mathbf{u}}^{\mathbf{T}}\mathbf{T}^{\mathbf{T}}\mathbf{W}\mathbf{T}\hat{\mathbf{u}} - \mathbf{u}^{\mathbf{T}}\mathbf{W}\mathbf{T}\hat{\mathbf{u}} - \hat{\mathbf{u}}^{\mathbf{T}}\mathbf{T}^{\mathbf{T}}\mathbf{W}\mathbf{u} + \mathbf{u}^{\mathbf{T}}\mathbf{W}\mathbf{u}). \end{aligned} \tag{5.21}$$

If the Hessian matrix $\mathbf{T}^{\mathbf{T}}\mathbf{W}\mathbf{T}$ of Eq. (5.21) is positive-definite, the minimum value of the cost function can be obtained by differential computation as follows:

$$\left(\frac{\partial \mathbf{J}}{\partial \hat{\mathbf{u}}}\right)^{\mathbf{T}} = \mathbf{T}^{\mathbf{T}}\mathbf{W}\mathbf{T}\hat{\mathbf{u}} - \mathbf{T}^{\mathbf{T}}\mathbf{W}\mathbf{u}. \tag{5.22}$$

For Eq. (5.22) to equate to zero, the virtual point displacement $\hat{\mathbf{u}}$ is required to satisfy the following:

$$\hat{\mathbf{u}} = \left(\mathbf{T}^{\mathbf{T}}\mathbf{W}\mathbf{T}\right)^{-1}\mathbf{T}^{\mathbf{T}}\mathbf{W}\mathbf{u}. \tag{5.23}$$

Hence, the result of $\hat{\mathbf{u}}$ allows for the estimation of the virtual point response. The residual displacement error can be also expressed as follows:

$$\mathbf{e_d} = \mathbf{u} - \mathbf{T}\left(\mathbf{T}^{\mathrm{T}}\mathbf{W}\mathbf{T}\right)^{-1}\mathbf{T}^{\mathbf{T}}\mathbf{W}\mathbf{u}. \tag{5.24}$$

Consequently, the above equations can be used to estimate the virtual point displacement at the actual coupling point (i.e., the non-measurable point).

5.2.2.2 Virtual point FRF

The virtual point FRFs that occur at the actual coupling points can also be obtained as described in Section 5.2.2.1. Prior to deriving the virtual point FRFs, the relationship at the interface point of the coupling system shown in Fig. 5.2 can be described as follows:

$$\mathbf{H}^{-1}\mathbf{u} = \mathbf{f}, \tag{5.25}$$

$$\mathbf{B}\mathbf{u} = 0, \tag{5.26}$$

where $\mathbf{u}$ denotes the displacement at the coupling point of the coupling system, $\mathbf{f}$ represents the external force vector [17], and $\mathbf{H}$ denotes the transfer function of the system. In addition, Eq. (5.26) describes an arbitrary constraint of a coupled system with the signed Boolean matrix $\mathbf{B}$ (e.g., $\mathbf{B} = [-\mathbf{I} \quad \mathbf{I}]$) [16].

To satisfy the constraints described in Eq. (5.26), Eq. (5.25) can be re-written as follows:

$$\mathbf{H}^{-1}\mathbf{u} = \mathbf{f} - \mathbf{B}^{\mathbf{T}}\boldsymbol{\lambda}, \tag{5.27}$$

where $\boldsymbol{\lambda}$ is a set of Lagrange multipliers to determine the optimized solution

of these equations [61].

Similarly, if the excitation points are the same as the response points, using the result of Eq. (5.23), Eq. (5.26) can be expressed as follows:

$$\hat{\mathbf{B}}\hat{\mathbf{u}} = \hat{\mathbf{B}}\left(\mathbf{T}^{\mathbf{T}}\mathbf{W}\mathbf{T}\right)^{-1}\mathbf{T}^{\mathbf{T}}\mathbf{W}\mathbf{u} = 0, \tag{5.28}$$

where $\hat{\mathbf{C}}$ is a signed Boolean matrix that describes a new set of constraints related to the virtual point displacement $\hat{\mathbf{u}}$, and $\hat{\mathbf{B}}\left(\mathbf{T}^{\mathbf{T}}\mathbf{W}\mathbf{T}\right)^{-1}\mathbf{T}^{\mathbf{T}}\mathbf{W}$ describes a new set of constraints of the actual point displacement $\mathbf{u}$ when the virtual point displacement $\hat{\mathbf{u}}$ is applied at the coupling point (here, the transformation matrix and weighting matrix are similar, as in the case of the virtual point displacement, given that the excitation points are the same as the response points). Thus, the following results are obtained:

$$\mathbf{u} = \mathbf{H}(\mathbf{f} - \mathbf{W}^{\mathbf{T}}\mathbf{T}\left(\mathbf{T}^{\mathbf{T}}\mathbf{W}\mathbf{T}\right)^{-1}\hat{\mathbf{B}}^{\mathbf{T}}\boldsymbol{\lambda}). \tag{5.29}$$

Moreover, the virtual point force vector $\hat{\mathbf{f}}$ can be derived similarly to the virtual point displacement described in Section 5.2.2.1. In particular, when the excitation and response points are the same, the virtual point force can be

expressed as follows:

$$\mathbf{f} = \mathbf{W}^{\mathbf{T}}\mathbf{T}\left(\mathbf{T}^{\mathrm{T}}\mathbf{W}\mathbf{T}\right)^{-1}\hat{\mathbf{f}}. \tag{5.30}$$

Finally, Eqs. (5.23), (5.29), and (5.30) can be combined and arranged to obtain the transfer function at the virtual point, as follows:

$$\hat{\mathbf{u}} = \hat{\mathbf{H}}\,\hat{\mathbf{f}}, \tag{5.31}$$

where

$$\hat{\mathbf{H}} = \mathbf{V}\mathbf{H}\mathbf{V}^{\mathbf{T}} - \mathbf{V}\mathbf{H}\mathbf{V}^{\mathbf{T}}\hat{\mathbf{B}}^{\mathbf{T}}\left(\hat{\mathbf{B}}\mathbf{V}\mathbf{H}\mathbf{V}^{\mathbf{T}}\hat{\mathbf{B}}^{\mathbf{T}}\right)^{-1}\hat{\mathbf{B}}\mathbf{V}\mathbf{H}\mathbf{V}^{\mathbf{T}}, \tag{5.32}$$

and

$$\mathbf{V} = \left(\mathbf{T}^{\mathrm{T}}\mathbf{W}\mathbf{T}\right)^{-1}\mathbf{T}^{\mathrm{T}}\mathbf{W}. \tag{5.33}$$

Thus, the virtual point FRF $\hat{\mathbf{H}}$ can be obtained using Eq. (5.32).

5.3 Validation of virtual point transformation

The proposed FBS model considering joint properties and virtual point displacement was validated through a series of physical experiments conducted using a test jig and vehicle suspension system.

5.3.1 Target system and system description

Vehicle suspension points are generally classified into two categories, namely, hard-mount suspension and the elastomeric rubber-bushing suspension [38,40,60], as shown in Figs. 5.5(a) and 5.5(b), respectively. The focus of this study was on the hard-mount vehicle suspension. A vehicle suspension system has a complex shape and presents many challenges with respect to measurements, given the lack of physical space for conducting tests such as the impact hammer test, to obtain FRFs. Therefore, as discussed in Section 5.2, the system characteristics cannot be accurately measure or predict using conventional methods. To apply and verify the method proposed in Section 5.2, a test jig similar to the crossmember of a vehicle suspension system was developed, as shown in Fig. 5.6. This test jig was designed with a coupling bolt at four mount points, similar to the connection of a suspension

crossmember to the vehicle body. Given that a crossmember usually consists of several welded plates, instead a solid bar, to reduce weight and cost, the test jig was also made of hollow components.

The physical measurements were conducted as shown in Fig. 5.7. To obtain the FRFs of the entire system, accelerometers were attached along each coupling point. The FRFs were then measured using an impact hammer (B&K 2806-002) for excitation and tri-axial accelerometers (PCB 365A15 ICP). In addition, force sensors (PCP 260A02) were used to obtain the transfer force between test jig substructures and an electromagnetic shaker (B&K 4824) was used to apply an external force to the system. All the signals were measured using a mobile FFT analyzer (LMS SCADAS) at a frequency resolution of 0.25 Hz.

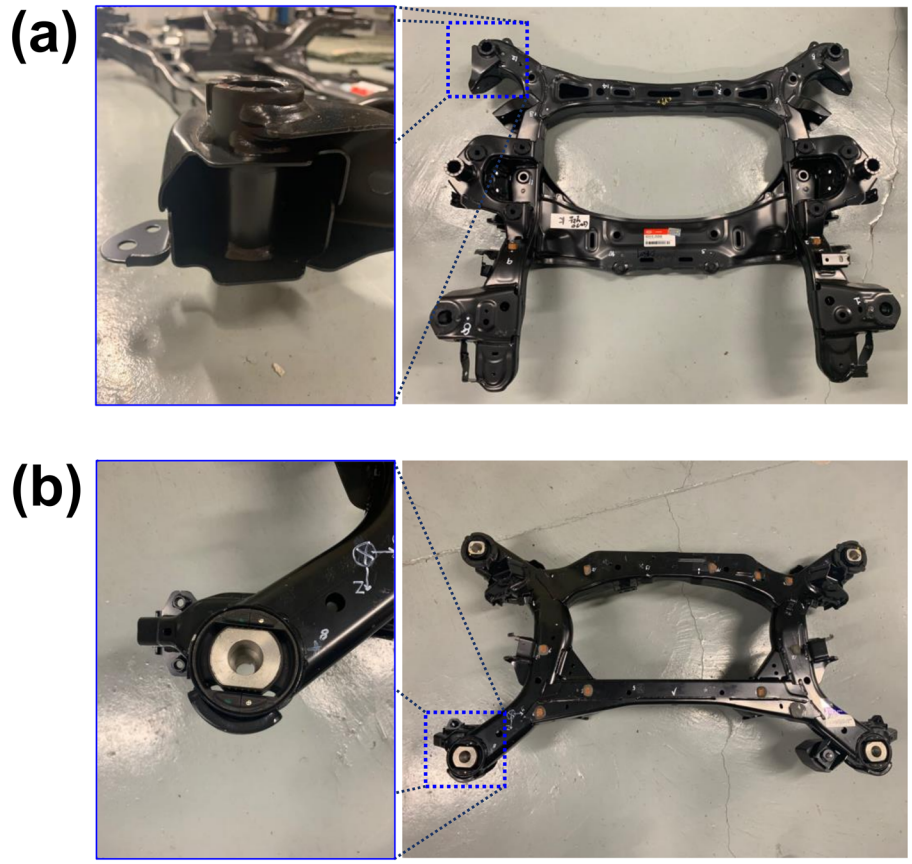

Figure 5.5 Vehicle suspension types: (a) hard-mount suspension and (b) rubber-bushing suspension.

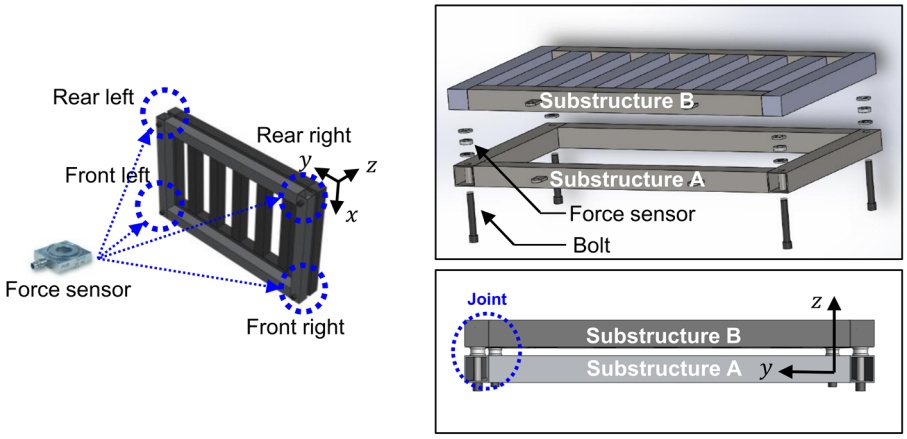

Figure 5.6 Test jig for validation of proposed method.

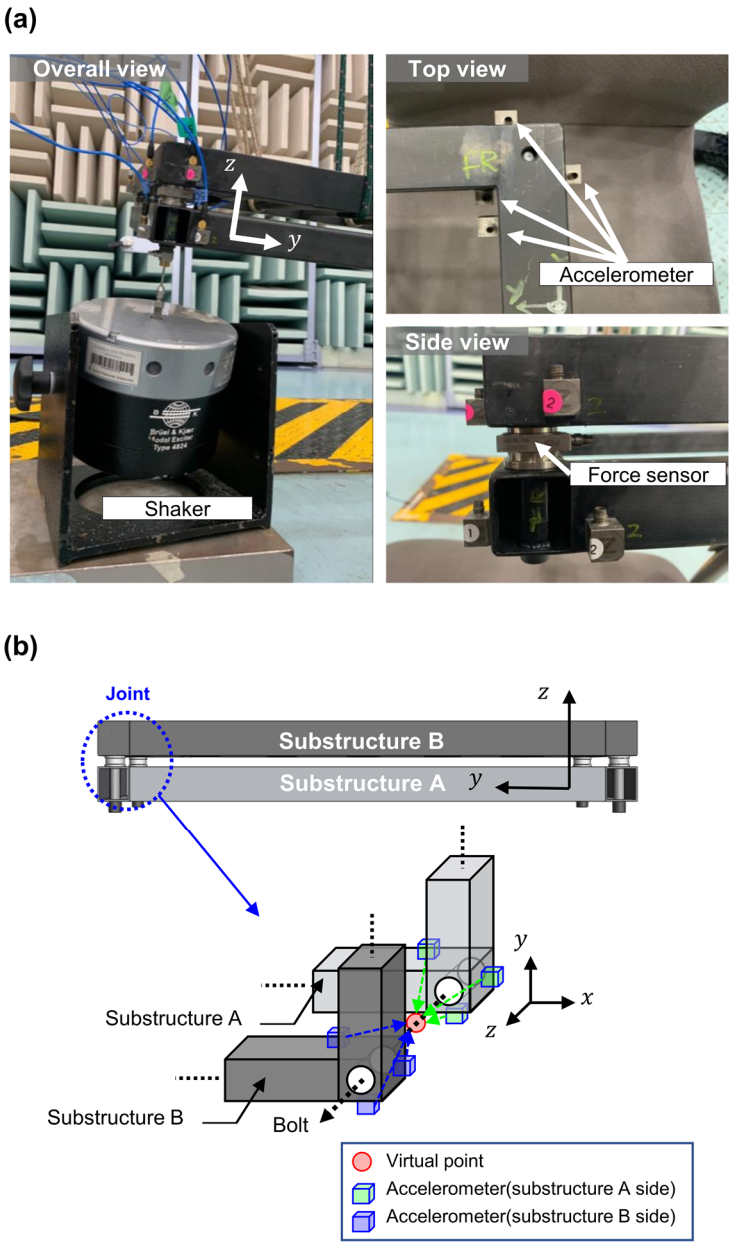

Figure 5.7 Validation test setup: (a) a test jig for verifying the proposed method and (b) virtual point for the test jig.

5.3.2 Validation of virtual point transformation

In this section, the general concepts of virtual points are validated with respect to the test jig. The primary focus in these subsections is the validation of the virtual point transformation technique at the coupling points of an assembled system. As mentioned in previous sections, general systems consist of substructures with bolts, and the dynamic substructuring technique can be employed to estimate the dynamic characteristics of an assembled system. In this process, accurate FRFs that express the characteristics of the system are required. However, in practical cases, there are non-measurable regions at the coupling points. Therefore, the VPT technique was employed to solve these problems. The next two subsections discuss the results of the virtual point displacement and virtual point FRF, as detailed in Section 5.2.

5.3.2.1 Validation of virtual point displacement

The test jig was used to verify the consistency of the VPT model presented in Section 5.2.2. Figure 5.8 presents a comparison of the tri-axial acceleration response data measured at each substructure side with an external

force applied to the coupled system as shown in Fig. 5.7. Based on the results, the responses at the coupling point should be the same for substructures A and B, depending on the assumptions for the application of the dynamic substructuring technique (i.e., force equilibrium and compatibility). However, as discussed in Section 5.2, due to the characteristics of an actual bolted joint, these assumptions cannot be directly implemented in practical use cases. In the z-direction, the similarity between the responses of Substructures A and B is the highest because of the rigidity of the bolt along the direction. However, in the x- and y-directions, different response modes are generated in each substructure. These differences can be attributed to the measurements carried out at the coupling periphery, instead of the actual coupling point. In addition, these results introduce inaccuracies to the dynamic substructuring model for system behavior estimation.

Therefore, the concept of the virtual point is introduced to overcome these limitations. As shown in Fig. 5.7(b), the response signals obtained from each substructure were used in Eq. (5.23) to estimate the virtual point displacement. To obtain the data, three triaxial accelerometers were installed on each of the substructures, and A and B and were excited in three orthogonal directions at each sensor location. From this process, the weighting matrix $\mathbf{W}$ was obtained from the coherence between the trials of the hammer

test, and the transformation matrix $\mathbf{T}$ was determined using the geometrical information between the accelerometer and the virtual point. Figure 5.8 presents a comparison of the responses measured in substructures A and B without postprocessing. In this case, the differences in responses occurred in each substructure, although the response of the coupling point should be the same in the dynamic substructuring model. Moreover, Fig. 5.9 presents the virtual point responses of the coupling point according to data measured at each substructure side when the proposed VPT was applied to the same system. In this case, the response of the actual coupling point (i.e., the virtual point) was estimated using the data collected at the three measurable points on each substructure side, as shown in Fig. 5.7. Compared with the results in Fig. 5.8, the results for both substructures in Fig. 5.9 were more similar. In particular, the inconsistencies of responses at the peak frequencies, as highlighted by circles in Fig 5.8, were improved. Moreover, the errors in the x- and y-directions from 400–500 Hz were due to the influence of the local mode of the measured FRFs in the system. The similarity of the results in the x- and y-directions generally improved, and the similarity in the z-direction improved at 490 Hz. These results were to be expected, given that the compatibility and rigidity at the system coupling point were established using the VPT model, thus confirming its validity. Therefore, the concept of the

virtual point can be applied to the dynamic substructuring model to improve its accuracy.

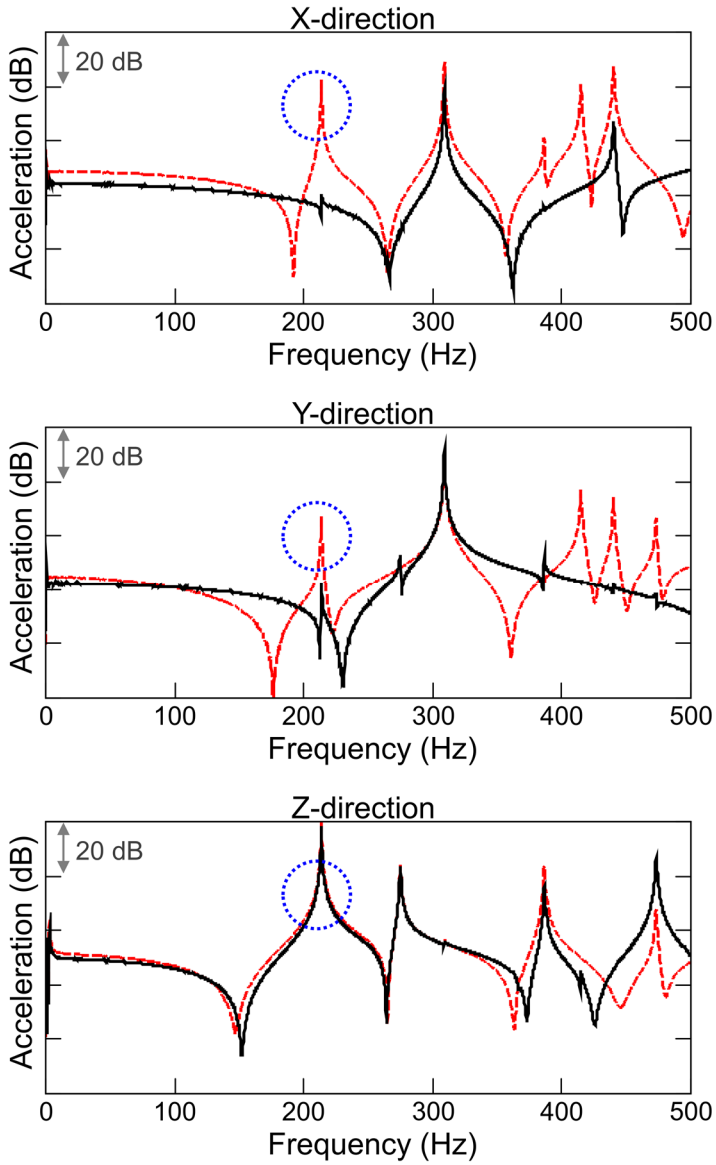

Figure 5.8 Measured acceleration responses of the subject coupling system around of a joint point without conducting VPT. The black solid line indicates the measured acceleration near the coupling point using the FRFs of substructure B, and the red dashed line indicates the measured acceleration near the coupling point using the FRFs of substructure A.

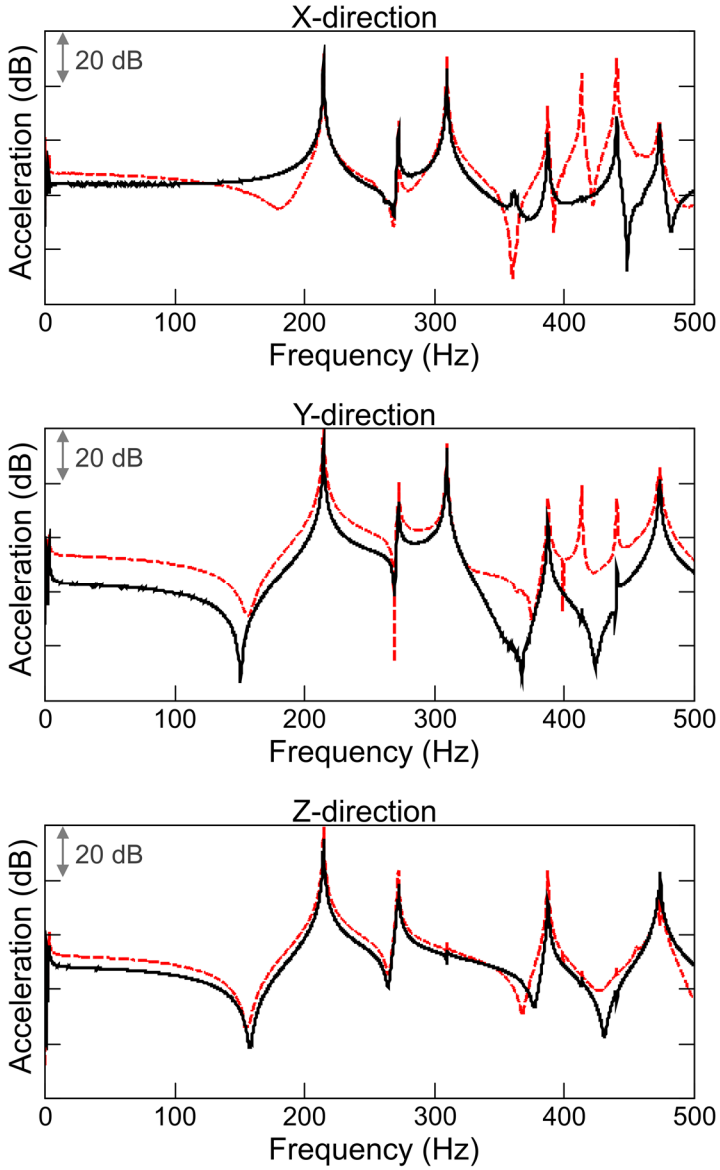

Figure 5.9 Virtual point acceleration responses of the subject coupling system around a joint point when performing VPT. The black solid line indicates the virtual point acceleration of the coupling system using the measured FRFs of substructure B, and the red dashed line indicates the virtual point acceleration of the coupling system using the measured FRFs of substructure A.

5.3.2.2 Validation of virtual point FRF

The FRFs at the virtual point can be verified in a similar manner as the results presented in Section 5.3.2.1. To estimate the accurate FRFs at the coupling points, the measured FRFs around the coupling points of the test jig were used in Eqs. (5.30), (5.31) and (5.32). As mentioned in section 5.3.2.1, three triaxial accelerometers and excitations at nine points near the accelerometers were used to calculate the characteristics of the virtual point. The weighting matrix $\mathbf{W}$ and the transformation matrix can be obtained in a similar manner to that introduced in Section 5.3.2.1. Figure 5.10 presents the measured FRFs on substructures A and B of the coupling point of the assembled system. As shown in this figure, there was a discrepancy between the FRFs measured on substructures A and B, thus violating the assumptions of dynamic substructuring. These results, similar to the virtual point displacement, lead to errors in the dynamic substructuring model.

However, as shown in Fig. 5.11, no significant differences were observed between the FRFs on Substructures A and B of the virtual point when generated using the VPT method. These results indicate improved accuracy when compared with the previous results, highlighted by circles in Fig. 5.10. As discussed in Section 5.3.2.1, it was also confirmed that the level of inertance

FRFs that did not coincide with the measured FRFs was more accurate in the virtual point FRFs. This improvement can be attributed to the use of the physical transformation matrix and weighting matrix obtained from the coherence of the FRF information in the VPT. Hence, the errors in the FRF measurement process can be eliminated by conducting VPT. Although there were errors in several frequency bands due to the influence of local modes ranging from 400–500 Hz, the results using the VPT were improved to match the overall trend of the FRFs. Based on these results, it can be concluded that it is preferable to use converted FRFs with the VPT, instead of measured FRFs near the coupling points. Thus, the virtual point FRFs can be used with the dynamic substructuring model to estimate the dynamic characteristics of a coupled system.

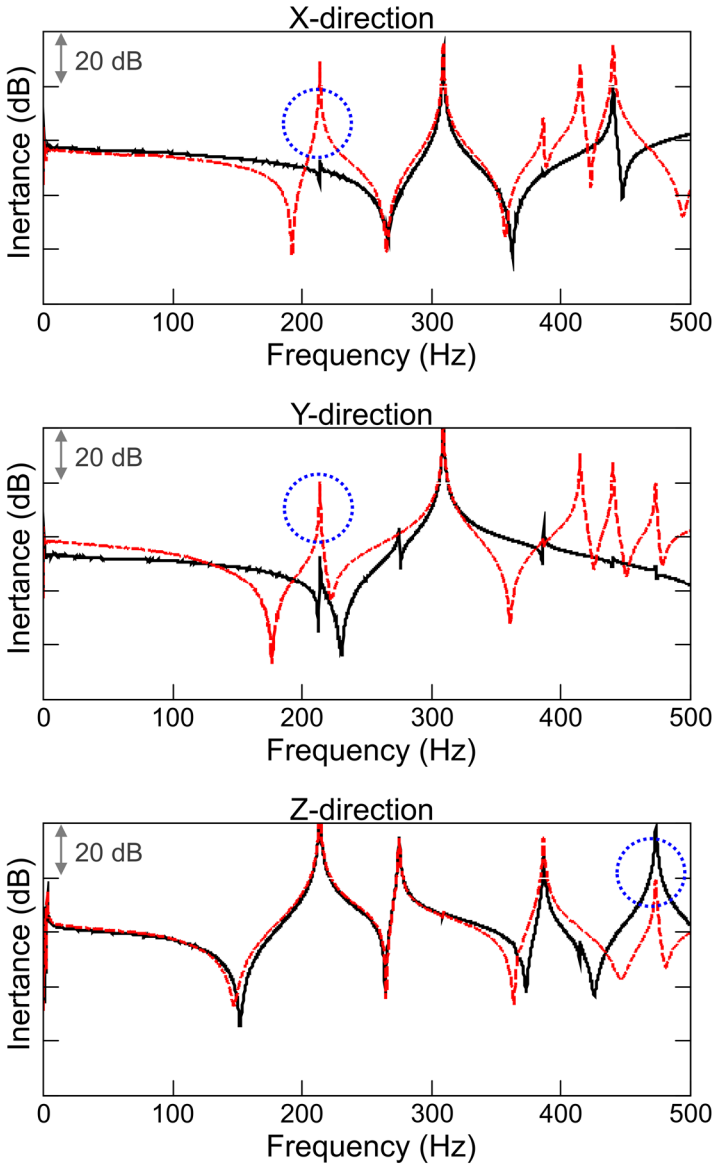

Figure 5.10 Measured FRFs of the subject coupling system at the joint point without performing VPT. The black solid line indicates the measured FRFs of substructure B, and the red dashed line indicates the measured FRFs of substructure A.

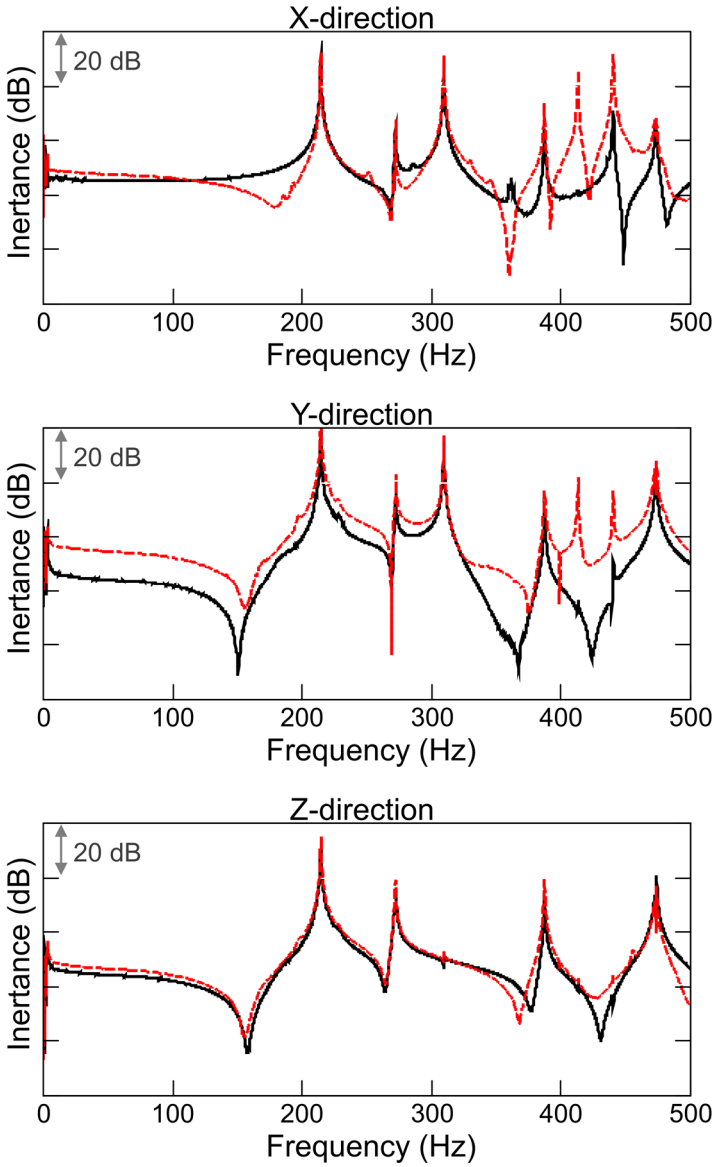

Figure 5.11 Estimated FRFs of the subject coupling system at the joint point performing VPT. The black solid line indicates the calculated virtual point FRFs, using the measured FRFs of substructure B, and the red dashed line indicates the calculated virtual point FRFs, using the measured FRFs of substructure A.

5.3.3 Dynamic substructuring with virtual point transformation

The problems due to the use of actual data in dynamic substructuring can be observed in the results presented in Section 5.3.2. The measured data is unreliable, as it dependent on the measurement position. In particular, the dynamic substructuring model is susceptible to FRF errors. Figure 5.12 presents a comparison of the estimated dynamic characteristics (i.e., inertance FRFs) of the coupled test jig obtained using Eq. (5.12) without (i.e., classical RC method) and with VPT, and the measured results of the actual coupled system. The estimated FRFs of the coupled system were obtained by applying Eq. (5.12) and using the FRFs measured from each single substructure and the GCPs obtained from the assembled system. When obtaining the GCPs for Fig. 5.12(b), the virtual point FRFs at the coupling point were substituted into Eq. (5.11). Table 5.1 presents the analysis results of Fig. 5.12. According to the results in Table 5.1, the proposed substructuring model yielded different FRF estimation results depending on whether the virtual point FRFs were used. When using the virtual point FRFs, the average estimation error of the peak frequency was reduced by 2.07% when compared with the case wherein the virtual point FRFs were not used. Based on the results, the use of the virtual

point FRFs resulted in an improved estimation accuracy.

Additional experiments were conducted using an actual vehicle suspension system to validate the practical application of the proposed dynamic substructuring technique based on the virtual point FRF and GCP concepts. The vehicle was divided into its body and its suspension. The FRFs of the fully assembled vehicle were then estimated using the FRFs of the suspension and vehicle body, in accordance with the proposed method. The vehicle test was conducted using a procedure similar to that used in the jig test.

The vehicle suspension system shown in Fig. 5.13 was used to estimate the dynamic characteristics at four mounting points (i.e., front left, front right, rear left, rear right mounts). Figure 5.14 presents the same suspension coupled to a test jig and vehicle body. In this experiment, the suspension was considered as Substructure A, and the test jig or vehicle body was considered as Substructure B. The FRFs of the suspension were measured at each mounting point under the free boundary conditions, whereas the FRFs of the vehicle body were measured at each coupling point. To obtain the dynamic properties of the coupling points, three tri-axial accelerometers were installed on the suspension side and on the substructure side, and the suspension was assembled at each of the four mount points. In addition, excitations were

induced in three directions at each accelerometer point. In particular, the total excitations were induced at 18 points. The FRFs obtained from this process were converted to virtual-point FRFs and were used to construct the GCPs, which were then used to estimate the dynamics at the coupling mount points of the vehicle. These substructures were then incorporated into the entire vehicle system. Finally, using the test jig, the GCPs were obtained according to Eq. (5.11), to evaluate the vibro-acoustic performance of the suspension. The dynamics at the coupling points of the vehicle and suspension coupling system were then estimated using the GCPs obtained from the test jig and suspension coupling system, in addition to the FRF information of the entire vehicle system, as shown in Fig. 5.15. Figure 5.16 presents the resulting estimated dynamic characteristics at a coupling point when the suspension was combined with the actual vehicle body.

The results in Fig. 5.16 indicate the importance of accurately determining the joint properties for the identification of the dynamic characteristics of the coupling system, in that the results obtained without considering the GCPs were less accurate. Therefore, the use of the GCPs leads to improved accuracy when compared with previous studies wherein the FBS method was used in practical cases [30]. The improved performance of the proposed method, as shown in Fig. 5.16, confirms that it can be accurately applied at a vehicle level.

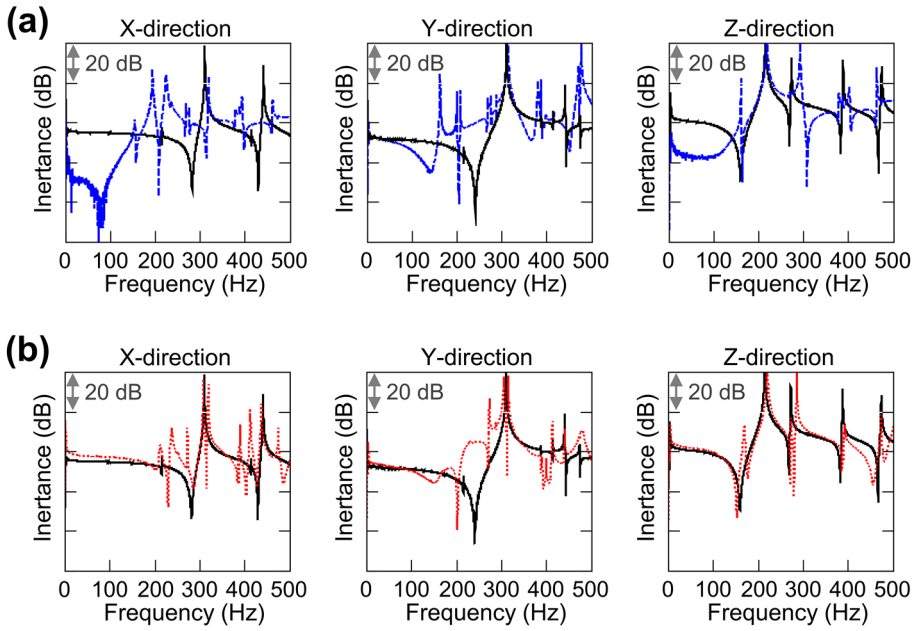

Figure 5.12 Comparison of inertance FRFs of the coupled test jig using the dynamic substructuring model. The black solid line indicates the measured FRF of the coupling system, the blue dashed line in (a) indicates the result of the dynamic substructuring model based only on substructure and joint measured FRFs, and the red dotted line in (b) indicates the result of the dynamic substructuring model based on substructure measured FRFs and virtual point FRFs.

Table 5.1 Comparison of estimated FRFs with and without virtual point FRFs in dynamic substructuring model.

Direction	FRF peak frequency (Hz)		
	Measured	Estimated (without VP FRFs)	Estimated (with VP FRFs)
X	309.75	317.75	307.50
	440.50	461.00	436.50
Y	309.75	312.75	305.00
	440.50	414.75	440.25
Z	214.50	217.50	219.75
	272.25	291.75	285.50
	387.50	378.25	387.00
	473.75	462.75	473.00
Average error (%)		3.42	**1.35**

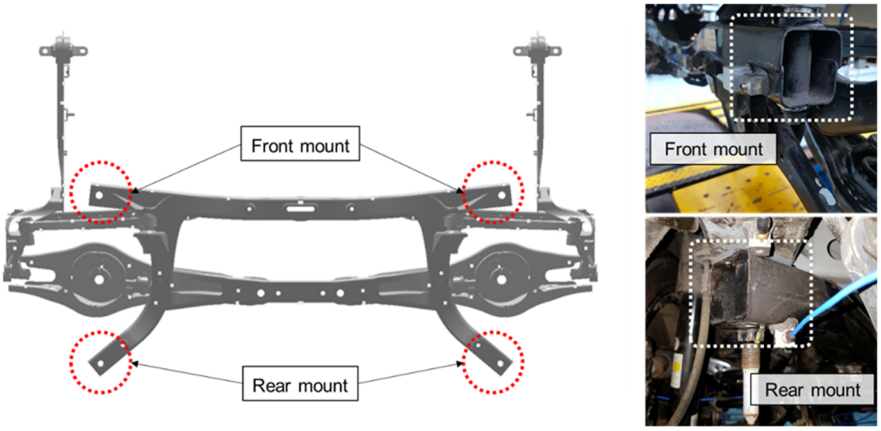

Figure 5.13 Vehicle suspension system.

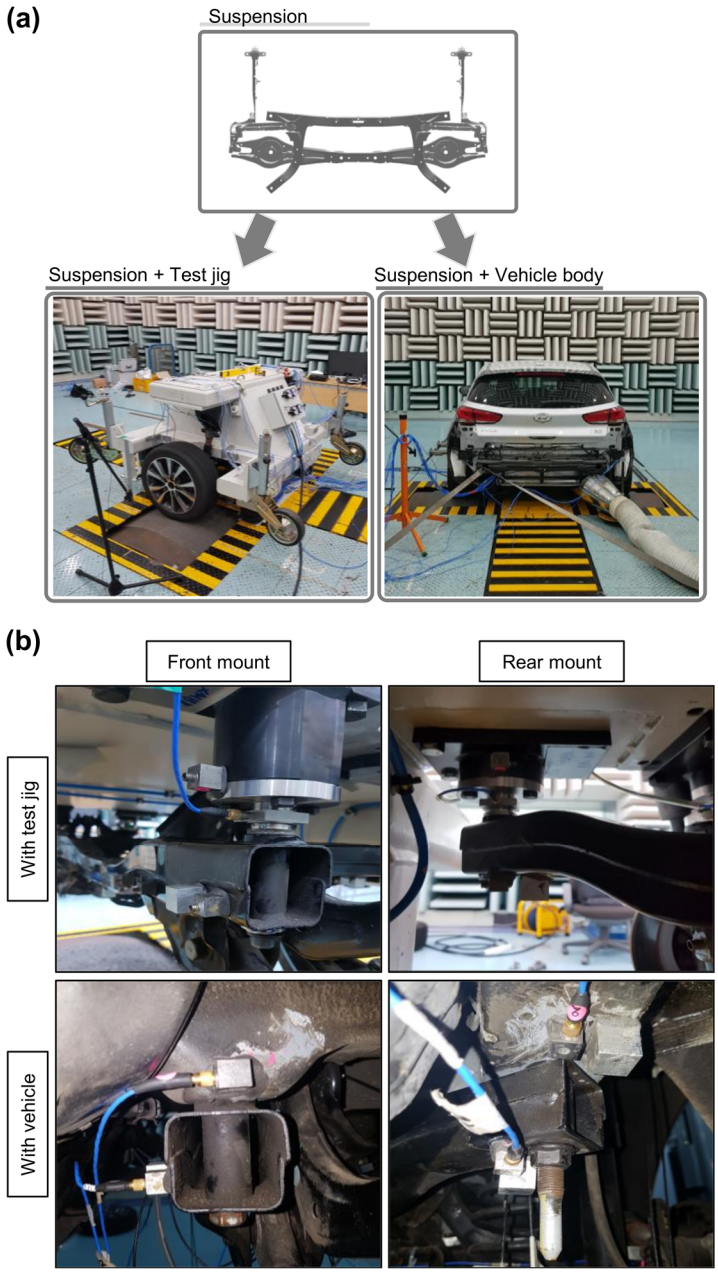

Figure 5.14 Vehicle test setup to validate the proposed dynamic substructuring method: (a) overall views of the suspension connected to the test jig and vehicle body and (b) each mount point of the test jig and vehicle cases.

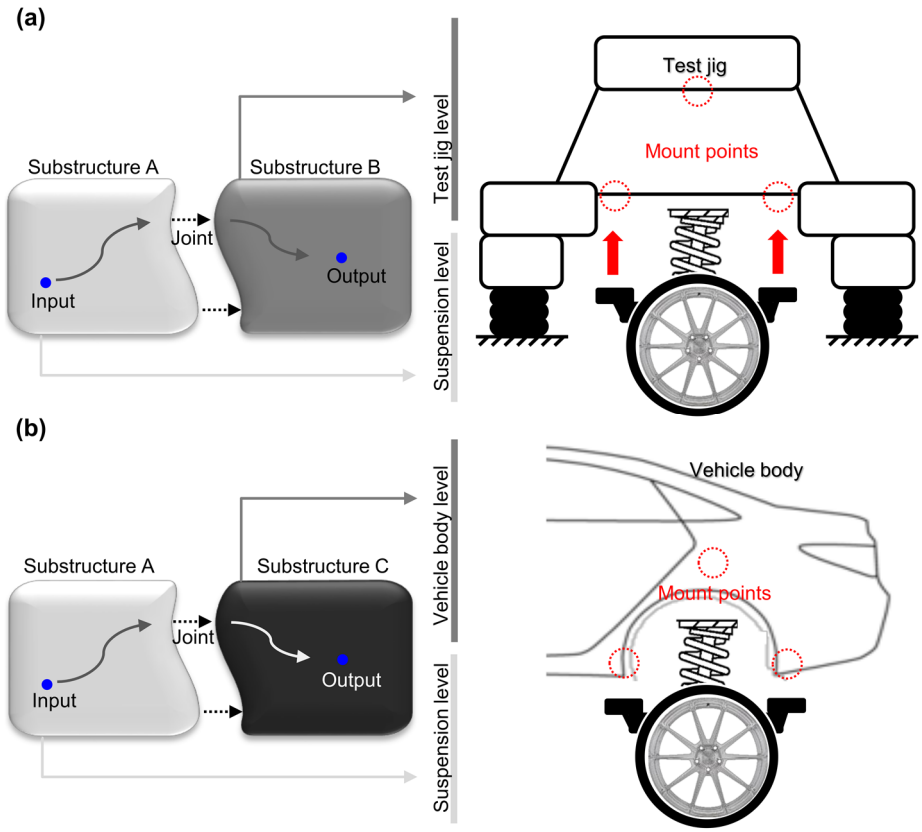

Figure 5.15 Vehicle suspension test case: (a) combined with the suspension test jig and (b) combined with the vehicle body.

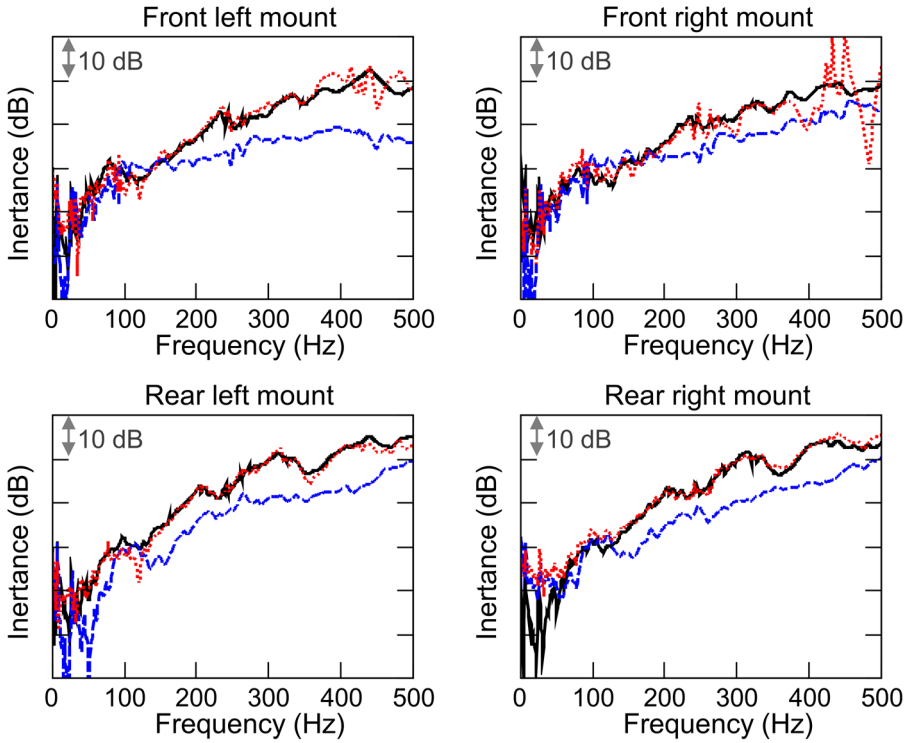

Figure 5.16 Comparison of inertance FRFs at coupled points of a vehicle with suspension. The black solid line indicates the measured FRF of the coupled system, the blue dashed line indicates the estimated FRFs using the dynamic substructuring model without GCPs, and the red dotted line indicates the estimated FRFs using the dynamic substructuring model with GCPs.

5.4 Summary

In this chapter, a practical method was proposed to improve the accuracy of a dynamic substructuring model. In most previous of the studies on dynamic substructuring, practical limitations due to measurement errors were identified. For example, in many real-world cases, frequency response functions (FRFs) cannot be accurately measured because of space constraints due to coupling geometries [62]. The proposed method is based on the FBS method and the application of VPT. The FRFs of the coupling system are estimated using the measured FRFs of the individual substructures and the virtual point FRFs. If the evaluated substructure is coupled with a new substructure, the dynamic characteristics of the new coupled system can be predicted using the generalized coupling properties (GCPs) of the evaluated coupling system.

The proposed method was validated using a series of test jig experiments to estimate the acceleration response and FRFs of the virtual points. This test jig was similar to a hard-mount vehicle suspension crossmember. Subsequently, the accuracy of the results obtained using the proposed method was verified via a comparison between the FRFs estimated using the dynamic substructuring model with GCPs obtained from virtual point FRFs and the

measured FRFs. Moreover, the GCPs obtained from a tested coupling system were then applied to a new coupling system, thus resulting in the improved accuracy of the existing FBS model using the RC method [11,66,67]. Finally, the same process was applied and validated using experiments on a vehicle suspension and vehicle body.

The proposed method allows for the accurate estimation of the dynamic characteristics of a coupling system based on physical measurements, thus reducing errors. This approach allows for the prediction of the dynamic characteristics of many mass-produced industrial products, which includes automotive products. Hence, the proposed method can be applied using the coupled joint properties of bolted connections measured during test jig evaluations in the last phase of production.

The proposed method is difficult to directly apply to isolation mounts (i.e., the elastomer rubber bushing of the suspension), as it assumes rigidity at the coupling joint point. Therefore, this factor should be considered in future studies. Moreover, the results of this study are significant, given that hard mounts are generally used in coupling systems. Thus, the proposed method is an effective tool for practical applications, which can contribute to the improvement of the evaluation of the vibration performance in the automotive industry and other assembly applications.

The results of the proposed method are more accurate than those of existing methods, as the data at an actual joint point between two substructures can be estimated, instead of using the data from coupling peripherals in physical tests or analytical models. Furthermore, the proposed method is applicable to all assumed rigid boundary conditions with respect to sensor attachment, which includes the bolt assembly. Thus, the proposed pre-test process using a test jig in the early design phase allows for the selection of suitable design parameters early in development process, especially to address noise and vibration issues.

CHAPTER 6

CONCLUSIONS AND RECOMMENDATIONS

6.1 Conclusions

This thesis dealt with experimental dynamic substructuring modeling to improve the vibroacoustic performance of a vehicle suspension. The dynamic substructuring technique is a tool that can predict the dynamic characteristics of a new coupled system from the dynamic characteristics information of several substructures. In general, NVH testing in the vehicle field requires a significant amount of effort and man-hours. Therefore, in this study, a method was developed to overcome these limitations, and practical methods were provided with respect to the NVH.

Chapters 1 and 2 provide literature reviews of the dynamic substructuring method and a comprehensive evaluation of the fundamental concepts of the dynamic substructuring modeling method. The method was derived based on two basic assumptions: force equilibrium and compatibility. These concepts were used throughout this study.

Chapter 3 introduces a method to estimate the rotational stiffness of a system using the dynamic substructuring method. In this chapter, a natural frequency shift was used, which occurred when a mass was added to the target. The concepts of trial masses, virtual trial masses, and virtual springs based on the dynamic substructuring model were introduced for the convenience of testing, to estimate the rotational stiffness. As a result, the rotational stiffness could be estimated without utilizing a dedicated test jig. This proposed method can estimate the stiffness with the information of FRFs measured under free-free boundary conditions. In particular, the virtual masses can replace actual trial masses, and virtual springs with infinite stiffness can replace free-free boundary conditions with free-fixed boundary conditions. The introduced method is more accurate and practically convenient than conventional rotational stiffness estimation methods, as it is less sensitive to measurement errors and excludes other mode effects. The model was validated using the experimental results for a vehicle component (shock absorber). As concluded, the proposed method is more efficient and convenient than other methods, as it does not require dedicated test jigs to fix a part.

In Chapter 4, the concept of virtual springs with infinite stiffness was applied to conduct a TPA. Thus, the transfer path can be evaluated without a practical decomposition and assembly process, which is different from

conventional TPA. Conventional methods lead to errors, as they do not accurately reflect the operational conditions of an actual system, such as the boundary condition to the exclusion of the source. A mathematical error is may therefore be induced in the matrix inversion method, which is used to estimate the operating forces of a source in the conventional TPA method. On the other hand, the proposed TPA does not require part removal or correlation information between the signals. Hence, the proposed method is applicable to actual vehicle development and the evaluation process, as it can predict trends without the experimental application of stiffness changes to the actual system. By arbitrarily changing the stiffness of the path, the reduction in SPL of the target system can be predicted without conducting experiments. This improves the efficiency of existing development processes with respect to the time required and cost, by reducing repeated vehicle prototype evaluations and improvements. In conclusion, this thesis proposes a novel transfer path evaluation method.

Chapter 5 presents an approach for the improvement of the estimation accuracy of the dynamic substructuring model. In real cases, FRFs cannot be accurately measured because of a lack of space due to coupling geometries. Thus, the VPT concept was introduced to solve this problem. In addition, the GCPs were used to estimate the FRFs of the coupling system. The FRFs of the

coupling system were estimated using the measured FRFs of the individual substructures and the virtual-point FRFs. If the evaluated substructure is coupled with a new substructure, the dynamic characteristics of the new coupled system can be predicted using the GCPs of the evaluated coupling system. The accuracy of the results obtained using the proposed method was verified by comparison between the FRFs estimated using the dynamic substructuring model with the GCPs obtained from the virtual-point FRFs and the measured FRFs. Moreover, the GCPs obtained from a tested coupling system were then applied to a new coupling system, thus resulting in the improved accuracy of the FBS model. Thereafter, the same process was conducted and validated by conducting experiments on a vehicle suspension and vehicle body.

The findings of this study provide allow for a better understanding of the control of the parameters related to NVH. In addition, the proposed methods allow for the selection of suitable design parameters in the early phase of development. These methods provide a practical solution that is easier to implement. Moreover, the estimation accuracy is superior to those of existing methods.

6.2 Recommendations

The dynamic substructuring model covered in this thesis could profit from additional elaborations. As for future work, it would be desirable to consider the following topics:

(i) Application of the rotational stiffness evaluation method: The evaluation method should be applied to more complex shapes. Although the method was verified for the damper strut of a vehicle in this study, generalization is required for the application of more complex shapes. This may require the modification of the trial mass formula to include more geometrical variables.

(ii) Studies should be conducted on extended application to systems with complex shapes or coupling conditions, and verification experiments should be conducted for the rotational stiffness estimation model. In systems with complex shapes, stronger coupling may require a greater number of virtual springs to consider the deformation and the rigid body motion of the part to be fixed.

(iii) For the proposed TPA, further investigation of the crosstalk effect is required. In a general TPA, the contribution of each path from the FRFs and phase information can be evaluated. However, in this study the crosstalk effect between the transfer paths was not extensively investigated. Therefore, further research is required for the effective application of the method.

(iv) The proposed TPA is only applicable to FRF data, and not the entire spectrum of an actual operation signal. In particular, the proposed method is a TPA method for FRFs; thus, the force characteristics should be used when representing actual phenomena. The FBS-based TPA requires more data and experience for a wider scope of application. Moreover, a virtual spring should be added at the attachment point of a link, and not to the link, for the TPA of suspension links, as discussed in Chapter 4.

(v) The weighting matrix should be assessed for the application of the VPT concept. In this work, to use the VPT, a weighting matrix was employed based on the coherence information between measurements. The mechanism of the transformation process should be described clearly and with good accuracy. In addition, further discussion is required with respect

to several frequency bands for which it is difficult to obtain reliable coherence data from measurements.

APPENDIX

This section presents a discussion of the effect of the volume of the trial mass on the rotational stiffness estimation. The properties of the rod that rotates around a hinge point are its mass (m), radius (r), moment of inertia (I_0), and density (ρ), as shown in Fig. A.1. The relationship between these properties is as follows:

$$m = \rho\pi r^2(L + h), \tag{A.1}$$

$$\begin{aligned} I_0 &= \frac{1}{4}mr^2 + \frac{1}{12}m(L + h)^2 \\ &= \frac{1}{12}\rho\pi r^2[L(3r^2 + L^2) + \{h^3 + 3Lh^2 + 3(L^2 + r^2)\}]. \end{aligned} \tag{A.2}$$

In addition, when the first trial mass is added to the rod, the frequency of the rotational mode, considering its volume, can be written as follows:

$$\begin{aligned} f_1 &= \frac{1}{2\pi}\sqrt{\frac{k_\theta}{I_{1.total}}} \\ &= \frac{1}{2\pi}\sqrt{\frac{k_\theta}{I_0 + I_1 + m_1[(z_1/2)^2 + h^2\,]}}. \end{aligned} \tag{A.3}$$

The frequency of the rotational mode, considering the volume of the second trial mass, is written analogously:

$$f_2 = \frac{1}{2\pi}\sqrt{\frac{k_\theta}{I_{2.total}}} = \frac{1}{2\pi}\sqrt{\frac{k_\theta}{I_0 + I_2 + m_2[(z_2/2)^2 + (L+h)^2\,]}}. \tag{A.4}$$

Based on these results, the moment of inertia of the system can be obtained as follows:

$$I_0 = \frac{f_2^2[I_2 + m_2\{(z_2/2)^2 + (L+h)^2\}] - f_1^2[I_1 + m_1\{\left(\frac{z_1}{2}\right)^2 + h^2\}]}{f_1^2 - f_2^2} = \frac{1}{12}\rho\pi r^2[L(3r^2 + L^2) + \{h^3 + 3Lh^2 + 3(L^2 + r^2)h\}]. \tag{A.5}$$

Finally, the third-order equation for h is derived as follows:

$$\frac{f_1^2 - f_2^2}{12}\rho\pi r^2 h^3 + \left(\frac{f_1^2 - f_2^2}{4}\rho\pi r^2 L + f_1^2 m_1 - f_2^2 m_2\right)h^2$$
$$+ \left(\frac{f_1^2 - f_2^2}{4}\rho\pi r^2 (L^2 + r^2) - 2f_2^2 m_2 L\right)h$$
$$+ f_1^2\left(I_1 + m_1\left(\frac{z_1}{2}\right)^2\right) \qquad \text{(A.6)}$$
$$- f_2^2\left(I_2 + m_2\left(\left(\frac{z_2}{2}\right)^2 + L^2\right)\right)$$
$$+ \frac{f_1^2 - f_2^2}{12}\rho\pi r^2 L(3r^2 + L^2) = 0.$$

Therefore, by solving the above equation for h, all the parameters required for estimating the rotational stiffness can be determined.

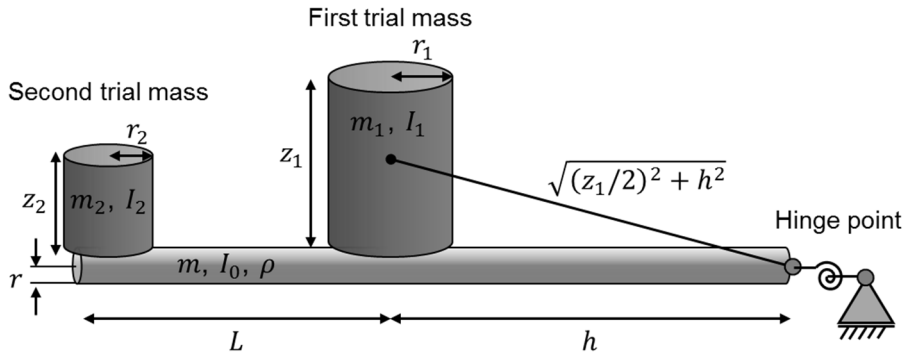

Figure A.1 Detailed modeling considering the volume of the trial mass.

REFERENCES

[1] K.H. Kang, K.J. Kim, Modal properties of beams and plates on resilient supports with rotational and translational complex stiffness, J. Sound Vib. 190 (1996) 207–220.

[2] I. Elishakoff, Y.K. Lin, L.P. Zhu, Random vibration of uniform beams with varying boundary conditions by the dynamic-edge-effect method, Comput. Methods Appl. Mech. Eng. 121 (1995) 59–76.

[3] T.P. Chang, G.L. Lin, E. Chang, Vibration analysis of a beam with an internal hinge subjected to a random moving oscillator, Int. J. Solids Struct. 43 (2006) 6398–6412.

[4] R.O. Grossi, M.V. Quintana, The transition conditions in the dynamics of elastically restrained beams, J. Sound Vib. 316 (2008) 274–297.

[5] D. Wang, Optimal design of an intermediate support for a beam with elastically restrained boundaries, J. Vib. Acoust. 133 (2011) 031014.

[6] M. Wang, D. Wang, G. Zheng, Joint dynamic properties identification with partially measured frequency response function, Mech. Syst. Signal Process. 27 (2012) 499–512.

[7] M. Mehrpouya, E. Graham, S.S. Park, FRF based joint dynamics modeling and identification, Mech. Syst. Signal Process. 39 (2013) 265–279.

[8] Ş. Tol, Dynamic characterization of bolted joints using FRF decoupling and optimization, Mech. Syst. Signal Process. 54 (2015) 124–138.

[9] H. Cao, S. Xi, W. Cheng, Model updating of spindle systems based on the identification of joint dynamics, Shock Vib. 2015 (2015).

[10] E. Segovia, J. Torres, J. Carbajo, J. Ramis, J.P. Arenas, Determination of the elastic parameters of a material from a standardized dynamic stiffness testing, J. Sound Vib. 460 (2019) 114885.

[11] D. Čelič, M. Boltežar, Identification of the dynamic properties of joints using frequency–response functions, J. Sound Vib. 317 (2008) 158–174.

[12] I.G. Araújo, J.E. Laier, Operational modal analysis approach based on multivariable transmissibility with different transferring outputs, J. Sound Vib. 351 (2015) 90–105.

[13] Y.-L. Zhou, E. Figueiredo, N. Maia, R. Perera, Damage detection and quantification using transmissibility coherence analysis, Shock Vib. 2015 (2016) 16.

[14] X. Li, Z. Peng, X. Dong, W. Zhang, G. Meng, A new transmissibility based indicator of local variation in structure and its application for damage detection, Shock Vib. 2015 (2015) 18.

[15] K.H. Joo, D. Min, J.G. Kim, Y.J. Kang, New approach for identifying boundary characteristics using transmissibility, J. Sound Vib. 394 (2017) 109–129.

[16] D.D. Klerk, D.J. Rixen, S.N. Voormeeren, General framework for dynamic substructuring: History, review and classification of techniques, AIAA J. 46 (2008) 1169–1181.

[17] M.V. van der Seijs, D. de Klerk, D.J. Rixen, General framework for transfer path analysis: History, theory and classification of techniques. Mech. Syst. and Signal Process. 68 (2015) 217–244.

[18] J.S. Tsai, Y.F. Chou, The identification of dynamic characteristics of a single bolt joint, J. Sound Vib. 125 (1988) 487–502.

[19] T. Yang, S.H. Fan, C.S. Lin, Joint stiffness identification using FRF measurements, Comput. Struct. 81 (2003) 2549–2556.

[20] Y. Ren, C.F. Beards, Identification of joint properties of a structure using FRF data, J. Sound Vib. 186 (1995) 567–587.

[21] Y. Ren, C.F. Beards, On substructure synthesis with FRF data, J. Sound Vib. 185 (1995) 845–866.

[22] Y. Ren, C.F. Beards, Identification of 'effective' linear joints using coupling and joint identification techniques, J. Vibrat. Acoust. 120(2) (1998) 331–338.

[23] W. Liu, D. Ewins, The importance assessment of RDOF in FRF coupling analysis, In Proceedings of the Seventeenth International Modal Analysis Conference, Orlando, FL (1999, February) pp. 1481–1487.

[24] J. Zhen, T.C. Lim, G. Lu, Determination of system vibratory response characteristics applying a spectral-based inverse sub-structuring approach. Part I: analytical formulation, Int. J. Vehicle Noise Vib. 1 (2004) 1–30.

[25] M.S. Allen, R.L. Mayes, E.J. Bergman, Experimental modal substructuring to couple and uncouple substructures with flexible

fixtures and multi-point connections, J. Sound Vib. 329 (2010) 4891–4906.

[26] A.T. Moorhouse, A.S. Elliott, T.A. Evans, In situ measurement of the blocked force of structure-borne sound sources, J. Sound Vib. 325 (2009) 679–685.

[27] M.V. van der Seijs, Experimental dynamic substructuring: Analysis and design strategies for vehicle development, 2016. ISBN 978-94-6186-671-4

[28] M.V. van der Seijs, E.A. Pasma, D. de Klerk, D.J. Rixen, A comparison of two component TPA approaches for steering gear noise prediction, in: Dynamics of Coupled Structures, Vol. 4, Springer, Cham., 2015, pp. 71–79.

[29] S.W. Klaassen, M.V. van der Seijs, D. de Klerk. System equivalent model mixing. Mech. Syst. and Signal Process. 105 (2018) 90–112.

[30] Y.J. Kang, J.G. Kim, D.P. Song, K.D. Ih, Derivation of road noise improvement factor within a suspension system using the inverse substructuring method, Proc. Inst. Mech. Eng., Part D: J. Automob. Eng. 233.14 (2019) 3775-3786, 0954407019835624.

[31] Y. Shuzi, A study of the static stiffness of machine tool spindles, Int. J. Mach. Tool Des. Res. 21 (1981) 23–40.

[32] Y. Wang, H. Liu, T. Huang, D.G. Chetwynd, Stiffness modeling of the Tricept robot using the overall Jacobian matrix, J. Mech. Robot. 1 (2009) 021002.

[33] D.J. Ewins, Modal testing: Theory, practice and application (Mechanical engineering research studies: engineering dynamics series), Research Studies Pre., second ed., ISBN-13: 978-0863802188, 2000.

[34] D.J. Ewins, P.T. Gleeson, A method for modal identification of lightly damped structures, J. Sound Vib. 84 (1982) 57–79.

[35] M.H. Richardson, D.L. Formenti, Global curve fitting of frequency response measurements using the rational fraction polynomial method, Proc. 3rd IMAC (1985) 390–397.

[36] J.H. Wang, C.M. Liou, Experimental identification of mechanical joint parameters, J. Vib. Acoust. 113 (1991) 28–36.

[37] F.S. Tse, I.E. Morse, R.T. Hinkle, Mechanical Vibrations: Theory and applications, Allyn & Bacon, 1978.

[38] X. Wang, Vehicle noise and vibration refinement, Woodhead, 2010.

[39] J.C. Dixon, The Shock Absorber Handbook, second ed. John Wiley & Sons, Ltd, 2008.

[40] B. Heißing, M. Ersoy (Eds.), Chassis handbook: Fundamentals driving dynamics, components, mechatronics, perspectives, Springer Science & Business Media, Berlin, 2010.

[41] J. Plunt, Finding and fixing vehicle NVH problems with transfer path analysis, Sound Vib. 39 (2005) 12–17.

[42] A.N. Thite, D.J. Thompson, The quantification of structure-borne transmission paths by inverse methods. Part 1: Improved singular value rejection methods, J. Sound Vib. 264 (2003) 411–431.

[43] A.N. Thite, D.J. Thompson, The quantification of structure-borne transmission paths by inverse methods. Part 2: Use of regularization techniques, J. Sound Vib. 264 (2003) 433–451.

[44] B.J. Dobson, E. Rider, A review of the indirect calculation of excitation forces from measured structural response data, Proc. Inst. Mech. Eng., Part C: J. Mech. Eng. Sci. 204 (1990) 69–75.

[45] M. Lohrmann, T. Hohenberger, Operational transfer path analysis: comparison with conventional methods, J. Acoust. Soc. Am. 123 (2008) 3534.

[46] J.S. Bendat, A.G. Piersol, H. Saunders, Random Data-Analysis and Measurement Procedures, 1989.

[47] K. Noumura, J. Yoshida, Method of transfer path analysis for vehicle interior sound with no excitation experiment, In FISITA2006 Proceedings F2006D183 (2006) pp. 1–10.

[48] D. de Klerk, A. Ossipov, Operational transfer path analysis: Theory, guidelines and tire noise application, Mech. Syst. Signal Process. 24 (2010) 1950–1962.

[49] N.M.M. Maia, J.M.M. Silva, A.M.R. Ribeiro, The transmissibility concept in multi-degree-of-freedom systems, Mech. Syst. Signal Process. 15 (2001) 129–137.

[50] I. Kido, A. Nakamura, T. Hayashi, M. Asai, Suspension vibration analysis for road noise using finite element model (No. 1999-01-1788), SAE Technical Paper, 1999.

[51] I. Kido, S. Ueyama, Coupled vibration analysis of tire and wheel for road noise improvement (No. 2005-01-2525), SAE Technical Paper, 2005.

[52] D. Čelič, M. Boltežar, The influence of the coordinate reduction on the identification of the joint dynamic properties, Mech. Syst. Sig. Process. 23(4) (2009) 1260–1271.

[53] S. Im, E. Kim, M. Cho, Reduction process based on proper orthogonal decomposition for dual formulation of dynamic substructures, Comput. Mech. (2019) 1–21.

[54] M.V. van der Seijs, E.A. Pasma, D.D. van den Bosch, M.W.F. Wernsen, A benchmark structure for validation of experimental substructuring, transfer path analysis and source characterisation techniques, in: Dynamics of Coupled Structures, Vol. 4, Springer Nature, Cham, 2017, pp. 295–305.

[55] D.P. Song, D. Min, Y.J. Kang, M. Cho, H.G. Kim, K.D. Ih, A methodology for evaluating the structure-borne road noise prior to a prototype vehicle using direct force measured on a suspension rig, Noise Control Eng. J. 64(3) (2016) 295–304.

[56] D.P. Song, Y.J. Kang, K.D. Ih, A validation study of the detachable shell dyno excitation method for structure-borne road noise evaluation, Noise Control Eng. J. 66(2) (2018) 142–160.

[57] Y.J. Kang, D.P. Song, K.D. Ih, Estimation of body input force transmission change due to parts' modification using the impedance method under rolling excitation, Proc. Inst. Mech. Eng., Part D: J. Automob. Eng. 233(2) (2019) 363–377.

[58] M. Häußler, D.J. Rixen, Optimal transformation of frequency response functions on interface deformation modes, in: Dynamics of Coupled Structures, Vol. 4, Springer Nature, Cham, 2017, pp. 225–237.

[59] M.V. van der Seijs, D.D. van den Bosch, D.J. Rixen, D. de Klerk, An improved methodology for the virtual point transformation of measured frequency response functions in dynamic substructuring, in: 4th International Conference on Computational Methods in Structural Dynamics and Earthquake Engineering, 2013.

[60] D. Schramm, M. Hiller, R. Bardini, Vehicle Dynamics: Modeling and Simulation, Heidelberg, Berlin, 2014, pp. 151.

[61] J.W. Tedesco, W.G. McDougal, C.A. Ross, Structural dynamics: Theory and Applications, Pearson, New York, 1999.

[62] M. S. Allen, D. Rixen, M. van der Seijs, P. Tiso, T. Abrahamsson, R. L. Mayes (Eds.), Substructuring in Engineering Dynamics: Emerging Numerical and Experimental Techniques, CISM International Centre for Mechanical Sciences, Courses and Lectures Vol. 594, Springer Nature, Cham, 2019.

[63] P. Gardonio, M.J. Brennan, On the origins and development of mobility and impedance methods in structural dynamics, J. Sound Vib. 249 (2002) 557–573.

[64] J.G. Kim, K.U. Nam, Y.J. Kang, Method to estimate rotational stiffness: Trial masses, virtual masses, and virtual springs, J. Sound Vib. 477 (2020) 115321.

[65] D.H. Lee, W.S. Hwang, C.M. Kim, Design sensitivity analysis and optimization of an engine mount system using an FRF-based substructuring method, J. Sound Vib. 255 (2002) 383–397.

[66] K.S. Kim, Y.J. Kang, Structural parameters identification using improved normal frequency response function method, Mech. Syst. Sig. Process. 22(8) (2008) 1858–1868.

[67] K.S. Kim, FRF-based system parameters identification with application to improved coupling method, Doctoral dissertation, 2009.

[68] X. Zhao, L. Dai, T. Wang, K.S. Sivakumaran, Y. Chen, A theoretical model for the rotational stiffness of storage rack beam-to-upright connections, J. Const. Steel Research 133 (2017) 269–281.

[69] T. Liu, J.Q. Yang, P. Feng, K.A. Harries, Determining rotational stiffness of flange-web junction of pultruded GFRP I-sections, Compos. Struct. 236 (2020) 111843.

[70] G.H. Golub, C.F. Van Loan, Matrix computations Vol. 3, JHU press, 2012.

[71] G. J. Turvey, Y. Zhang, Characterisation of the rotational stiffness and strength of web-flange junctions of pultruded GRP WF-sections via web bending tests, Composites Part A 37(2) (2006) 152–164.

[72] A. S. Mosallam, L. Feo, A. Elsadek, S. Pul, R. Penna, Structural evaluation of axial and rotational flexibility and strength of web–flange junctions of open-web pultruded composites, Composites Part B 66 (2014) 311–327.

[73] H. Xin, A. Mosallam, Y. Liu, C. Wang, Y. Zhang, Impact of hygrothermal aging on rotational behavior of web-flange junctions of structural pultruded composite members for bridge applications, Composites Part B 110 (2017) 279–297.

국 문 초 록

일반적으로 기계시스템은 다양한 하위 부분구조물로 구성되며, 이들은 많은 소음 및 진동 문제를 야기한다. 본 논문은 이러한 하위 부분구조물의 동특성 정보만을 사용하여 전체 대상 시스템의 동적 특성을 추정하기 위한 동특성 합성기법을 다루고 있다.

먼저, 본 논문의 첫 장에서는, 동특성 합성기법을 활용한 결합 시스템의 회전 강성 추정 기법을 제시하였다. 기존 시험기반의 회전 강성 평가법들은 측정 오류에 민감 할 뿐 아니라, 측정을 위한 별도의 고정용 지그가 필요하다. 그러나, 본 연구에서 제시된 방법은 시스템에 부가되는 질량에 의한 고유 주파수 편이 현상을 사용하기 때문에 기존 방법에 비해 측정오차가 상대적으로 작고, 다른 모드의 간섭을 배제함으로써 추정 정확도의 향상을 기대할 수 있다. 또한, 본 기법은 주파수 응답함수 기반 합성 모델을 사용하여 실제 고정 지그를 사용하는 대신, 고정 경계조건을 수식적으로 대체함으로써 기존 방법의 복잡성을 해결하였다. 이 과정에서 시험 질량, 가상 질량 및 가상 스프링의 개념이 도입되었으며, 실제 차량의 충격 흡수 장치를 이용하여 모델의 검증을 수행하였다.

다음으로, 본 논문의 두 번째 장에서는, 동특성 합성 모델을 이용한 새로운 전달 경로 분석 기법을 제시하였다. 본 연구에서는 대

상 시스템의 실제 전달경로를 제거하는 대신, 무한대의 강성을 갖는 가상의 스프링을 주파수 응답 함수의 형태로 반영함으로써, 특정 전달경로의 제거 효과를 구현하였다. 본 기법은 기존의 전달경로 분석법에 비하여 실험적으로 구현이 쉬우며, 측정에 소요되는 작업량과 계산량 또한 획기적으로 줄일 수 있다. 해당 기법은 차량 현가계의 특정 진동 전달 현상을 이용하여 실험적으로 유효성이 검증되었다.

본 논문의 마지막 장에서는, 동특성 합성 모델의 정확도 개선을 위한 연구가 수행되었다. 일반적으로 결합시스템은 두 개 이상의 결합물이 볼트를 이용하여 결합되며, 결합 시스템의 동특성 예측을 위해서는 결합부의 정확한 동특성이 요구된다. 하지만 대부분의 경우, 물리적 공간의 제약으로 인하여 실제 결합 지점에서의 측정이 불가능하기 때문에, 가상 지점의 개념을 도입하여 결합지점에서의 주파수 응답함수를 추정하였다. 해당 방법 역시, 실제 차량과 서스펜션 시험 지그를 이용하여 검증되었다. 본 연구는 많은 실제 응용 분야에서 정확한 시스템의 동특성 추정에 기여하고 있다.

주요어 : 동특성 합성기법, 주파수 응답 함수 기반 합성법,
시험 질량, 가상 질량, 가상 스프링, 회전 강성,
전달 경로 분석, 가상 지점 변환
학 번 : 2015-20723